BULK AND INTERFACIAL PROPERTIES OF CHAIN FLUIDS

A MOLECULAR MODELLING APPROACH

A dissertation presented to the
Departament d'Enginyeria Química of the

Universitat Rovira i Virgili

in partial fulfillment of the requirements for the degree of
Doctor in Chemical Engineering

by

Josep C. Pàmies

under the supervision of Dr. Lourdes F. Vega

Tarragona, Spain
October, 2003

BULK AND INTERFACIAL PROPERTIES OF CHAIN FLUIDS

A MOLECULAR MODELLING APPROACH

Memòria de la tesi presentada al
Departament d'Enginyeria Química de la

Universitat Rovira i Virgili

per a optar al títol de
Doctor per la Universitat Rovira i Virgili

Josep Pàmies Corominas

Tesi dirigida per la Dra. Lourdes Vega

Tarragona,
octubre de 2003

BULK AND INTERFACIAL PROPERTIES OF CHAIN FLUIDS
A MOLECULAR MODELLING APPROACH

Thesis committee:

Prof. Keith E. Gubbins
North Carolina State University, NC, USA

Prof. Walter G. Chapman
Rice University, TX, USA

Prof. George Jackson
Imperial College, UK

Dr. Carlos Vega
Universidad Complutense de Madrid, Spain

Dr. João A. P. Coutinho
University of Aveiro, Portugal

Dr. Felipe J. Blas (substitute)
Universidad de Huelva, Spain

Dr. Daniel Duque (substitute)
Institut de Ciència de Materials de Barcelona (ICMAB-CSIC), Spain

External evaluators (requirement for the mention of "European doctor"):

Dr. Thomas Kraska
University at Cologne, Germany

Dr. Amparo Galindo
Imperial College, UK

La sotasignant

FA CONSTAR

que el present treball, que porta per títol

BULK AND INTERFACIAL PROPERTIES OF CHAIN FLUIDS: A MOLECULAR MODELLING APPROACH

i que presenta en Josep Pàmies Corominas per a optar al grau de Doctor per la Universitat Rovira i Virgili, ha estat realitzat en aquesta universitat sota la seva direcció, i que tots els resultats presentats i l'anàlisi corresponent són fruit de la investigació realitzada per l'esmentat candidat.

I per a que se'n prengui coneixement i als efectes que correspongui, signa aquest certificat.

<div align="right">

Lourdes Vega Fernández
Investigadora Científica
Institut de Ciència de Materials de Barcelona
Centro Superior de Investigaciones Científicas (CSIC)

</div>

Tarragona, 31 d'octubre de 2003.

Declaration

The work reported in this thesis was carried out, in the most part, at the Molecular Modelling Group, Departament d'Enginyeria Química, Universitat Rovira i Virgili (Avinguda dels Països Catalans, 26, 43007, Tarragona, Spain) with financial support from the Departament d'Universitats, Recerca i Informació of the Generalitat de Catalunya. No part of this thesis has been submitted elsewhere for any other degree or qualification and it is all my own work unless referenced to the contrary in the text.

<div align="right">

Josep Pàmies
October 2003

</div>

Als meus pares,
i a tots els que han mogut alguna peça del trencaclosques

La vida és breu, l'art llarg, l'ocasió fugissera,
l'experiment perillós, i el judici difícil.

Hipòcrates

Contents

Agraïments / Acknowledgements

Aquest treball no hagués arribat mai fins aquí sense l'ajuda i el suport de moltes persones durant els darrers quatre anys. A tots ells els dedico aquesta tesi i, encara que només sigui mitjançant aquestes dues planes, mereixen un reconeixement.

Per començar, vull donar les gràcies a la Dra. Lourdes Vega. Sense la Lourdes, el projecte de tesi hagués estat quelcom prou avorrit com per esgotar les ganes d'intentar treure-li suc. Amb la Lourdes, el camí ha estat un viatge divertit ple de detalls engrescadors i gratificants, tan en el terreny científic com el personal. I amb ella, he après molt més que ciència. Recordo el bon grapat de cops que m'ha dit "si no ho saps explicar de forma senzilla, és que no ho entens". Si trobeu aquesta tesi entenedora, li heu d'agrair sobretot a ella.

It is a great pleasure to thank professors Keith Gubbins, Walter Chapman, George Jackson, Carlos Vega and João Coutinho for accepting to be members of the evaluation committee. I believe it is impossible to ask for a better committee for this thesis. I apologize in advance if I forgot any important reference of their multiple works in this field.

It is also a pleasure to thank Dr. Thomas Kraska and Dr. Amparo Galindo for the evaluation of this work. It is laudable to read this thesis and make a report in only two weeks.

És un plaer agrair al Dr. Felipe Blas y al Dr. Daniel Duque que hagin acceptat llegir aquesta tesi i ser membres suplents del tribunal. Al Felipe li dec molt perquè aquesta tesi és en molta part una continuació natural del seu treball. Els seus codis i notes m'han estat molt útils en moltes ocasions. Al Dani li he d'agrair la lectura crítica i minuciosa d'aquest treball.

I would like to thank professor Peter Cummings for inviting me to Knoxville and taking care of me and some of my expenses and, together with Dr. Clare McCabe, for helping me on many scientific questions while I was learning and working on molecular simulation. I am also very grateful to professor Cor Peters for inviting me to Delft, for enlightening many ideas, and making that stay a very pleasant one. I would also like to thank other researchers at Delft: professor Theo de Loos, for his interest on my work, and Louw Florusse, for his experimental data on the solubility of hydrogen.

Regarding this piece of work, I should thank Dr. Henk Meijer from Shell for the critical reading of the manuscript. I can not forget to thank Dr. João Coutinho for inviting me to Aveiro and for his comments on the works about interfacial properties and perfluoroalkanes. For this I should also thank Dr. Isabel Marrucho. Also in Aveiro, I was very happy to work with Antonio Queimada. Very special thanks go to Ana Dias. I owe a lot to her both professionally and as a friend. The weeks in Aveiro would have been very different without Ana and her family.

Agraeixo també el suport econòmic de la Universitat Rovira i Virgili, la concessió d'una beca predoctoral del Departament d'Universitats, Recerca i Societat de la Informació de la Generalitat de Catalunya, i els projectes PB96-1025, PPQ2000-2888-E i PPQ-2001-0671 del Ministerio de Ciencia y Tecnología del govern espanyol.

Els meus companys de despatx a Tarragona també es mereixen un reconeixement especial. El Carlos, l'Oliver, la Susana, la Silvia, el Zaid i, més recentment, el Carmelo, el Henry i el Saravana. Tots ells han fet que sempre fos molt agradable, fins i tot divertit, treballar al despatx. A l'Oliver i el Carlos els he d'agrair també la seva ajuda amb els problemes informàtics, i al Carmelo, que sempre em fa riure, el seu bon treball sobre el model TACH. A la resta d'amigues dels nombrosos cafès gratificants, la Isabela, la Clara i la Vanessa, els molt bons moments. Sense tots ells, aquestes línies serien segur pessimistes. I no em puc deixar el Fèlix que, a més d'haver de fer de taxista, ha aconseguit que el codi de la soft-SAFT sigui molt més valuós.

La Dra. Rosa Marcos, el Luisfer Turrens, i el Dr. Miguel Ángel Santos, que foren membres del grup de modelització molecular a Tarragona, i els estudiants del Laboratori d'Investigació, sobretot a l'Òscar Garcia, la Cristina Linares i la Montse Andreu, també mereixen un agraïment per la seva ajuda, que no ha estat poca.

No puc deixar d'anomenar alguns companys de viatge, els quals m'han ajudat d'alguna o d'altra forma, encara que potser ells no ho sàpiguen. L'Eduardo Sanz, que sempre troba la vessant còmica de qualsevol situació, la Laura Rovetto, sempre disposada a xerrar de qualsevol cosa, la Pilar Garate, que s'ha doctorat en paciència esperant els meus resultats, i el José Luis Rivera, que em va portar a tot arreu per Knoxville, fins i tot més enllà.

La penya d'amics de Tarragona, encara que no vulguin que els hi expliqui què és això de la mecánica estadística, són per mi de bon tros els millors cantants i músics d'aquestes terres. Quasevol agraïment cap a tots ells es quedarà curt.

Mons pares i germans han ajudat molt a que aquesta tesi hagi arribat a un final gratificant. A ells no els necessito demostrar res. Per a ells, la meva tesi és meravellosa; per a mi, aquest treball tambés és, en part, seu.

I per últim, li dedico molt especialment aquesta tesi a la Raquel que, encara que ja estigui farta de sentir parlar-ne, segur que li agradarà veure-la acabada. Ella, més que ningú, és qui mereix el meu agraïment més sincer.

Summary

This work concerns the development of tools from molecular modelling, specifically Statistical Associating Fluid Theory (SAFT) and molecular simulation (both Monte Carlo and molecular dynamics), and their application in the modern molecular thermodynamics area. These tools have been used to study the behaviour of bulk properties of fluid systems at thermodynamic equilibrium, mainly vapour-liquid equilibria, but also liquid-liquid coexistence and critical behaviour. Properties of planar interfaces from a SAFT together with a density gradient approach are also subject of this work. The real systems treated include pure n-alkanes, 1-alkanols, n-perfluoroalkanes, hydrogen, oxygen, xenon, carbon dioxide and a number of mixtures of them.

Thermophysical properties affect most aspects of chemical plant design and operation. On the one hand, property data and predictive methods are the raw material of chemical process design. On the other, process simulation has become the main tool for the development, design, scale-up and optimization of chemical processes. Thermophysical properties, particularly, those of phase equilibria, are therefore key inputs for the development of such process models.

Thermophysical properties can be obtained experimentally and from theoretical models, both from phenomenological and molecular points of view. However, nowadays experimental measurements are only carried out for systems or conditions at which existing models fail or they are not accurate enough. Phenomenological models are a physically reasonable way to represent experimental data but, due to their limited prediction capability, they may not reliably work outside the range where their parameters were fitted. A molecular perspective, contrarily, allows deriving fundamental relationships between the underlying inter- and intra-molecular forces and the resulting macroscopic behaviour of fluids. An important advantage of using a molecular model is that parameters are physically meaningful and independent of thermodynamic conditions. Furthermore, the use of molecular theory and simulations provides a means to separately determine the effect of intermolecular forces and the effect of the assumptions made in molecular theory on the macroscopic behaviour.

As explicitly stated in the title of this thesis, this work fits the molecular modelling field. It has been devoted to the development of reliable and accurate tools from molecular modelling for the prediction of the thermodynamic behaviour of complex fluids. The statistical associating fluid theory (SAFT), the density gradient theory, and molecular simulations, both Monte Carlo and molecular dynamics, have been employed to study the behaviour of bulk and interfacial properties of chain fluids at thermodynamic equilibrium. The real systems treated include pure n-alkanes, 1-alkanols, n-perfluoroalkanes, hydrogen, oxygen, xenon, carbon dioxide and a number of mixtures of them.

A Lennard-Jones version of the SAFT equation of state, the so-called soft-SAFT equation, has been used to study phase equilibrium and critical behaviour of chain systems. Sets of optimized molecular parameters for the first members of the n-alkane, 1-alkanol and n-perfluoroalkane series are proposed, which linearly correlate with the carbon number of the chain. Using them in a transferable way allows the accurate prediction of the phase envelope of long chains and mixtures, without the need of optimization of mixture parameters in many cases. The equation is proven to be successful for phase equilibria predictions and critical behaviour of normal alkanes and asymmetric binary mixtures of them. It is also shown that the soft-SAFT equation is able to quantitatively predict available critical properties for relatively long chain lengths, showing a crossover to mean-field behaviour when the infinite chain length regime is reached. Moreover, assuming that the volume and dispersive energy per molecule keep their proportionality to molecular weight for very long chains, it was found that the equation predicts a value of 1/5 for the critical compressibility factor of chains of infinite length.

The solubility of hydrogen in long n-alkanes is shown to be another successful application of the soft-SAFT equation of state. It is proven that the soft-SAFT model is able to provide very accurate and reliable results for these very asymmetric systems. The extension of the equation to cross-associating systems allows a correct description of the solubility of oxygen in n-perfluoroalkanes. It is demonstrated again the importance of physically meaningful parameters, by showing reasonable trends and comparing parameter values to those from other models when possible. The study of carbon dioxide binary mixtures concluded that, for an accurate description of these systems, the effect of the quadrupole of the carbon dioxide has to be included in the SAFT model.

The soft-SAFT equation has been coupled with the Cahn-Hilliard density gradient theory for the calculation of properties of planar interfaces of n-alkanes, 1-alkanols, and mixtures of them. It is shown that interfacial properties for pure compounds and mixtures at subcritical conditions can be accurately predicted with this approach. Moreover, it is expected that a crossover treatment of the soft-SAFT equation will

greatly improve the description of mixtures in which a critical point is involved.

Although most of the work was directed towards the development of a reliable and accurate tool based on SAFT for the prediction of the thermodynamic behaviour of complex fluids, molecular simulations were also used for the computation of bulk and interfacial properties of simple fluids. In particular, a molecular dynamics code was extended for the computation of interfacial properties. The influence of the cut-off radius of the interaction potential on the coexisting densities is also presented.

This work has demonstrated that the keys of an appropriate use of molecular modelling tools are the selection of a suitable specific model representative of the structure and relevant interactions of the real system, and the use of parameters that should show physical trends (within a chemical series) and be transferable (within a chemical series and to other compounds) whenever possible.

Notation

Abbreviations

AAD(s)   Absolute Averaged Deviation(s)
DFT   Density Functional Theory
DGT   Density Gradient Theory
eq(s)   equation(s)
EOS(s)   Equation(s) Of State
LCST   Lower Critical Solution Temperature
LJ   Lennard-Jones
LLE   Liquid-Liquid Equilibrium/a
PVT   Pressure-Volume-Temperature
RDF   Radial Distribution Function
RHS   Right-Hand Side
SAFT   Statistical Associating Fluid Theory
UCST   Upper Critical Solution Temperature
VLE   Vapour-Liquid Equilibrium/a

Roman symbols

A Helmholtz free energy per mole
a Helmholtz free energy density
c influence parameter of the density gradient theory
C two-body direct correlation function
CN carbon number
g pair correlation function
k volume of association
k_B Boltzmann constant
M_w molecular weight
m chain length

N_A	Avogadro's number
P	pressure
R	ideal gas constant
r_c	cut-off radius
T	temperature
X	fraction of nonbonded molecules
x	mole fraction
Z	compressibility factor

Greek symbols

γ	interfacial tension
Δ	association strength
ϵ	energy well-depth of the intermolecular potential / dispersive energy
ε	association energy
η	size parameter of the generalized Lorentz-Berthelot combination rules
Θ_c	general variable for a critical property
μ	chemical potential per mole
ξ	energy parameter of the generalized Lorentz-Berthelot combination rules
ρ	density
ρ_c	critical density
σ	size parameter of the intermolecular potential / diameter
ϕ_c	critical volume fraction
Ω	grand thermodynamic potential

List of Figures

List of Tables

Chapter 1

Introduction

In day to day life, we intuitively know how the world works. There are very basic laws of physics that we instinctively understand showing everywhere: gravity makes things fall to the ground, pushing something makes it move, two things cannot occupy the same place at the same time. At the turn of the nineteenth century, scientists thought that all the basic rules of Newtonian classical physics should apply to everything in nature, but then they began to study the world of the atoms, electrons and light waves. None of these things followed known rules. Thanks to physicists like Max Planck, Albert Einstein and Niels Bohr, new physics laws were discovered. These laws constitute today the basic laws of quantum mechanics.

Several years after the "birth" of quantum mechanics, in 1929, Dirac [1] wrote "The underlying physical laws necessary for the mathematical theory of a large part of physics and the whole of chemistry are thus completely known, and the difficulty is only that the exact application of these laws leads to equations much too complicated to be soluble."

One could therefore argue that chemistry and derived disciplines just follow the laws of quantum mechanics and they are nothing but applied physics. However, as music does not end when all types of instruments, notes and rhythms are established, science does not end when its basic laws are known. The "playing" part can still be a hard job. Even with the powerful computers available today, the application of quantum mechanical models can be extremely complex for all but the simplest systems. Any other theoretical approach needs some experimental data in order to provide an accurate description of the real world.

As explicitly stated in the title of this thesis, this work belongs to the molecular modelling field. As defined in reference [2], molecular modelling starts from the chemical constitution of a material, and proceeds to derive estimates of properties by

deductive reasoning based upon the principles of quantum and statistical mechanics. Molecular modelling encompasses theory, simulation and phenomenological models. The approaches that comprise molecular modelling are: (1) Molecular orbital theory (*ab initio* models); (2) Statistical mechanics; (3) Classical or Newtonian theory; (4) Computer simulations (molecular dynamics and Monte Carlo); (5) Phenomenological models. The approaches we used in this research work come from statistical mechanics and computer simulations, and results are compared to phenomenological models and experiments.

Since this thesis work is specifically devoted to the description of bulk and interfacial properties of fluids from a molecular point of view and using tools from statistical thermodynamics, it belongs to the area of modern molecular thermodynamics. Prausnitz [3] stated that molecular thermodynamics is now in a post-van der Waals era. This does not mean that methods based on the van der Waals concept are no longer useful, but rather that molecular thermodynamics is now increasingly using ideas and tools from a variety of advanced concepts in chemical physics, mathematics and computer simulations.

Physical property data and methods are the raw material of chemical process design. Nowadays process simulation has become the main tool for the development, design, scale-up, and optimization of chemical processes. It is evident, hence, that thermodynamic properties (in particular, phase equilibria) and kinetic data are key inputs for the development of such process models. The need for accurate physical property data and models is well documented in the literature [4–7].

Thermodynamic properties of pure fluids and mixtures are usually obtained by means of equations of state. Experimental measurements are only carried out for systems or conditions at which existing models fail or they are not accurate enough. There are, in principle, two types of equations suitable for real systems: empirical, and semi-empirical. Empirical equations or correlations are usually arbitrary functions with parameters fitted to experimental data. They are very accurate only for the systems for which the parameters were obtained and in the range of thermodynamic conditions used in the fitting procedure. On the other hand, semi-empirical models use phenomenological knowledge and/or theoretical approximations, which make them general in the sense that they can be valid for many systems. These models are able to accurately describe real systems by treating some of their parameters as adjustable to experimental data.

It is well known the limited prediction capability of empirical and many semi-empirical models, like traditional cubic equations of state, outside the range where their parameters were fitted. On the contrary, parameters of molecular models based on statistical mechanics are physically meaningful and independent of the thermodynamic conditions. Another important advantage of using a molecular-based theory,

versus simple mean-field approaches, is that one can explicitly consider intramolecular as well as intermolecular interactions. Furthermore, the details of the applied intermolecular potential will be reflected in the accuracy of the thermodynamic properties calculated by using the theory.

Almost fifteen years have passed since Chapman, Gubbins, Jackson and Radosz [8, 9], and Huang and Radosz [10, 11] developed an equation of state for associating fluids, the so-called SAFT equation (which stands for Statistical Associating Fluid Theory), based on Wertheim's first-order thermodynamic perturbation theory [12–15]. As pointed out in a recent review by Müller and Gubbins [16], more than 200 papers have been published in the last ten years on the development and applications of equations of state based on the SAFT approach. Nowadays SAFT is becoming a standard equation for engineering purposes, as well as a challenging approach to test the accuracy of such types of molecular theory in predicting the properties of complex fluids.

One may consider the success of the SAFT equation, developed essentially to deal with associating fluids, for which traditional macroscopic equations usually fail. SAFT is an approach in which the different microscopic contributions that control the macroscopic properties of the fluid are explicitly considered when building the theory. In this sense, nonideal contributions, such as molecular shape and association, are introduced in the development of the equation. In spite of this great advantage versus equations of state based on the van der Waals approach, it is exciting to see how a simple equation like SAFT can give quantitative predictions, comparable to simulation and experimental data, for thermodynamic properties of a lot of pure substances and multicomponent mixtures. There may be several reasons that underlie this success, but it is clear that its strong statistical-mechanical basis makes it a robust and versatile equation, to which refinements and extensions can be implemented in a systematic way. For this reason, several versions of the SAFT equation exist today. Besides the SAFT equation of Huang and Radosz [10, 11], which was parameterized for many real fluids and is by far the most widely used, other implementations are outstanding because of their applicability: the SAFT-VR of Jackson and co-workers [17], the PC-SAFT of Gross and Sadowski [18] and the soft-SAFT EOS of Vega and co-workers [19]. Specific applications where they are successful, as well as their similarities and differences are emphasized in the reviews by Müller and Gubbins [16], Economou [20] and Paricaud *et al.* [21], and throughout the present manuscript when necessary.

1.1 Scope, objectives and organization of this thesis

This work concerns the development of tools from molecular modelling, in particular, SAFT and molecular simulation, and their application in the modern molecular thermodynamics area. The mentioned tools have been used to study the behaviour of bulk properties of fluid systems at thermodynamic equilibrium, mainly vapour-liquid equilibria, but also liquid-liquid coexistence and critical behaviour. Interfacial properties of planar interfaces from a SAFT + density gradient theory approach are also subject of this work. The real systems treated include pure n-alkanes, n-alkanols, n-perfluoroalkanes, hydrogen, oxygen, xenon, carbon dioxide and a number of mixtures of them. Thermodynamic properties of some of these systems had already been approached from many models, both from phenomenological and molecular points of view. However, our principal aim is directed toward the development of a reliable and accurate tool based on SAFT for the prediction of the thermodynamic behaviour of complex fluids, complemented with molecular simulations. By appropriate use we understand the selection of a suitable specific model representative of the structure and relevant interactions of the real system, and molecular parameters that show physical trends (within a chemical series) and may be transferable (within a chemical series and to other compounds). A few specific objectives are also addressed:

- Application of the soft-SAFT EOS to equilibrium calculations of binary systems of short + long chains and polymers

- Study of the capability of the soft-SAFT EOS in predicting solubility of gases in long chains

- Obtaining of reliable and transferable molecular parameters for real systems

- Extension of the soft-SAFT EOS for cross-associating models and application to real systems

- Extension of a molecular dynamics code for the computation of interfacial density profiles of pure systems

- Integration of the soft-SAFT EOS to the Cahn and Hilliard density gradient theory. Application to interfacial tension calculations in vapour-liquid interfaces of pure and binary mixtures

- Development of a single, modular and multi-feature computer code, easy to systematically extend, and of friendly use.

After this general introductory chapter, the next two chapters are devoted to theory. Chapter 2 exposes the physical background of Wertheim's theory of association

and the SAFT equation. The last section of that chapter focuses on the soft-SAFT EOS. We emphasize there the particular features of this equation and then make a brief description of the characteristics of the soft-SAFT computer program. Chapter 3 is dedicated to the physical and mathematical description of the Cahn-Hilliard gradient theory. Results from the application of these theories are given in subsequent chapters.

Chapter 4 is devoted to the study of equilibrium and critical behaviour of chain systems by the soft-SAFT EOS. In the first section vapour-liquid equilibrium properties and critical constants for the n-alkane series and mixtures of short and long alkanes are studied. The next section deals with the dependence of the critical behaviour on chain length for pure homopolymer systems. In the third place, we present a study of the solubility of hydrogen in long chains. An application to equilibrium properties of perfluoroalkane systems and the solubility of oxygen and xenon in these compounds comes into the fourth section. The last section concerns the prediction of vapour-liquid equilibria and critical properties of binary mixtures of CO_2 + n-alkanes and CO_2 + 1-alkanols.

In chapter 5 we use molecular simulations for the computation of bulk and interfacial properties of methane and propane. In addition, a study of the influence of the cut-off radius on the accuracy of the properties is performed. The details of the molecular simulation techniques used are specified in the same chapter. We believe that any additional theoretical explanation about molecular simulation is unnecessary in this thesis work, given the existence of a vast literature [22] on the fundamentals in which they are based, and also on their implementation and applications.

Chapter 6 is devoted to the application of the soft-SAFT + Cahn-Hilliard density gradient theory. The vapour-liquid interfacial tensions of pure n-alkanes, 1-alkanols, and mixtures of them are studied.

Finally, in chapter 7, we summarize the conclusions of this thesis and future work is outlined.

Chapters 5 and 6, and every section in Chapter 4 are self-contained. This means that they have their particular introduction and conclusions.

Chapter 2

Statistical Associating Fluid Theory (SAFT)

The background of the SAFT equation of state is presented in this chapter, after a description of Wertheim's theory of association. The assumptions underlying the theory and the approximations made in the derivation of the equation are explained throughout the text. The description of the soft-SAFT equation of state follows, with remarks on the differences with respect to the original SAFT equation. The last section also contains a description of the features of the soft-SAFT computer code, at the present state of development.

2.1   Wertheim's theory of association

Association in fluids implies the existence of strong and highly directional attractive molecular interactions, which lead to the formation of relatively long-lived molecular clusters. Hydrogen bonding and charge transfer are cases of such chemical association between molecules. Association has a significant effect on the properties of fluids, which are responsible for large deviations from ideality. The strong and directional nature of the association bonds, whose internal energy shows a higher dependence on temperature than the weaker van der Waals interactions, makes possible the close-loop phase behaviour [23], not seen in fluids without hydrogen bonding.

Several attempts to understand the behaviour of associating fluids have arisen from chemical theory and statistical mechanics. The oldest method for predicting phase equilibria of associating mixtures is the chemical theory of solutions first developed by Dolezalek [24]. This approach, rigorously based on thermodynamics, considers

the existence of distinct molecular species in solution, which are assumed to be in chemical equilibrium. The strong anisotropic physical interactions of the associating fluid are treated as chemical reactions with corresponding equilibrium constants. The main drawback of this theory lies in the arbitrary way in which the user decides which species are present. After a scheme is assumed, one has to determine the equilibrium constants and their temperature dependence. Unless one assumes that the mixture of complexes is an ideal solution, the activity coefficients of the species must be also estimated. Although this implies that chemical theories have little predictive value, they have been used to correlate thermodynamic data for highly nonideal solutions.

Several theories emerged with a firm base on statistical mechanics, like lattice theories, and those developed from the ideas of Andersen and Wertheim. Lattice theories assume that the fluid structure can be approximated by a solid-like lattice structure. These theories are successful when the structure is well defined, such as in gas hydrates, otherwise they have not been in good agreement with molecular simulation results for associating fluids. The representation of the structure of a liquid by a lattice is undoubtedly an oversimplification, and this limits their applicability to the basic qualitative features of associating fluid systems. The quasichemical approximation due to Guggenheim [25] and several excess Gibbs energy models [26, 27] are based on lattice theories, and have been applied to a broad variety of liquid mixtures.

Andersen [28, 29] was one of the first to introduce the geometry of the interaction at an early stage of the theory for the description of highly directional hydrogen-bonding fluids. Andersen developed the ideas of physical clusters and proposed a cluster expansion in terms of the total number density. Although the nature of the association attractive sites of his model restricts the system to single bonds at each site thus, in principle, making the theory simpler, graph cancellation due to steric effects is cumbersome and inefficient. Nevertheless, his works influenced later theories for associating fluids. Other authors introduced the possibility of molecular association into commonly used integral equation theories [30, 31]. For a review of the various approaches, see [32]. The rest of the section will be devoted to Wertheim's approach because of its simplicity in form and accuracy in comparison with molecular simulations.

Wertheim, following the ideas of Andersen, developed a theory [12, 13] based on a resumed cluster expansion in terms of both the total number density and the monomer density. In this way the correct low-density limit for the second virial coefficient is guaranteed. Wertheim also simplified the complex graphical expansions by assuming steric effects due to the repulsive core of each molecule that restrict the formation to a single bond at each attractive site. The result of Wertheim's development is a final expression written in the form of a first-order thermodynamic perturbation theory (TPT1), which relates the change in residual Helmholtz free energy due to

association to the monomer density. Wertheim first presented his development for pure hard-core molecules with one attractive site, but he subsequently extended the theory to systems with multiple bonding sites per molecule [14, 15]. Chapman *et al.* later generalized Wertheim's theory to binary mixtures of components A and B in which only AB dimers can form [33, 34].

Wertheim's theory assumes that the potential has a short-range highly directional component that causes the formation of associated species (e.g. dimers, trimers, tetramers, etc.), but does not presuppose a particular intermolecular potential, which has to be specified to implement the theory. Jackson *et al.* used Wertheim's theory to study the effect of molecular associations on the phase coexistence properties of hard-sphere molecules with one or two bonding sites [35], showing excellent agreement with Monte Carlo simulations. The hard-sphere model as a reference fluid is the easiest to use because its equation of state (EOS) and pair distribution function are known, and accurate analytical expressions are available. In 1987, Wertheim [36] and Chapman *et al.* [37], independently, found that, in the limit of infinite association, the system of associating species could become a polymer. In this sense, Chapman *et al.* [37] obtained an EOS for hard-sphere chains from Wertheim's theory, by imposing the condition of total bonding and the correct stoichiometry of segments with bonding sites. This means that to form a chain from m segments of the same diameter d, a stoichiometric ratio of m segments with either one or two association sites is required, and the condition of zero nonbonded segments is imposed. They also separated the effects of molecular association and chain size on the coexistence properties. Later Chapman used the Lennard-Jones (LJ) potential as reference and compared results from the theory to Monte Carlo simulations, obtaining an excellent agreement [38].

The derivation of Wertheim's TPT1 involves some approximations, which lead to the relatively simple expressions shown below in this chapter and must be taken into account when using the theory. Firstly, the graphs corresponding to the formation of ring-like bonding structures were neglected in the theory, and only tree-like structures were included. Secondly, as previously mentioned, only a single bond is allowed at each association site. Furthermore, the activity of a site is independent of bonding at other sites in the same molecule, i.e., sites on a given molecule are independent of each other. Therefore, terms involving the repulsions between two molecules which are attempting to bond to two different sites on a third molecule were also neglected in TPT1. As a direct result, the theory is incapable of describing the effects of steric hindrance when two bonding sites are set so close together that both sites cannot bond simultaneously.

Three steric hindrance approximations follow from the restriction of single bonding at a specific attractive site. First, the repulsive cores of two bonded molecules prevent a third molecule to come close enough to bond to any of the occupied sites. Second,
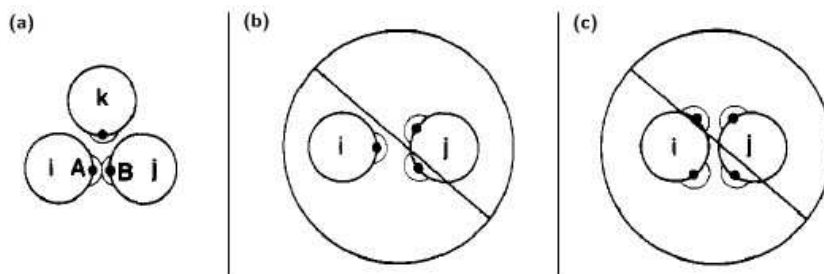
Figure 2.1: Approximations in first-order Wertheim's theory due to steric incompatibility. (a) The repulsive cores of the molecules i and j prevent molecule k from bonding at site A or B. (b) No site on molecule i can bond simultaneously to two sites on molecule j. (c) Double bonding between molecules is not allowed. Figure taken from [9].

no site on a molecule can bond simultaneously two sites on another molecule. Lastly, no double bonding between two molecules is allowed. Figure 2.1 schematically depicts these approximations.

In the first-order theory of Wertheim, the angle between bonding sites is not defined. Only the distance from the centre of the repulsive core and the short-range interaction potential of the bonding site must be specified. This means that the properties of the fluid will be independent of the angle between sites. Hence, the theory should be most accurate when the angle between the centre of the core and any two bonding sites on the molecule is close to π. Cases in which bonding at one site is dependent of bonding at other sites on the same molecule can be accounted for with the extension of Wertheim's theory to second order. Nevertheless, except for special cases [39], it is not of practical use due to the more structural information required, which is not always available.

2.2 SAFT equation of state

As mentioned in the last section, Wertheim provided a relationship between the residual Helmholtz free energy due to association and the monomer density by means of expanding the Helmholtz energy in a series of integrals of molecular distribution functions and the association potential. Wertheim showed that a simple expression can be obtained when many integrals in the series are set to zero on the basis of the physical arguments explained above in the last section.

Wertheim's theory was extended to mixtures of spheres and chains of spheres and

tested against Monte Carlo simulations [32–35, 37, 40]. In 1989, Chapman, Gubbins, Jackson and Radosz presented an equation of state model of associating fluids [8, 9] based on the first-order theory of Wertheim. The essence of their approach is the use of Wertheim's theory to describe a reference fluid which includes both the molecular shape and molecular association, instead of the much simpler hard-sphere model employed in most engineering equations of state. The effect of weaker intermolecular forces, like dispersion and induction, were included through a mean-field perturbation term. They called this approach the Statistical Associating Fluid Theory (SAFT). Later on, Huang and Radosz applied the SAFT equation to many real pure fluids and mixtures [10, 11]. There are small differences between the SAFT model presented by Chapman and co-workers and that presented by Huang and Radosz, which affect the expressions corresponding to dispersion forces and the association strength. Several versions of the SAFT equation have arisen in the following years [20] and it is still being improved in a systematic way due to its formulation, which is general, in the sense that only basic, physically sound assumptions were made. Comparison with computer simulations and experimental data have greatly helped in the improvement and test of its applicability, which has been shown to be very broad [16, 20].

The general expression of the SAFT EOS is given in terms of the residual Helmholtz free energy per mole (with respect to an ideal gas at the same temperature and density), denoted by A, as a sum of contributions due to the interaction among segments, the formation of chains from identical segments, and the formation of association bonds between two segments (or chains),

$$
\begin{aligned}
A^{res} = A - A^{ideal} \quad = \quad & A^{\text{seg}}(m\rho, T; \sigma, \epsilon) + A^{\text{chain}}(\rho, T, x_i; \sigma_i, \epsilon_i, m_i) \\
& + A^{\text{assoc}}(\rho, T, x_i; \sigma_i, \epsilon_i, \varepsilon^{\alpha_i \beta_j}, k^{\alpha_i \beta_j}) + ... ,
\end{aligned} \qquad (2.1)
$$

where ρ is the (chain) molecular density, T the absolute temperature, and x_i the composition of species i in the mixture. Molecular parameters are m, the number of spherical segments forming a chain molecule, and the diameter σ and dispersive energy ϵ of the segments. The strength of the association bond between site α on specie i and site β on specie j depends on the energy $\varepsilon^{\alpha_i \beta_j}$ and volume of association $k^{\alpha_i \beta_j}$. Note that the segment term is a function of the total number density of segments present in the system, while the chain and association contributions depend on the number density of chains. The dots indicate that other terms can be added in a perturbation manner, such as multipolar contributions.

2.2.1 Segment term

A^{seg} is defined as the residual Helmholtz free energy of nonassociated spherical segments, and it is not specified within SAFT. Both Chapman *et al.* [8, 9] and Huang

and Radosz [10, 11] versions of the SAFT equation, hereafter indistinctly referred to as the original SAFT EOS, use a perturbation expansion with a hard-sphere fluid as a reference and a dispersion term as a perturbation. The hard-sphere Helmholtz free energy is calculated through the expression of Carnahan and Starling and the dispersion term through correlations of molecular simulation data for the LJ fluid, which are functions of the reduced temperature and density. The reader is referred to the source articles for details. Other intermolecular potentials, such as the square-well [41–43] and the Yukawa potential [44], have been used as the model for the segment interactions. Jackson *et al.* proposed a generalized potential function with an attractive part of variable range in the so-called SAFT-VR approach [17]. The availability of an analytical EOS for the LJ fluid [45, 46] led to other versions of the SAFT equation [47, 48], like the soft-SAFT EOS, described below in the next section.

As already introduced, a nonassociating pure fluid requires three parameters in SAFT, namely m, σ and ϵ. In order to model mixtures, which may consist of chains with different number of segments, which in turn can be of different size and/or dispersive energy, one must make use of averaged parameters that simulate an "averaged" fluid which has the same thermodynamic properties as the mixture. This is done by means of mixing rules. Several options exist [49] but the van der Waals' one fluid theory turns out to be the most used. It is a well-established conformal solution theory that defines parameters of a hypothetical pure fluid having the same residual properties as the mixture of interest. Van der Waals' mixing rules are in good agreement with molecular simulation data for spheres of similar size [50]. The corresponding expressions for the size and energy parameters of the conformal fluid are:

$$\sigma^3 = \frac{\sum_i \sum_j x_i x_j m_i m_j \sigma_{ij}^3}{\left(\sum_i x_i m_i\right)^2},$$ (2.2)

$$\epsilon \sigma^3 = \frac{\sum_i \sum_j x_i x_j m_i m_j \epsilon_{ij} \sigma_{ij}^3}{\left(\sum_i x_i m_i\right)^2}.$$ (2.3)

The effective chain length of the conformal fluid is given by

$$m = \sum_i x_i m_i,$$ (2.4)

which agrees with the principle of congruence.

The expressions 2.2-2.4 involve the mole fraction x_i and the chain length m_i of each of the components of the mixture of chains, denoted by the indices i and j, and

the unlike ($j \neq i$) interaction parameters σ_{ij} and ϵ_{ij}, which are determined by means of combination rules, those from Lorentz-Berthelot being the most employed. The generalized Lorentz-Berthelot combining rules read

$$\sigma_{ij} = \eta_{ij} \frac{\sigma_{ii} + \sigma_{jj}}{2}, \tag{2.5}$$

$$\epsilon_{ij} = \xi_{ij} \sqrt{\epsilon_{ii} \epsilon_{ij}}, \tag{2.6}$$

where the factors η_{ij} and ξ_{ij} modify the arithmetic and geometric averages, respectively, between components i and j. Both parameters are usually set to 1 for mixtures of segments of similar size and energy. In this case, eqs 2.5 and 2.6 reduce to the simple Lorentz-Berthelot rules. Further information about the appropriateness of several combination rules can be found in reference [51]

2.2.2 Chain term

As mentioned, the SAFT approach accounts for chain length by taking the limit of complete bonding in Wertheim's TPT1 [36, 37, 40]. The Helmholtz free energy due to the formation of chains from m_i spherical monomers is

$$A^{\text{chain}} = RT \sum_i x_i \left(1 - m_i\right) \ln g_{\text{R}}(\sigma), \tag{2.7}$$

where $R = k_{\text{B}} N_{\text{A}}$ is the ideal gas constant, being k_B the Boltzmann constant and N_{A} the Avogadro's number. The pair correlation function g_{R} of the reference fluid for the interaction of two segments in a mixture of segments, evaluated at the segment contact σ, provides structural information to the theory at the first-order level. At this point, it is convenient to stress that, at the first level of approximation, thermodynamic properties do not depend on the angles between the vectors from the centre of the segment to the various attractive sites. Hence, when the bonding site angles are small enough for the segment cores to prevent simultaneous bonding at the sites, the theory fails. Consequently, the steric self-hindrances of the chain structures are neglected. Furthermore, this means that the first-order theory implies conformality between branched and linear isomers of the same number of segments. For instance, the theory assumes that a n-alkane has the same reduced EOS as a *neo*-alkane. One can overcome this situation by using the second-order level of the theory, which accounts for the simultaneous bonding of three molecules [36, 39]. However, each level of approximation requires the corresponding structural information for the fluid. Hence, a three-body correlation function, which additionally depends on the bond angles, is needed in a second-order perturbation theory. A nth-order perturbation theory, where $n = m - 1$, would describe each of the bond angles in the chain of m-mers, but would require knowledge of the m-body correlation function of the reference

fluid. At present, the knowledge of high-order correlation functions is limited, hence they are usually approximated by a closure involving just pair correlation functions. Müller and Gubbins [52] suggested that, for hard-sphere chain fluids, the additional effort of applying the second-order perturbation theory may not be justified unless the chains have rigid bond angles less than 110°.

Another important consequence of Wertheim's first-order approach is that it does not contain information about the chain conformation or the attractive chain self-interaction beyond the formation of bonds, thus predicting a zero configurational energy at the zero-density limit. Computer simulation results from Johnson *et al.* [53] have shown that, at sufficiently low densities, the contribution to the internal energy of the chains is mainly due to the intramolecular interactions. Hence, at low densities, the SAFT theory predicts an appreciably higher energy than that observed from simulations, because of the coiling up of the chains. This weakness of the theory does not arise at high and moderate densities, at which the internal energy is accurately predicted by the theory, because chain-chain interpenetrations become more important and intramolecular interactions less significant.

Wertheim's theory does not require a reference fluid with a spherically symmetric intermolecular potential. In eq 2.7 it was assumed that the reference fluid is a spherical segment with a diameter σ equal to the distance at which the intermolecular potential vanishes. Moreover, the bond length is restricted to be equal to σ, thus the chain model corresponds to a fluid of tangent spheres. It is known that predictions from TPT are improved when additional information is added into the reference fluid. For that reason, in a similar way as done in generalized Flory theories [54], both Chang and Sandler [55] and Ghonasgi and Chapman [56] independently derived a dimer reference TPT1 for hard chains. The Helmholtz free energy due to the formation of chains from m_i dimers is

$$A^{\text{chain}} = RT \sum_i x_i \left[\frac{-m_i}{2} \ln g_{\text{R}}(\sigma) + \left(1 - \frac{m_i}{2}\right) \ln g_{\text{R}}^{\text{D}}(\sigma) \right] \text{ for } m_i \geq 2, \qquad (2.8)$$

where g_{R}^{D} is the pair correlation function of the reference fluid of dimers and g_{R}, as defined in eq 2.7, the pair correlation function of the monomer reference fluid. Obviously, for chains with less than two monomers, i.e., $m_i < 2$, a dimer reference fluid does not hold.

2.2.3   Association term

Associating fluids are able to form clusters of associated molecules. Therefore, the SAFT model for associating fluids not only accounts for monomers, but also for associated clusters. Within SAFT, the mole fraction of (in general, chain) molecules

of specie i that are not bonded at site α (obviously on the same specie) is denoted by X_i^α. Consequently, the mole fraction of molecules of specie i bonded at site α is $1 - X_i^\alpha$. The mole fraction of nonassociated molecules (the fraction of monomers) of specie i is given by $\prod_\alpha X_i^\alpha$. The fraction of clusters of a given size can be estimated by using general statistical arguments [57]. As an example, in a pure fluid with two identical bonding sites, A and B, in which only AB bonding is allowed, only chain and ring-shaped aggregates can be formed. Because in this example the sites are identical, i.e., have the same intermolecular potential function and parameters, $X^A = X^B = X$. For the use of simple statistics, it is necessary to assume the number of ring-shaped clusters to be negligible. Since TPT1 assumes that the activity of a site is independent of bonding at other sites on the same molecule, the fraction of molecules in the system that are present as dimers can be estimated considering the probability of seeing two free sites and one association bond, which is given by $X^2(1 - X)$. In general, the fraction of molecules present as a cluster of size N is estimated to be

$$X(N-\text{mer}) = NX^2\left(1 - X\right)^{N-1},\tag{2.9}$$

and the cluster average size is given by

$$\bar{N} = \frac{1}{X}.\tag{2.10}$$

Eq 2.9 is the "most probable distribution" of Flory [57], that is in agreement with experimental results for polymer polydispersity.

The Helmholtz energy change due to association is calculated from [12–15, 37]

$$A^{\text{assoc}} = RT \sum_i x_i \sum_\alpha \left(\ln X_i^\alpha - \frac{X_i^\alpha}{2}\right) + \frac{M_i}{2},\tag{2.11}$$

where M_i is the number of association sites on each molecule of specie i and $\sum_\alpha$ represents a sum over all association sites (on molecules of specie i). From the solution of mass balances, the mole fractions

$$X_i^\alpha = \frac{1}{1 + N_A \rho \sum_j x_j \sum_\beta X_j^\beta \Delta^{\alpha_i \beta_j}}\tag{2.12}$$

are obtained, which involve a summation over all sites on all the species, thus taking into account self-association and cross-association among species. $\Delta^{\alpha_i \beta_j}$ is the association strength between site α on molecule i and site β on molecule j, and it is defined as

$$\Delta^{\alpha_i \beta_j} = \int g_R^{ij}(12) f^{\alpha_i \beta_j}(12) d(12),\tag{2.13}$$

where $g_{\mathrm{R}}^{ij}(12)$ is the reference fluid pair correlation function, f is the Mayer function of the association potential, $f^{\alpha_i\beta_j}(12) = \exp\left(-\phi^{\alpha_i\beta_j}(12)/k_{\mathrm{B}}T\right) - 1$, and $d(12)$ denotes an unweighed average over all orientations and an integration over all separations of molecules 1 and 2. The correlation function $g_{\mathrm{R}}^{ij}(r)$ of two of the segments of a chain reference fluid is not readily available. As it has already been said, Wertheim's TPT1 approach does not specify the angle between association sites on a given molecule, neither where on the chains the sites are placed. Therefore, in principle, for chains formed by more than 2 cores, there will be various choices for $g_{\mathrm{R}}^{ij}(r)$, depending on the location (end, middle of the chain, etc.) of the segments. The usual approximation [37] is to employ the pair correlation function of nonbonded spheres g_{R} at the same temperature, and density equal to $m\rho$. That is, the segment pair correlation function is assumed to be equivalent to that of the segment as part of a chain. This is a reasonable approximation if the bonding site is located diametrically opposed to the backbone of the chain [58].

The square-well potential

$$\phi^{\alpha_i\beta_j} = \left\{ \begin{array}{ll} -\varepsilon^{\alpha_i\beta_j} & \text{if } r^{\alpha_i\beta_j} < \sigma_{\mathrm{a}} \\ 0 & \text{if } r^{\alpha_i\beta_j} \geq \sigma_{\mathrm{a}} \end{array} \right. \tag{2.14}$$

is very convenient to represent the hydrogen bonding potential of real molecules and provides certain mathematical simplifications over other existing models, such as the somewhat more realistic fractional point charge model [59]. In eq 2.14, $r^{\alpha_i\beta_j}$ is the centre to centre distance between the association sites and σ_{a} the diameter of the association site.

The geometry of the association sites is chosen to be spherical for simplicity and it is believed to be more realistic than others also employed [59]. For a reference fluid of hard-spheres, such as that of the original SAFT EOS, the association sites are placed with its centre lying on the surface of the reference spherical core. The evaluation of the integral in eq 2.13 is not straightforward and no accurate analytical expression for it is available. However, a reasonable approximation is to consider that $r^2 g_{\mathrm{HS}}(12)$ is constant and equal to the value at contact $\sigma^2 g_{\mathrm{HS}}(\sigma)$ [35]. With this approximation, $\Delta^{\alpha_i\beta_j}$ becomes

$$\Delta^{\alpha_i\beta_j} = 4\pi g(\sigma)_{\mathrm{HS}} F^{\alpha_i\beta_j} k^{\alpha_i\beta_j}, \tag{2.15}$$

where $F^{\alpha_i\beta_j} = \exp\left(\varepsilon^{\alpha_i\beta_j}/k_{\mathrm{B}}T\right) - 1$.

When a soft reference fluid is used, association sites can be embedded in the reference core, tangent to the surface. Figure 2.2 depicts two association sites placed at a distance b from the centre of a reference fluid core (which can be polyatomic). This placement forces two bonded molecules to have some degree of overlap, as should be expected for real associating fluids. With this geometry and bonding potential, eq
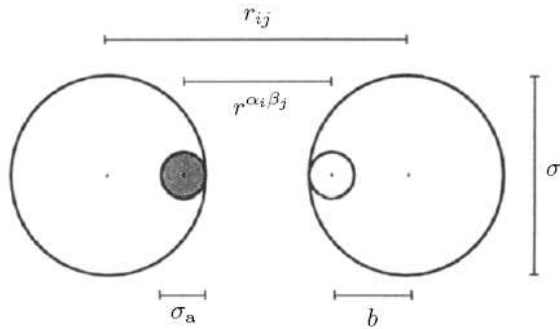
Figure 2.2: Two dimensional view of the association geometries. The large circles represent the cores of the reference fluid and the small ones the off-centre association sites. Figure taken from [47]

2.13 can be simplified to [59, 60]

$$\Delta^{\alpha_i \beta_j} = 4\pi F^{\alpha_i \beta_j} k^{\alpha_i \beta_j} I^{ij}, \qquad (2.16)$$

where I is a dimensionless integral defined as

$$I^{ij} = \frac{1}{24b^2\sigma^3} \int_{2b-\sigma_a}^{2b+\sigma_a} g_R(r) \left(\sigma_a + 2b - r\right)^2 \left(2\sigma_a - 2b + r\right) r \, dr. \qquad (2.17)$$

In contrast with the previous case, the integral in eq 2.17 can be evaluated numerically for a given reference fluid and specific geometry, using accurate values for g_R obtained from molecular simulations, and the results can be fitted to an empirical analytical expression as a function of the reduced temperature and density [47].

It has to be mentioned that results from Wertheim's theory are fairly sensitive [61] to approximations used to estimate g_R, the pair correlation function of the reference fluid. In particular, the Weeks-Chandler-Andersen approximation for g_{LJ} [62] and the low-density correction for it cause significant deviations between simulation and theory for the coexistence properties of a LJ fluid with an association site.

2.3 Soft-SAFT equation of state

A SAFT equation based on a reference LJ potential was presented in 1997 by Blas and Vega [19]. The use of a soft potential as opposed to a hard (repulsive) potential as a reference simplifies the overall perturbation approach, since both the repulsive and dispersive contributions are taken into account simultaneously. They tested the accuracy of the so-called soft-SAFT EOS versus Monte Carlo simulations for homonuclear

and heteronuclear associating and nonassociating LJ mixtures of chain molecules. Vapour-liquid phase equilibrium (VLE) and supercritical conditions were studied as a function of chain length and interaction parameters. The agreement between theory and simulation was shown to be excellent except at low densities, where the theory predicts a significantly higher internal energy. As explained in the above section, this comes from the fact that Wertheim's TPT1 accounts for the energetic contribution due to the formation of bonds but does not contain information about chain conformations. In other words, any SAFT model which is based only on TPT1 considers chains as formed by freely-jointed segments, hence the angle between consecutive bonds is not defined.

The soft-SAFT EOS is a modification of the original SAFT equation, also based on Wertheims TPT1. The main differences between the original SAFT and the soft-SAFT equations are that (a) the latter uses the LJ potential for the reference fluid, hence accounting in a single term for dispersive and repulsive forces, while the original equation employs a perturbation scheme based on a hard-sphere fluid (reference) + dispersion contribution (perturbation term), and (b) the original SAFT uses the radial distribution function (or pair correlation function) of hard spheres in the chain and association terms, while in soft-SAFT both terms depend on the radial distribution function of a LJ fluid of nonbonded spheres. The specific intermolecular potential chosen will certainly influence thermodynamic properties computed through the theory. It is therefore expected that the more realistic LJ potential (as opposed to a hard potential) provides a better description of the output properties. The modified version of SAFT proposed by Ghonasgi and Chapman [63] and the EOS for LJ chains of Johnson *et al.* [53] also use a LJ potential and radial distribution function. Additionally, the LJ-SAFT equation of Kraska and Gubbins [64,65] considers dipole-dipole interactions.

As already commented, in contrast to the hard-sphere potential, the use of a soft potential allows the association sites to be fully embedded inside the reference core. This allows some overlapping between the segments that contain the two association sites involved in a bond, which is a more realistic situation. According to this, the soft-SAFT model places association sites tangent to the reference core, as defined by the parameters $b = 0.4\sigma$ and $\sigma_{\mathrm{a}} = 0.2\sigma$ (see Figure 2.2). This geometry has been previously used [47,59,60]. The integral in which the radial distribution function of the LJ fluid is involved, see eq 2.17, is computed in soft-SAFT making use of the analytical expression provided by Müller and Gubbins [47].

Empirical analytical equations with parameters fitted to molecular simulation data are also available for the radial distribution function of the LJ fluid evaluated at the bonding distance, as a function of the reduced temperature and density. They are explicitly needed in the chain term (see eqs 2.7-2.8). The expressions fitted by Johnson

et al. [53] and Johnson [66] for a LJ fluid of monomers and dimers, respectively, are employed.

The LJ segment term of the soft-SAFT EOS corresponds to the residual Helmholtz free energy of a LJ fluid of spheres. Two very accurate EOS for the LJ fluid are available in the literature, namely the Benedict-Webb-Rubin EOS from Johnson *et al.* [45] and the EOS based on a perturbed virial expansion with a reference hard-sphere term from Kolafa and Nezbeda [46]. Both equations have 32 parameters that have been fitted to extensive computer simulation data for the LJ fluid. Although the latter is theoretically more robust, the former is slightly more accurate, as will be shown in Figure 4.14.

Since the basic SAFT equations have been presented in the previous section, the mathematical formulation of the soft-SAFT EOS is omitted here for brevity. Nonetheless, the complete set of expressions needed to implement the equation are given in Appendix A. In subsequent chapters the features of the soft-SAFT model are emphasized when necessary.

2.3.1   Computer code

As part of the present thesis work, the soft-SAFT EOS has been implemented into a computer code. The first function of it was the prediction of VLE properties for pure chain molecules and their mixtures. However, there was a need for much more. For instance, when applying the theory to real systems, molecular parameters have to be fitted using experimental data. Hence the soft-SAFT computer program also does this task. In addition, the Cahn and Hilliard density gradient theory has also been implemented in the same code. To be concise, a list of the current features of the computer program is next:

- Applicability to pure systems and binary mixtures of associating and nonassociating molecules

    - Fluid phase equilibria (two and three coexisting phases) and single phase properties (subcritical or supercritical)

    - Critical properties

    - Interfacial properties of planar interfaces

- Models available

    - Reference fluid of LJ monomers and dimers with van der Waals one-fluid mixing rules and generalized Lorentz-Berthelot combining rules

- Several self-association and cross-association models with up to 4 association sites

- Additional features

  - Parameters optimization to the given experimental data and calculation of deviations

  - Generation of isotherms, isobars and isopleths for equilibrium calculations in binary mixtures

  - Automatic search for appropriate initial values (guesses) for the determination of coexistence densities

Some of the characteristics mentioned above had already been implemented into various old codes, each one having its own applicability. For practical purposes, a single soft-SAFT computer code has been started from scratch in this thesis work. The program is written in *Fortran 77* in a modular manner and it is friendly for the user. It has a single, easy-to-use input file, and a number of output files depending on the type of calculation performed. The use of the program for thermodynamic property calculations and parameter optimization is not restricted to soft-SAFT. Any other EOS can be implemented into the program as a subroutine.

As an example of output data from the soft-SAFT program, Figures 2.3-2.5 show reduced values of thermodynamic properties for the LJ spherical fluid, including both single phase and equilibrium curves. Note that the SAFT approach is not used in this case, because no chain and association contributions apply. For the obtaining of these plots, the soft-SAFT code only used the reference equation of Johnson *et al.* [45].

For phase-equilibria calculations, the commonly used fugacity method is employed [67]. That is, chemical, thermal and mechanical stability are satisfied by imposing the equality of chemical potentials of each component in the coexisting phases at fixed temperature and pressure. Because SAFT is formulated as an explicit function of temperature, density and phase compositions (see eq 2.1), the fugacity method is applied by equating chemical potentials and the pressure at a fixed temperature. The density and compositions of the coexisting phases remain as unknowns. This method is not completely reliable because it is initialization-dependent, and may converge to a point that is a local but not a global minimum, thus leading, in some cases, to nonphysical or trivial solutions (identical phases). This is due to the fact that the equality of chemical potentials is a necessary but not a sufficient condition for the minimization of the total Gibbs energy of the entire system. The total Gibbs energy should be minimum globally, which means that for a given temperature and pressure, a global minimum of the Gibbs energy function describes the true equilibrium phase compositions. Nevertheless, when the number of phases is specified a
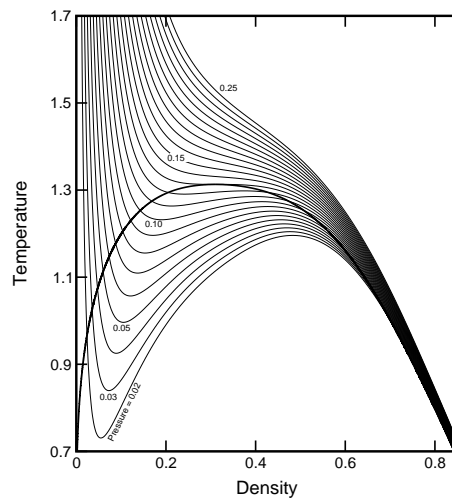
Figure 2.3: Temperature-density plot for the LJ fluid
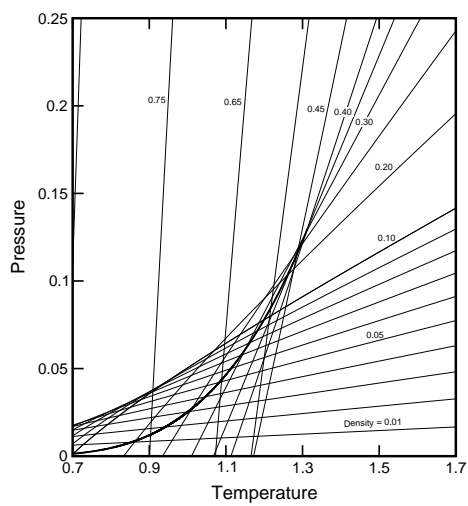
Figure 2.4: Pressure-temperature plot for the LJ fluid
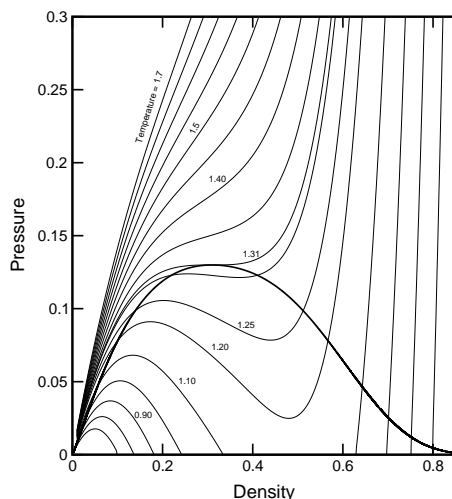
Figure 2.5: Pressure-density plot for the LJ fluid

priori, as required by the soft-SAFT program, the criteria of any trained user are good enough to overcome these inconveniences. It has also to be mentioned that a new methodology based on an interval Newton/generalized bisection algorithm has been published recently [68], which is a completely reliable technique for the computation of phase stability and equilibrium properties. The authors demonstrate that efforts toward the implementation of this new method in SAFT are worthwhile.

Critical properties of pure systems and mixtures are obtained by numerically solving the necessary conditions [69], which involve second and third derivatives of the Helmholtz free energy with respect to the molar volume (pure systems) or the composition (in mixtures). Derivatives are approximated by finite differences with fourth order error.

For the solution of the system of nonlinear algebraic equations that arise from the fugacity method, a modification of the Powell's hybrid method [70] is used. When optimizing parameters, because there are more restrictions than unknowns, one has to face a nonlinear optimization problem. It is solved in soft-SAFT by a Levenberg-Marquardt nonlinear least squares algorithm [71], which is one of the most widely employed nonlinear curve fitting methods. Both solvers are used as linked subroutines, which come in the minpack library of Fortran routines [72].

Chapter 3

Density gradient theory (DGT)

An overview of the density gradient theory is presented, together with the necessary set of equations needed to relate it to an equation of state model. In particular, the expressions for the determination of interfacial tensions and density profiles in planar interfaces between fluids are provided.

3.1   Fundamentals

The Cahn and Hilliard density gradient theory of inhomogeneous systems provides a means for relating an equation of state to interfacial properties of a classical fluid system. Cahn and Hilliard [73] rediscovered in 1958 the van der Waals' gradient theory [74, 75] of 1894, which leads to a general expression for the Helmholtz energy density of an inhomogeneous system. Carey *et al.* [76–78] made this theory easy to use for predictions of interfacial tensions.

The van der Waals' gradient theory [74, 75] gives a density functional for the local Helmholtz free energy density of a fluid system, which consists of a 'homogeneous' term and a 'nonhomogeneous' term. The former is represented by the Helmholtz free energy density of a homogeneous fluid, evaluated at a local density in between the bulk densities, while the latter is proportional to the square of the molar density gradient. Cahn and Hilliard, in their derivation, assumed that the Helmholtz free energy density $\tilde{a}$ of the inhomogeneous fluid is a function of the mole density and its derivatives with respect to the space coordinates. It was also assumed that the density gradient is small compared to the reciprocal value of the intermolecular distance, thus allowing

to treat the density and its derivatives as independent variables. They expanded $\tilde{a}$ in a Taylor series about $\tilde{a}_0(\tilde{\rho})$, the Helmholtz free energy density of the homogeneous fluid at the local density $\tilde{\rho}$, and truncated after the second order term. This series may not converge but, because of the short range of the intermolecular potential, it is assumed to have at least an asymptotic validity [79]. In the absence of an external potential, the expression for the Helmholtz free energy of the system $\tilde{A}$ reads*

$$\tilde{A} = \int \left[\tilde{a}_0(\tilde{\rho}) + \sum_i \sum_j \frac{1}{2} \tilde{c}_{ij} \nabla \tilde{\rho}_i \cdot \nabla \tilde{\rho}_j \right] d^3 \tilde{r}, \qquad (3.1)$$

where the integration is performed in the entire system volume and ρ_i is the molar density of component i. The parameter $\tilde{c}$ for the components i and j is defined below.

An attractive feature of the density gradient theory is that it does not prescribe from what theory an expression should be obtained to define the 'homogeneous' term in the free energy density. For instance, this might be from an expression based on statistical mechanics, but also from semi-empirical equations of state without a strong molecular basis. Definition of this 'homogeneous' free energy density leads to a unique definition of the Helmholtz free energy of the inhomogeneous system. The only quantity required then is an expression for the coefficient of proportionality that goes before the square gradient, the so-called influence parameter c_{ij}, in terms of density and/or temperature. The influence parameter was originally related to the mean square range of the direct correlation function $C_{ij,0}$ of a homogeneous fluid,

$$\tilde{c}_{ij} = \frac{\tilde{T}}{6} \int \tilde{r}^2 C_{ij,0}(\tilde{r}, \tilde{\rho}) d^3 \tilde{r}. \qquad (3.2)$$

Details on the derivation of this expression are given elsewhere [80–82]. Because no direct correlation functions are available for most systems of practical interest, several estimations have been used [83]. For instance, Carey *et al.* [77,78] connected this parameter to those from the Peng-Robinson EOS, arguing that the ratio $c/ab^{2/3}$ for real nonpolar fluids might be a slowly varying function of temperature and density. Other authors [84,85] neglect the dependence on thermodynamic properties and treat c as a constant parameter.

The density gradient theory makes use of the second law of thermodynamics, which states that the internal state of a closed, isothermal system minimizes the Helmholtz free energy at equilibrium. By minimization of the total free energy of the

---

*Variables with a tilde on it are reduced. All the equations in this chapter are presented in a dimensionless form for coherence and easy relation with the soft-SAFT EOS expressions given in Appendix A.

system, density profiles are obtained. Davis and Scriven [86] proved that the chemical potential of a species remains constant across the interface. From the application of these statements to eq 3.1, the following Euler-Lagrange equations result:

$$\sum_j \nabla \cdot (\tilde{c}_{ij} \nabla \tilde{\rho}_j) - \frac{1}{2} \sum_k \sum_j \frac{\partial \tilde{c}_{kj}}{\partial \tilde{\rho}_i} \nabla \tilde{\rho}_k \cdot \nabla \tilde{\rho}_j = \frac{\partial (\tilde{a}_0(\tilde{\rho}) - \sum_i \tilde{\rho}_i \tilde{\mu}_{0i})}{\partial \tilde{\rho}_i} \qquad (3.3)$$

$$i, j, k = 1, ..., N$$

Eq 3.2 is mathematically a nonlinear boundary value problem. For details of the various numerical approaches to solve this equation, one is referred to the works by Davis *et al.* [86] and the Ph. D. thesis of Cornelisse [87]. The existence of a fluid microstructure (e.g., planar interface, spherical drop, thin film, periodic structure) is governed by the right hand side of eq 3.3 and c_{ij}, which was named influence parameter because it affects the stability and characteristic length scales of these microstructures.

3.2 Interfacial tension and density profiles

The interfacial tension is a macroscopical consequence of the density profile. Considering a planar interface and assuming that the density dependence of the influence parameter can be neglected, an expression that relates the interfacial tension to the square of the density gradients can be derived from eq 3.1 [78, 86],

$$\tilde{\gamma} = \sum_i \sum_j \int_{-\infty}^{\infty} \tilde{c}_{ij} \frac{d\tilde{\rho}_i}{d\tilde{z}} \frac{d\tilde{\rho}_j}{d\tilde{z}} d\tilde{z} = 2 \int_{-\infty}^{\infty} \left[\tilde{a}_0(\tilde{\rho}) - \sum_i \tilde{\rho}_i \tilde{\mu}_{0i} - \tilde{p}_0 \right] d\tilde{z}, \qquad (3.4)$$

where μ_{0i} and p_0 are the equilibrium chemical potential and pressure, respectively, and z is the direction perpendicular to the interface. The approximation $\partial \tilde{c}_{ij}/\partial \tilde{\rho} = 0$ is supported by the works of McCoy and Davis [88] and those of Carey *et al.* [77, 78].

Eq 3.4 would be of more practical use if it were expressed in terms of density space. Poser and Sanchez [89] employed a transformation from location space to density space, the integration of which provides a way to calculate density profiles:

$$\tilde{z} = \tilde{z}_0 + \int_{\tilde{\rho}_2(\tilde{z}_0)}^{\tilde{\rho}_2(\tilde{z})} \sqrt{\frac{\tilde{c}'}{\Delta \tilde{\Omega}(\tilde{\rho}_1, \tilde{\rho}_2)}} d\tilde{\rho}_2. \qquad (3.5)$$

From this point, for simplicity, equations will be shown for the case of binary mixtures. The expressions for pure fluids can be straightforwardly derived. In eq 3.5, $\tilde{z}_0$ denotes an arbitrarily chosen origin, $\tilde{\Omega}(\tilde{\rho}_1, \tilde{\rho}_2) \equiv \tilde{a}_0(\tilde{\rho}) - \sum_i \tilde{\rho}_i \tilde{\mu}_i$ is the reduced grand thermodynamic potential, $\Delta \tilde{\Omega}(\tilde{\rho}_1, \tilde{\rho}_2) \equiv \tilde{a}_0(\tilde{\rho}) - \sum_i \tilde{\rho}_i \tilde{\mu}_i + \tilde{p}_0$ and $\tilde{c}'$ results

from the influence parameters of the pure components and the density profiles across the interface:

$$\tilde{c}' = \tilde{c}_2 + 2\,\tilde{c}_{12}\left(\frac{d\tilde{\rho}_1}{d\tilde{\rho}_2}\right) + \tilde{c}_1\left(\frac{d\tilde{\rho}_1}{d\tilde{\rho}_2}\right)^2. \tag{3.6}$$

The cross parameter $\tilde{c}_{12}$ was assumed to be given by the geometric mean combination rule

$$\tilde{c}_{12} = \beta\sqrt{\tilde{c}_1\tilde{c}_2}, \tag{3.7}$$

which leads to a useful simplification of eq 3.3. β is an adjustable parameter, which can be fitted to interfacial tension measurements of the mixture.

Using the above mentioned transformation, Poser and Sanchez [89] derived also an equation for the interfacial tension in binary mixtures that considers the change in the partial densities ρ_1 and ρ_2 within the interface:

$$\tilde{\gamma} = \sqrt{2}\int_{\tilde{\rho}_2^I}^{\tilde{\rho}_2^{II}}\sqrt{\tilde{c}'\Delta\tilde{\Omega}(\tilde{\rho}_1,\tilde{\rho}_2)}\,d\tilde{\rho}_2. \tag{3.8}$$

The limits of integration are the bulk densities of component 2 in the coexisting phases, indistinctly labelled by I and II.

The computation of the grand thermodynamic potential for binary mixtures can be performed, with the following expression:

$$
\begin{aligned}
\Delta\tilde{\Omega}(\tilde{\rho}_1,\tilde{\rho}_2) &= (\tilde{\rho}_1+\tilde{\rho}_2)\,\tilde{A}(\tilde{\rho}_1,\tilde{\rho}_2) - \tilde{\rho}_1\tilde{\mu}_1^I(\tilde{\rho}_1^I,\tilde{\rho}_2^I) - \tilde{\rho}_2\tilde{\mu}_2^I(\tilde{\rho}_1^I,\tilde{\rho}_2^I) + \tilde{p}_0 \\
&= \tilde{\rho}_1\left[\tilde{\mu}_1(\tilde{\rho}_1,\tilde{\rho}_2) - \tilde{\mu}_1^I(\tilde{\rho}_1^I,\tilde{\rho}_2^I)\right] \\
&\quad + \tilde{\rho}_2\left[\tilde{\mu}_2(\tilde{\rho}_1,\tilde{\rho}2) - \tilde{\mu}_2^I(\tilde{\rho}_1^I,\tilde{\rho}_2^I)\right].
\end{aligned}
\tag{3.9}
$$

For binary mixtures, it is clear from eqs 3.5-3.9 that the determination of $\Delta\tilde{\Omega}(\tilde{\rho}_1,\tilde{\rho}_2)$ and $\tilde{c}_{12}$ requires the knowledge of $\tilde{\rho}_1$ for each value of $\tilde{\rho}_2$ within the interface. This dependence conforms to the density profiles across the interface. Minimisation of the interfacial tension leads to a system of equations [89] by which the partial density profiles can be obtained:

$$\left(\frac{\partial\Delta\tilde{\Omega}(\tilde{\rho}_1,\tilde{\rho}_2)}{\partial\tilde{\rho}_1}\right) = \tilde{c}_1\left(\frac{\partial^2\tilde{\rho}_1}{\partial\tilde{z}^2}\right) + \tilde{c}_{12}\left(\frac{\partial^2\tilde{\rho}_2}{\partial\tilde{z}^2}\right) \tag{3.10}$$

$$\left(\frac{\partial\Delta\tilde{\Omega}(\tilde{\rho}_1,\tilde{\rho}_2)}{\partial\tilde{\rho}_2}\right) = \tilde{c}_{12}\left(\frac{\partial^2\tilde{\rho}_1}{\partial\tilde{z}^2}\right) + \tilde{c}_2\left(\frac{\partial^2\tilde{\rho}_2}{\partial\tilde{z}^2}\right). \tag{3.11}$$

This second-order system of partial differential equations can be numerically solved by finite-difference or finite-element methods. For a detailed discussion about the numerical solution of these coupled equations, the reader is referred to [87].

The above system of equations can be reduced to a single algebraic equation if the simple geometric mixing rule for $\tilde{c}_{12}$ (eq 3.7 with $\beta = 1$) is used:

$$\sqrt{\tilde{c}_2} \left(\frac{\partial \Delta \tilde{\Omega}(\tilde{\rho}_1, \tilde{\rho}_2)}{\partial \tilde{\rho}_1} \right) = \sqrt{\tilde{c}_1} \left(\frac{\partial \Delta \tilde{\Omega}(\tilde{\rho}_1, \tilde{\rho}_2)}{\partial \tilde{\rho}_2} \right). \tag{3.12}$$

Combining eqs 3.9 and 3.12, the simple relation

$$\sqrt{\tilde{c}_2} \left[\tilde{\mu}_1(\tilde{\rho}_1, \tilde{\rho}_2) - \tilde{\mu}_1^I(\tilde{\rho}_1^I, \tilde{\rho}_2^I) \right] = \sqrt{\tilde{c}_1} \left[\tilde{\mu}_2(\tilde{\rho}_1, \tilde{\rho}_2) - \tilde{\mu}_2^I(\tilde{\rho}_1^I, \tilde{\rho}_2^I) \right] \tag{3.13}$$

can be used to compute $\tilde{\rho}_1$ at every sampling point value of $\tilde{\rho}_2$ within the interface.

Chapter 4

Bulk properties. A soft-SAFT approach

Application of the soft-SAFT EOS model to the correlation and prediction of phase-equilibria properties is presented. The systems considered include pure and binary mixtures of chainlike molecules within the n-alkane, 1-alkanol and n-perfluoroalkane series, and light gases, such as carbon dioxide, xenon, oxygen and hydrogen. We checked the performance of soft-SAFT on the prediction of vapour-liquid equilibria and critical properties of pure n-alkanes and mixtures of short and long n-alkanes, the dependence of the critical properties of homopolymers on chain length, the solubility of gases in n-alkanes and n-perfluoroalkanes, and the modelling of carbon dioxide binary mixtures with n-alkanes and 1-alkanols. Molecular parameters were optimized carefully in order that they show meaningful trends.

4.1   VLE and critical behavior of heavy n-alkanes

[*]A new set of molecular transferable parameters for the n-alkane series is proposed. Phase-equilibria calculations of pure heavy members of the series, up to n-octatetra-contane (n-$C_{48}H_{98}$), and of ethane + n-decane and ethane + n-eicosane mixtures are performed with the soft-SAFT EOS. Using the new set of parameters, the equation is able to accurately predict the phase behavior of pure heavy n-alkanes. The dependence of the critical properties of pure n-alkanes with the carbon number is

---

*Section published as an article in *Ind. Eng. Chem. Res.* **40**, 2532 (2001).

also predicted to be in quantitative agreement with experimental data, validating, at the same time, some recent simulation results of heavy members of the series. The physical meaning and transferability of these parameters are also discussed.

4.1.1   Introduction

It is well-known that alkanes are thermally unstable above $\sim$650 K, which makes experimental determination of critical points of normal alkanes longer than n-decane extremely difficult. However, heavier n-alkanes are present in multicomponent mixtures commonly found in the petrochemical industry. Because the number of components in these mixtures can be quite large, most thermophysical predictions use correlations based on the principle of corresponding states, with parameters directly related to the critical properties of the pure components. Therefore, although the pure components may be unstable at these conditions, the critical properties of heavy hydrocarbons are needed in the design of petrochemical processes. On the other hand, it has been observed that normal alkanes show a great regularity in their behavior with respect to the carbon number. Therefore, the search of transferable parameters becomes an attractive route to obtain the thermodynamic properties of components otherwise hard to find.

Recently, there has been some progress in the estimate of critical properties of n-alkanes. Anselme and co-workers [90] were able to measure the critical properties of the n-alkane series up to n-octadecane with a novel experimental technique. An interesting conclusion of their study, contradictory to most of the available correlations at that time, is the fact that the critical density reaches a maximum when plotted versus the carbon number, and then monotonically decreases as the number of carbons in the chain increases. A few years later Siepmann et $al.$ [91,92] were able to calculate the phase envelope of long n-alkane chains, up to n-octatetracontane, from molecular simulations. They used the Gibbs ensemble technique combined with configurational bias Monte Carlo, confirming the presence of a maximum in the critical density.

A main advantage of molecular-based models, such as those used in molecular simulations, versus traditional models, is the fact that the molecular parameters are independent of the thermodynamic conditions. Hence, once the molecular model is tested against available experimental data, the same model can be used to predict, with confidence, the thermodynamic properties of the same system at other conditions. Much effort has been devoted since the work of Siepmann and co-workers [91] to develop intermolecular potential models for the phase behavior of real fluids using molecular simulations [93–99]. The procedure used in this model development is, roughly, the following: first a potential model is proposed for the interaction sites in the molecules, and then the phase envelope is calculated with an appropriate molec-

ular simulation technique. In most of the cases, the united-atom approach is used, in which molecules are separated into methyl and methylene groups, with an interaction site placed at each of the carbon centers. A more realistic all-atom representation is also possible. With an all-atom model, interaction sites are placed at each of the atom centers, including the hydrogen atoms [98]. Although feasible, this increases the number of interaction sites by approximately a factor of 3, increasing the computational demand by roughly an order of magnitude. The molecular parameters of the model are obtained by adjusting the simulation results (usually coexisting densities and the estimated critical point) to experimental data.

Among the simulation models proposed for n-alkanes with the united-atom approach, the most accurate currently available are the NERD [95,96], the TraPPE [97], and the one proposed by Errington and Panagiotopoulos [99], which we will name EP. The TraPPE and NERD models reproduce well the critical parameters and the saturated liquid densities of n-alkanes over a wide range of chain lengths, although they are less accurate for the saturated vapour densities and vapour pressures. On the other hand, the EP model is able to describe more accurately the vapour pressures and critical properties. All of these models have been used to predict, with no additional fitting, the phase diagram of binary mixtures of n-alkanes, including short and long chains, finding, in general, good agreement with experimental data. The three of them confirm the existence of the maximum in the critical density.

It is clear that having transferable molecular parameters for a series of chemical compounds is an outstanding step toward predicting with accuracy the needed properties of systems otherwise expensive or impossible to obtain. In principle, these properties could also be estimated from other modelling approaches, such as molecular-based theories or macroscopic EOSs especially developed for n-alkanes. Although there are several advantages of molecular simulations versus simple EOS, a clear disadvantage is their computational cost. Therefore, it would be desirable to have EOSs able to predict, with at least the same confidence and the same degree of accuracy, the properties obtained by molecular simulations when experimental data are not available.

Several researchers have taken this approach, attaining different degrees of accuracy depending on the approximations made in the theory. In particular, Vega and MacDowell [100] computed the VLE of n-alkanes from a simple perturbation theory. In their study, an accurate EOS for the repulsive n-alkane chain was combined with a mean-field term accounting for the contribution of attractive forces to the total free energy. Although a quantitative agreement between the model and the experimental data was not obtained, as expected, they observed that the theory was able to capture the main features of the critical properties of n-alkanes.

The phase behavior of pure alkanes and their mixtures has also been calculated using the SAFT equation. There are different versions of this equation, depending,

mainly, on the reference fluid used [101, 102]. Blas and Vega used the so-called soft-SAFT EOS [19] to calculate the phase behavior of several hydrocarbons. Comparisons with available experimental phase diagrams of pure, binary, and ternary systems of short members of the n-alkane series showed excellent agreement except near the critical region. If one is interested in the critical region, it has been demonstrated that the set of molecular parameters rescaled to the critical point gives results in quantitative agreement with experimental data [102]. As done with other versions of SAFT [103–105], they also proposed transferable molecular parameters for the n-alkane series, as a correlation with the n-alkane molecular weight.

We propose here a new set of transferable molecular parameters that provide a significant improvement, with respect to the one from Blas and Vega [101], on the predictions of the phase envelope of heavy members of the n-alkane series. A correlation for the critical properties of heavy n-alkanes is also proposed. The main goal of this study is to test the predictive capabilities of transferable molecular parameters for the n-alkane series with the soft-SAFT EOS. This test will be performed by means of (1) the prediction of phase equilibria of pure and binary systems of heavy n-alkanes and (2) the prediction of the dependence of the critical properties with the n-alkane carbon number. In particular, we present phase equilibria and critical properties of some pure heavy n-alkanes up to n-octatetracontane. In addition, calculations are performed for the mixtures ethane + n-decane and ethane + n-eicosane at different thermodynamic conditions. The accuracy of the predictions from the soft-SAFT EOS is checked versus experimental data, when available, and comparisons are made with predictions from the Peng-Robinson (PR) EOS and with recent molecular simulation data.

4.1.2   Molecular model

Following our previous work, n-alkanes are described as homonuclear chainlike molecules, modeled as m Lennard-Jones segments of equal diameter σ, and the same dispersive energy ϵ, bonded tangentially to form the chain. This is an approximation, because the actual molecules are heteronuclear due to the presence of CH_3 and CH_2 chemical groups, and it has been used previously [10, 11, 48, 64, 101–105]. When the number of carbon atoms increases, the amount of CH_2 groups versus CH_3 ones increases largely, making the approximation better.

We must emphasize that, although the molecular parameters have physical meaning (chain length, segment diameter, and dispersive energy per segment), they are effective parameters and, hence, care must be taken when using them for other applications, as will be discussed later. Although the model is simple compared to more realistic models, such as those used in recent simulations [65, 95–99], it conserves the

relevant features of the real system, and it has proven to predict with high accuracy the phase equilibria of *n*-alkane multicomponent mixtures [101] as well as the critical properties of *n*-alkane binary mixtures [102, 106].

4.1.3   Transferable parameters

According to our model, *n*-alkanes need three molecular parameters, m, σ, and ϵ, to describe all thermodynamic properties. As mentioned already, one of the most promising results of applying the soft-SAFT EOS to these systems is that, as seen with other versions of SAFT [103–105], these parameters increase linearly with the molecular weight. In a previous work, Blas and Vega [101] obtained these molecular parameters for the first eight members of the *n*-alkane series by fitting experimental saturated liquid densities and vapour pressures, and proposed a correlation of the three molecular parameters. In a similar manner, Kraska and Gubbins [48] obtained the molecular parameter values from methane to *n*-nonane by fitting the predictions of the so-called LJ-SAFT EOS to experimental data. For pure *n*-alkanes, the LJ-SAFT equation differs from the soft-SAFT EOS in the choice of the LJ reference term: while the first one uses the equation of Kolafa and Nezbeda [46], soft-SAFT uses here the one proposed by Johnson *et al.* [45], for consistency with previous works. Nevertheless, in VLE calculations, we found that both equations for the LJ fluid are equally accurate.

    A third set of transferable parameters, also from the eight first members of the series, is proposed here. It has been obtained by fitting experimental saturated densities more accurately than vapour pressures, and selecting appropriately the thermodynamic range of the experimental data, that is, excluding values in the near-critical region. This new set of parameters, given in Table 4.1, in addition to providing a significant improvement on the predictions of phase equilibria of heavy *n*-alkanes, agrees with those obtained by molecular simulation united-atom models. See the Results and discussion section for details.

    For simplicity, we will name the three sets of transferable parameters and their respective correlations after the initials of the authors in the corresponding paper. Hence, the BV correlation refers to the one proposed by Blas and Vega [101], KG parameters are those fitted by Kraska and Gubbins [48], and the new correlation proposed here is called the PV correlation, which is given by the next equations.

$$m \;\;=\;\; 0.0255M_{\mathrm{w}} + 0.628 \tag{4.1a}$$

$$m\sigma^3 \;\;=\;\; 1.73M_{\mathrm{w}} + 22.8 \tag{4.1b}$$

$$m\epsilon/k_{\mathrm{B}} \;\;=\;\; 7.89M_{\mathrm{w}} + 38.0 \tag{4.1c}$$

Units of σ and ϵ/k_{B} are Å and K, respectively. M_{w} is the *n*-alkane molecular weight,

Table 4.1: New proposed set of molecular parameters for the n-alkanes (the PV set), found by fitting to experimental data from the NIST Chemistry Webbook [107] (methane, ethane, propane, and n-butane) and from the compilation of Smith and Srivastava [108] (the rest of the n-alkanes).

	m	σ (Å)	ϵ/k_{B} (K)
methane	1.000	3.728	147.2
ethane	1.392	3.756	202.5
propane	1.776	3.811	219.5
n-butane	2.134	3.871	237.7
n-pentane	2.497	3.901	246.6
n-hexane	2.832	3.929	254.4
n-heptane	3.169	3.960	260.3
n-octane	3.522	3.970	264.4

expressed in g/mol. Parameters from this correlation deviate with respect to the fitted parameters with an absolute averaged deviation (AAD) equal to 1.1%, whereas the corresponding deviations for the BV and KG linear relationships are 2.7 and 1.7%, respectively.

Like any analytical EOS, soft-SAFT overestimates the critical point. Recently, Kiselev and Ely [109] have proposed a crossover SAFT EOS for pure fluids, which incorporates the scaling laws asymptotically close to the critical point and is transformed into the original SAFT of Huang and Radosz [10] far from the critical point. They applied the equation to PVT and VLE data for pure n-alkanes, improving the performance of the original equation, especially near the critical region. Although this is the correct approach to treat the critical region with analytical EOS when studying VLE, a different approach can be used if one is interested just in the behavior of the critical properties. In particular, Blas and Vega [102] showed that the soft-SAFT equation is able to quantitatively predict the critical properties of binary mixtures of hydrocarbons when the molecular parameters of the pure components are rescaled to the experimental critical points. Following this later path, we present here an additional correlation in order to enhance the prediction of the critical properties of the n-alkane series. We first rescale the molecular parameters of the PV correlation with the available experimental critical densities and temperatures [110], i.e., up to n-octadecane, and then correlate this new set of parameters. The resulting

relationships, shown in eqs 4.2a-4.2c, will be referred as the PVr correlation.

$$m = 0.0255M_{\mathrm{w}} + 0.628 \tag{4.2a}$$

$$m\sigma^3 = 1.34M_{\mathrm{w}} + 37.2 \tag{4.2b}$$

$$m\epsilon/k_{\mathrm{B}} = 7.17M_{\mathrm{w}} + 58.1 \tag{4.2c}$$

Units are the same as those in eqs 4.1a-4.1c.

4.1.4 Results and discussion

Before presenting phase-equilibria results, we first compare the molecular parameters of the BV, KG, and PV correlations, discussing their physical meaning and possible transferability. Afterward, predictions from the soft-SAFT equation with these parameters are presented and compared to experimental data, when available, to the PR EOS computed with the commercial package Hysys Plant 2.1, and to Monte Carlo simulation data from the literature. This is actually a double check: a comparison versus available experimental data will show the accuracy and predictive capability of the soft-SAFT EOS and its transferable parameters. If this is satisfactory and the same equation is used to compare with simulation data when experimental values are not available, the accuracy of the simulation data can therefore also be proven.

Comparison of molecular parameters

It is often claimed that one of the main advantages of molecular-based equations versus macroscopic models is the fact that they have fewer parameters, and that these have physical meaning. However, care should be taken, in general, when fitting molecular parameters to experimental systems: as a consequence of the nonlinear optimization needed, one could find different sets of parameters compatible with the desired accuracy of the fitting. Therefore, we will discuss the physical meaning and transferability of these parameters before presenting the phase-equilibria results. Here, by physical meaning we mean whether the parameters follow the expected behavior from the model used. Because we have modeled n-alkanes as homonuclear chains, different values of m, σ, and ϵ are expected for each member of the series. However, σ and ϵ should tend to an asymptotic value as the chain length increases, because the addition of new groups to longer chains does not essentially modify the structure of the molecule.

It should be noted that eqs 4.1b and 4.1c give a linear dependence of $m\sigma^3$ and $m\epsilon$ with M_{w}, not just σ and ϵ, respectively. This is consistent with the physical meaning of the parameters mentioned above: the dispersive energy and segment size
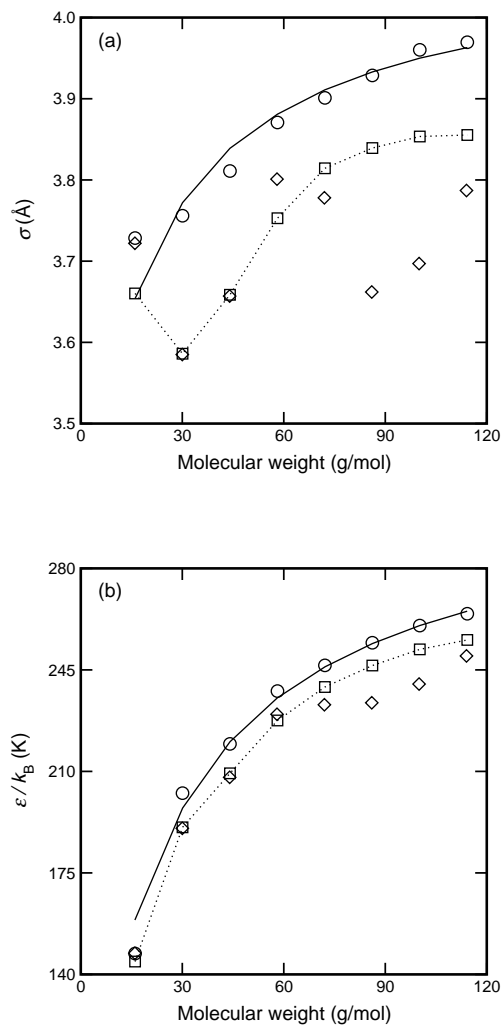
Figure 4.1: Molecular parameters from Blas and Vega [101] (diamonds), Kraska and Gubbins [48] (squares), and the new proposed set (circles), as a function of the molecular weight: (a) segment diameter; (b) dispersive energy. Solid lines show the values from the PV correlation (eqs 4.2a-4.2c). Dotted lines are a guide for the eye.

Table 4.2: Values of the size parameter σ from the three sets of transferable molecular parameters used in this work and from molecular simulation models (values in Å).

chemical group[a]	BV	KG	PV	TraPPE	NERD
CH$_4$	3.722	3.660	3.728	3.73	
CH$_3$ (ethane)	3.585	3.586	3.756	3.75	3.825
CH$_2$ (*n*-octane)	3.787	3.855	3.970	3.95	3.93
CH$_2$ (correlation)	3.782	3.994	4.078		

[a]See text for details.

parameters strongly increase with the number of carbon atoms for the low members of the series.

Figure 4.1 shows the segment size and energy parameters fitted by BV, KG, and PV versus the *n*-alkane molecular weight. In Figure 4.1a it is seen that the BV size parameter does not follow the expected trend of reaching an asymptotic value, but it randomly fluctuates. At the same time, there is no physical explanation for the sudden increase of the BV energy parameter for *n*-heptane and *n*-octane in Figure 4.1b. The parameters fitted by KG and PV follow, in general, the expected trend corresponding to the homonuclear model used. However, as Figure 4.1a shows, the KG correlation has the minimum value of the size parameter in ethane, which disagrees with values used in computer simulation models, as will be seen later in this section.

Although it is clear that all of these parameters are effective, it is also claimed that they are transferable. The transferability is understood here as using the parameters to predict, with the same procedure, the behaviour of compounds of the same family not included in the fitting. A question remains as whether the parameters obtained by this modelling approach could be used to guide some other molecular models, such as simulations. We present in Table 4.2 a comparison between the size parameter values from the three sets of transferable parameters used in this work and from molecular simulation united-atom models where the LJ potential for the nonbonded interactions is used. It should be emphasized that the molecular models are not identical: in simulations bending and torsional potentials are included, in addition to the LJ, while in soft-SAFT only LJ interactions are considered. Hence, this comparison is approximated and gives an idea of the volume occupied by the groups forming the molecules. Because our model is homonuclear, the size parameter for ethane is chosen to compare with the CH$_3$ parameter used in molecular simulation models, while the size parameter for *n*-octane and the asymptotic value from the correlations are shown for comparison with the CH$_2$ parameter. It can be seen that the proposed PV set

of parameters provides values very close to those used in the simulation models, especially in the TraPPE model, reinforcing the robustness of this correlation.

A direct comparison of other parameters could be performed for the compounds for which, in the simulation models, intramolecular interactions do not exist or are negligible, as happens for methane, ethane, and propane. For these compounds, we have decided to compare two additional molecular values by means of an AAD that includes the three alkanes: the total bond length of a molecule and the intermolecular dispersive energy between two molecules. The former is calculated in SAFT as $(m - 1)\sigma$, while it is a fixed value in the simulation models. The second one is a summation of the dispersive energy values of all possible pairs of segments interacting between the two molecules. The deviations of the total bond length are, with respect to the values from the TraPPE model, 18.9, 20.5, and 2.81% for the BV, KG, and PV parameters, respectively. In a similar way, AAD values of the dispersive energy are 13.7, 17.7, and 0.90%. It can be seen that the PV correlation is the only one that captures the values of the molecular simulation models.

Phase equilibria of pure heavy n-alkanes

We have chosen to calculate the phase envelope of selected n-alkanes, according to the available experimental and simulation data, for comparison. We first study n-octane, for which there are abundant simulation and experimental data. The phase equilibrium of this n-alkane as predicted using the parameters from the three correlations is shown in Figure 4.2. For comparison, we also include molecular simulation data and predictions from the PR EOS. It is not surprising that the PR EOS used here accurately predicts the whole phase envelope. As we have mentioned, the version we use is taken from a commercial package and it has specific well-fitted parameters for each member of the series. However, as happens with all macroscopic EOS, this equation does not explicitly consider the structure of the molecules and, in particular, the nonsphericity; hence, its performance deteriorates for compounds not included in its fitted parameters. All molecular simulation models presented in Figure 4.2a predict the phase envelope of n-octane in a very accurate way. The predictive accuracy of these models will allow us to use them as a reference for comparison when experimental data are unavailable.

The vapour pressure of n-octane in a logarithmic scale is plotted versus the inverse of the temperature in Figure 4.2b. We also include here simulation data from the TraPPE [97] and the EP [99] models, not included in Figure 4.2a. The reasons why these data were not included in the temperature-density diagram are that they do not present phase-equilibria results for the heavier n-alkanes we present next and also that they perform equally well as the rest of the models presented.
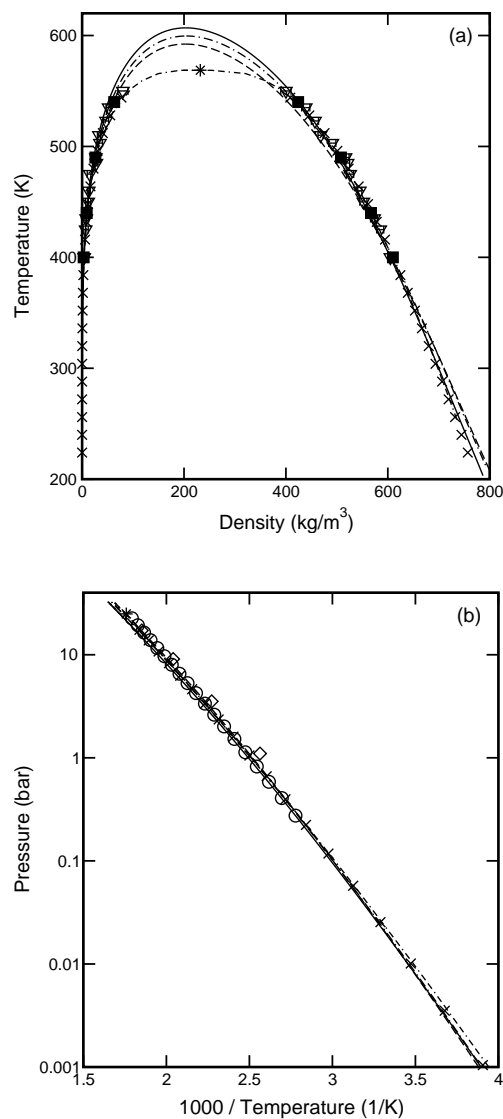
Figure 4.2: Phase equilibrium of *n*-octane: (a) coexisting densities; (b) vapour pressures. Crosses are experimental coexistence data [108] and the star is the experimental critical point [110]. Triangles, squares, diamonds, and circles represent molecular simulation data from the SKS [92], NERD [95], TraPPE [97], and EP [99] models, respectively. Lines correspond to predictions from the PR EOS (dot-double-dashed) and the soft-SAFT EOS using the BV (dashed), KG (dot-dashed), and PV (solid) correlations of molecular parameters.
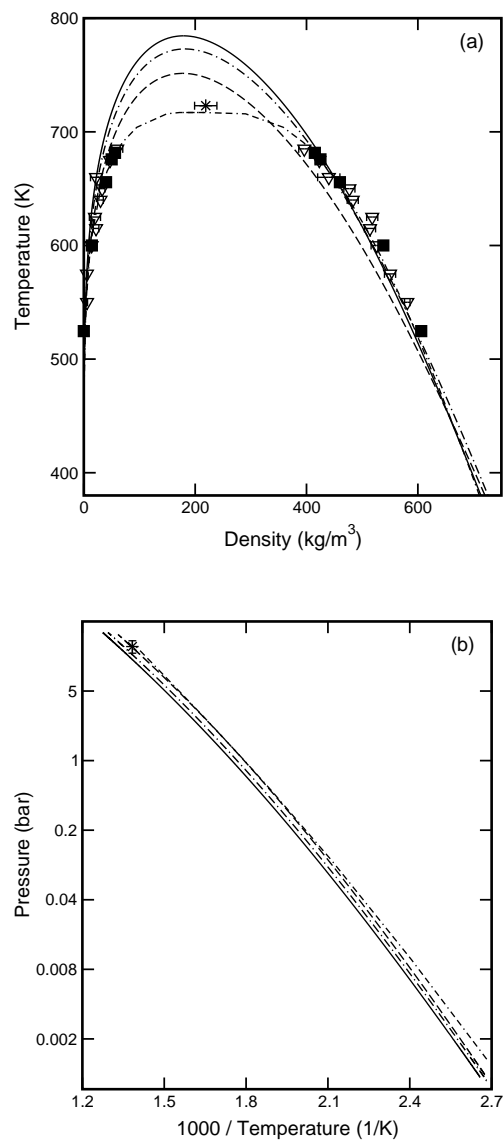
Figure 4.3: Phase equilibrium of n-hexadecane: (a) coexisting densities; (b) vapour pressures. Symbols are the same as those in Figure 4.2.
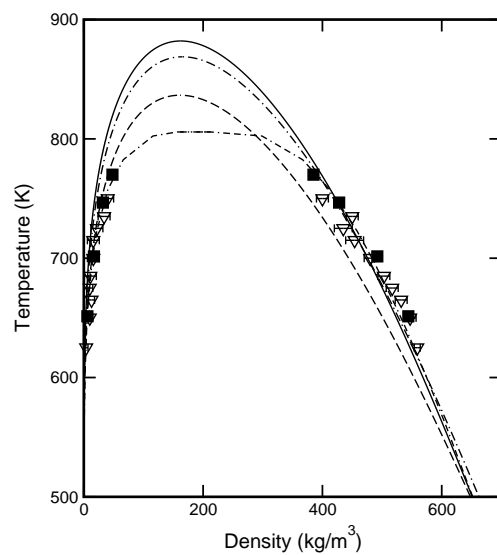
Figure 4.4: Coexisting densities of *n*-tetracosane. Symbols are the same as those in Figure 4.2.
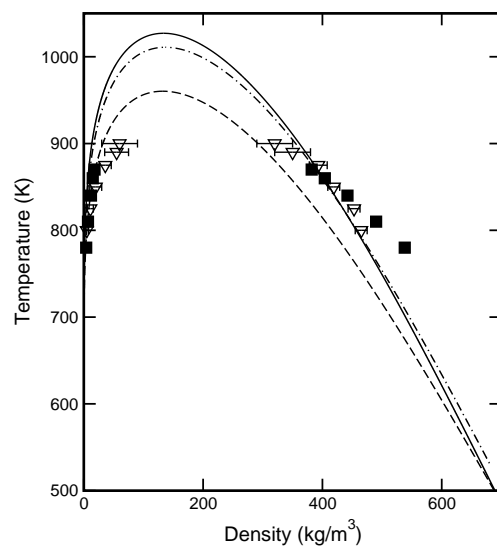
Figure 4.5: Coexisting densities of *n*-octatetracontane. Symbols are the same as those in Figure 4.2.

Temperature-density plots of n-hexadecane, n-tetracosane (n-$C_{24}H_{50}$), and n-octatetracontane (n-$C_{48}H_{98}$) are presented in Figures 4.3a, 4.4, and 4.5, respectively. Taking predictions of the PR EOS and molecular simulation results as a reference, because of the lack of experimental data, it can be appreciated that predictions using the BV parameters deteriorate when the n-alkane carbon number increases, while differences between the KG and PV curves remain practically constant and with an excellent accuracy. As for n-octane, the PV parameters give improved saturated liquid density predictions in the lowest temperature region and the saturated vapour densities are increasingly overestimated when approaching the critical region in all cases. We expect that the soft-SAFT equation with a reference fluid of dimers [111] will enhance the predictions for the vapour phase. It is observed that the soft-SAFT EOS predictions from the PV and KG parameters are in excellent agreement with the coexisting densities of the NERD model [95], as well as with the SKS model [92] and the PR EOS. We do not present predictions from the PR equation for n-octatetracontane because this component is not included in the Hysys Plant 2.1 library we have used.

Phase equilibria of binary mixtures of ethane and a long n-alkane

As was done with phase equilibria of pure n-alkanes, we selected several binary mixtures depending on simulation and experimental data available. Our goal here is to test the transferability of the parameters on mixtures of asymmetric compounds of the same series. Because no additional differences among correlations other than those commented on the pure compounds section were observed in mixtures, only predictions using parameters from the PV correlation are presented here. We first use the parameters of the pure compounds to predict the behaviour of the mixtures without any fitting. Because the binary mixtures studied are very asymmetric, additional phase-equilibria plots are shown, where the two binary interaction parameters η and ξ of the generalized Lorentz-Berthelot combining rules (eqs 2.5-2.6) have been fitted to experimental data. These binary parameters, because they do not depend on the thermodynamic conditions, are then used to predict the behaviour of the mixtures at other thermodynamic conditions.

Predictions from the soft-SAFT equation as well as predictions from the PR EOS are compared to experimental and simulation data. Nath *et al.* [96] studied the same binary mixtures using computer simulations and compared their results to the original SAFT EOS. They found that, in general, the PR EOS performs better than the original SAFT for these asymmetric mixtures, although predictions from both deteriorate as the chain length increases. We will show here how the soft-SAFT equation greatly improves predictions for these mixtures.

Figure 4.6 shows the phase-equilibrium diagram of the ethane + n-decane mixture at 96.526 bar. Molecular parameters from the PV correlation with no binary parameters fitted are used with the soft-SAFT equation. Although soft-SAFT overestimates the liquid compositions and underestimates those of the vapour phase, the general trend of the mixture is correctly given. Note that this is a mixture with two critical points, and critical points cannot be accurately predicted by the equation using the PV correlation. Nevertheless, predictions can be improved if fitted binary parameters are used, as will be shown later.

The temperature-composition diagram of the ethane + n-eicosane mixture at 96.526 bar is shown in Figure 4.7. This is a very challenging mixture for modelling, because the components are very asymmetric and the working pressure is very high. It is striking to see how predictions from the soft-SAFT EOS, with no fitting to the mixture, give the same degree of accuracy as the simulation models. Of course, as expected, the LCST point of the mixture is underestimated with this approach. It should also be noted that predictions from the PR EOS deteriorate with respect to the previous mixture, giving an accuracy similar to that of the soft-SAFT equation.

The pressure-composition diagram of the ethane + n-decane mixture at two different temperatures, 411 and 511 K, is presented in Figure 4.8. Again, predictions from the soft-SAFT EOS with the PV correlation are compared to experimental and simulation data. It is observed that the equation describes quite well the subcritical region of the mixture, especially the liquid phase. The EP model [99] is in better agreement with the experimental data (and our predictions) than the NERD model [96]. As for the temperature-composition diagram of this mixture (see Figure 4.6), the PR EOS predictions are in quantitative agreement with experiments.

Figure 4.9 displays the pressure-composition diagram of the ethane + n-eicosane mixture at 340 and 450 K. Because no simulation data are available for these conditions, only the experimental and PR values are plotted with the soft-SAFT EOS line. It is observed that, for this very asymmetric mixture, predictions from the soft-SAFT equation are more accurate than those obtained from the PR EOS: the soft-SAFT equation is able to predict the phase envelopes in almost quantitative agreement with experimental data, except near the critical region.

The previous figures show that the soft-SAFT EOS is able to capture the phase behaviour of very asymmetric mixtures of n-alkanes at different thermodynamic conditions, just by using the transferable parameters proposed for the pure components. However, there are several applications which may require more accurate predictions. As with any other modelling approach to mixtures, predictions can be enhanced if binary interaction parameters are fitted. In Figures 4.10 and 4.11 we present the same binary mixtures as those shown in Figures 4.6 and 4.9 but using fitted binary parameters. We just fit these parameters to experimental data at a given thermody-
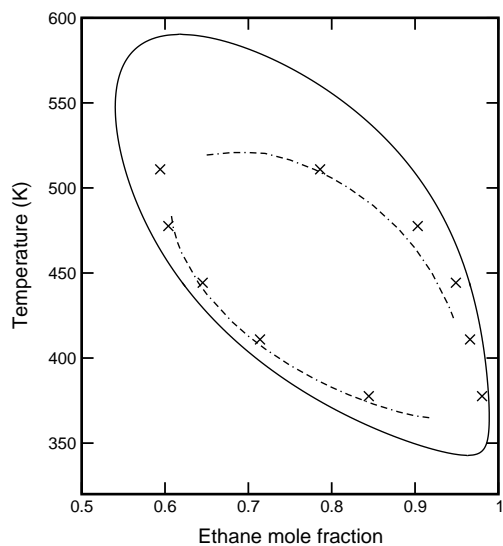
Figure 4.6: Phase diagram for a mixture of ethane and n-decane at 96.526 bar. Crosses correspond to experimental coexistence data [112], the dot-double-dashed line to the PR EOS, and the full line to the soft-SAFT EOS predictions.
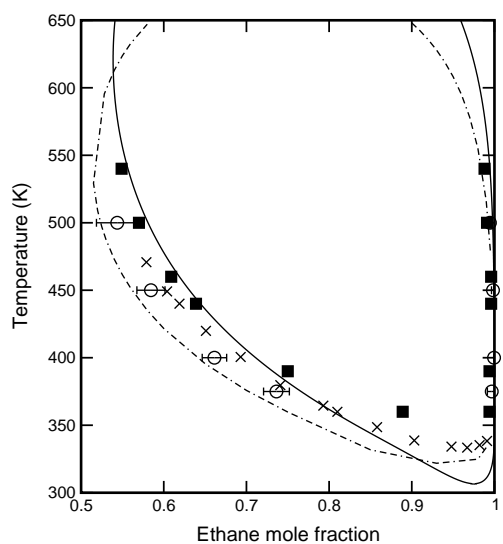
Figure 4.7: Phase diagram for a mixture of ethane and n-eicosane at 96.526 bar. Crosses, squares, and circles correspond to experimental coexistence data [113] and to simulation data from NERD [96] and EP models [99], respectively. The lines correspond to the PR EOS (dot-double-dashed) and the soft-SAFT EOS (full).
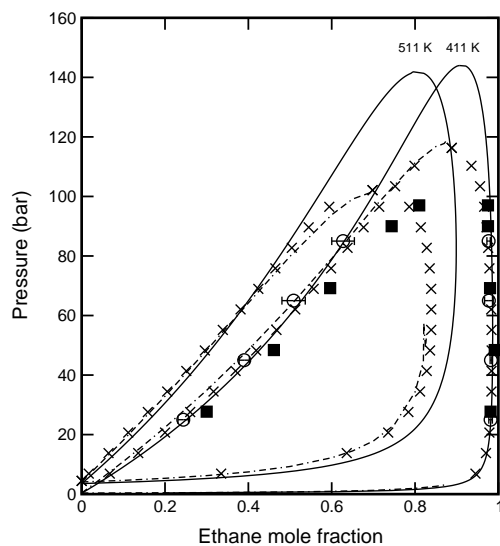
Figure 4.8: Phase diagram for a mixture of ethane and n-decane at 411 and 511 K. The source of experimental data is the same as that in Figure 4.6. The rest of the symbols are the same as those in Figure 4.7.
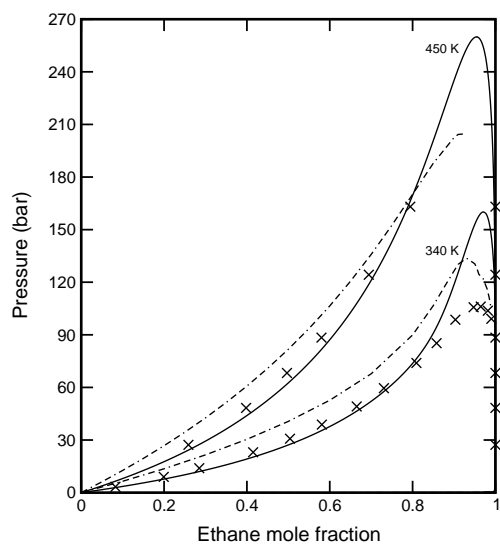
Figure 4.9: Phase diagram for a mixture of ethane and n-eicosane at 340 and 450 K. Symbols are the same as those in Figure 4.7.
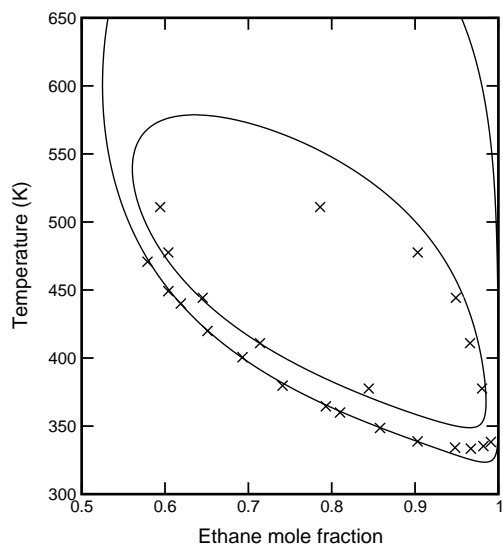
Figure 4.10: Phase diagram for the ethane + n-decane and ethane + n-eicosane mixtures at 96.526 bar. Symbols are experimental data and lines are SAFT calculations with fitted binary interaction parameters.
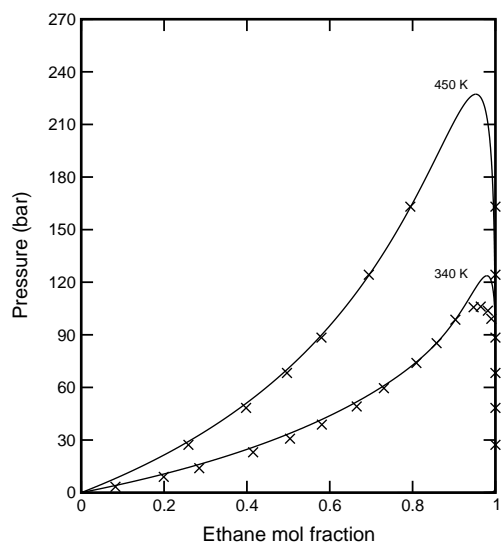
Figure 4.11: Phase diagram for a mixture of ethane and n-eicosane at 340 and 450 K. Symbols are experimental data and lines are SAFT calculations with fitted binary interaction parameters.

namic condition and use the same parameters in a transferable way; i.e., we predict the behaviour of the same mixture at different thermodynamic conditions without any further fitting. The binary parameters fitted for the ethane + *n*-decane mixture are $\eta = 1.028$ and $\xi = 0.9865$, and those for the ethane + *n*-eicosane mixture are $\eta = 1.029$ and $\xi = 0.9769$. Note that all of them are very close to unity.

Figure 4.10 shows the temperature-composition diagram of ethane + *n*-decane and ethane + *n*-eicosane mixtures at 96.526 bar. Experimental data are the same as those in Figures 4.6 and 4.7. Lines represent now the soft-SAFT EOS results with the fitted binary parameters. The agreement between the theoretical and the experimental results is remarkable, especially for the ethane + *n*-eicosane mixture. A similar behaviour is observed in Figure 4.11, where the pressure-composition diagram of ethane + *n*-eicosane is presented again. The only deviation observed between the soft-SAFT EOS predictions and the experimental data is the overestimation of the critical point, an expected fact, as mentioned already.

Critical properties of pure *n*-alkanes

The critical temperature and density as a function of the carbon number, for *n*-alkanes up to *n*-octatetracontane, are shown in Figures 4.12 and 4.13, respectively. It is observed that the PV correlation is able to capture the trend of the critical temperature with the carbon number, although, as expected, it is overestimated. Quantitative agreement is obtained when the PVr correlation is used. Note that all simulation models are also able to quantitatively predict this property.

Figure 4.13 shows that, using the (nonscaled) PV correlation, the soft-SAFT EOS qualitatively predicts the behaviour of the critical density, presenting a maximum, as was obtained experimentally by Anselme *et al.* [90] A quantitative agreement with experimental data is achieved when parameters from the rescaled PVr correlation are employed. Critical densities are overestimated by the TraPPE model and slightly underestimated by the NERD model, while simulations results from Errington and Panagiotopoulos are in excellent agreement with experiments and with the soft-SAFT EOS predictions. Because, to our best knowledge, experimental data of heavier *n*-alkanes are not available, and soft-SAFT is able to correlate the existing experimental results, predictions from the equation can be seen as a validation of the molecular simulation values for *n*-tetracosane and *n*-octatetracontane from the EP model [99].

The fact that the soft-SAFT EOS slightly overestimates the maximum critical density and underestimates the value of methane is due to the intrinsic effects of performing a correlation: the PVr correlation comes from a minimum square analysis of the molecular parameters up to *n*-octadecane. Hence, heavy *n*-alkanes will be favorably described by the correlation.
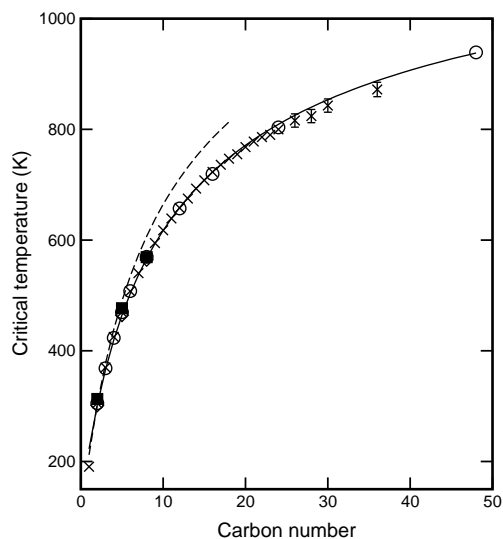
Figure 4.12: Critical temperature as a function of the *n*-alkane carbon number. Dashed and solid lines correspond to the soft-SAFT predictions with the PV and PVr correlations, respectively. Crosses are experimental data from references [110] (up to *n*-tetracosane) and [114] (*n*-hexacosane and heavier). Other symbols are the same as those in Figure 4.2.
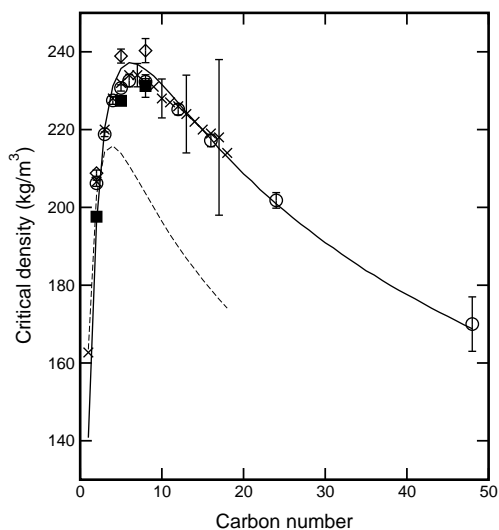
Figure 4.13: Mass critical density as a function of the *n*-alkane carbon number. Comparison among the soft-SAFT EOS predictions and available experimental and molecular simulation data. Symbols are the same as those in Figure 4.12.

Anselme *et al.* [90] showed that a nonlinear dependence of the critical density on the carbon number was necessary to correctly describe its behaviour. We have used the functional form suggested by Wilding *et al.* [115] to fit the soft-SAFT EOS predictions for the critical density of n-alkanes up to a chain of $n = 100$ carbons, obtaining

$$\rho_c = \frac{M_w}{91.31 + 26.33n^{1.293}} \quad n \geq 1, \tag{4.3a}$$

$$\rho_c = \frac{M_w}{153.7 + 22.08n^{1.333}} \quad n \geq 15, \tag{4.3b}$$

where ρ_c is the critical density in g/mL, M_w is the molecular weight in g/mol, and n is the carbon number. Although the fit of eq 4.3a to soft-SAFT EOS predictions has an AAD value of 0.74%, eq 4.3b, with an AAD of 0.14%, is an enhanced fitting of the power dependence of the critical density on n. Coefficients from eq 4.3b were calculated by successively extracting the lightest members of the series, until a reduction of the AAD of less than 0.01% is found. According to eq 4.3b, we find that, for the chain lengths considered in the fitting, the soft-SAFT equation provides that the critical density decreases as $n^{-1/3}$, while a decrease proportional to $n^{-1/2}$ was found by MacDowell *et al.* [116] when applying the Wertheim's thermodynamic perturbation theory to very long chain fluids. We have obtained [117], however, that the critical exponent of $-1/3$ is not the value predicted by the soft-SAFT equation for very long chains. In the limit of infinitely long chains, the critical exponent becomes $-1/2$, as expected [116]. A detailed discussion on the scaling of critical properties of infinitely long chains will be presented in the next section.

We also provide a fit to the critical temperature predictions from the soft-SAFT EOS using the PVr correlation, with the same functional form used in the critical density:

$$T_c = \frac{1}{8.058 \times 10^{-4} + 4.321 \times 10^{-3}n^{-0.7257}} \quad n \geq 2. \tag{4.4}$$

In this case, methane and ethane have been taken out of the data set to improve the fitting up to an AAD of 0.035%.

4.1.5   Conclusions

A new set of molecular parameters for the n-alkane series is proposed. They were obtained with the soft-SAFT EOS by fitting the experimental data for the first eight members of the series. A correlation of them versus the molecular weight, called the PV correlation, is able to accurately predict the phase envelope of pure heavy n-alkanes and asymmetric binary mixtures of them, when used with the soft-SAFT equation.

The performance of the PV correlation has been compared with two other published parameters for the same chemical family: the BV correlation, from Blas and Vega [101], and the parameters from Kraska and Gubbins [48], that we correlated in the KG relationship. Comparisons are also made to available experimental and simulation data. It is observed that, in general, PV and KG correlations perform equally well for heavy n-alkanes, but the new correlation is the most appropriate for liquid densities and, furthermore, its molecular parameters agree with those used in simulation models, showing the robustness of the soft-SAFT equation and the importance of fine-tuning the fitted parameters to the best values. Results were also compared with the PR EOS predictions available in a commercial package (Hysys Plant 2.1), which gives excellent agreement with experimental data for pure n-alkanes, because it has well-optimized parameters for them.

The new proposed set of transferable parameters has been used to predict the phase behaviour of ethane + n-decane and ethane + n-eicosane mixtures at several thermodynamic conditions. Comparisons of the soft-SAFT EOS predictions with available experimental and simulation data show that the equation is able to capture the main features of the phase envelope, providing, in some cases, the same degree of accuracy as simulation models. An excellent quantitative agreement with experimental data for these mixtures has been obtained when two fitted binary interaction parameters, independent of the thermodynamic conditions, were used. Comparisons with predictions from the PR equation for mixtures show that, as for the case of pure components, this equation accurately predicts the phase envelope of mixtures for which parameters for the pure components were fitted, but its performance deteriorates for very long chains. Nath *et al.* [96] have shown that, in the absence of any adjustable binary parameter, the PR EOS performed better than the original SAFT [8, 10, 11] for these mixtures. The improved predictions of the soft-SAFT EOS demonstrate that using a SAFT approach to model these fluids is better than the use of other macroscopic models, if the appropriate reference fluid in the SAFT-type equation is used.

The PV correlation is able to capture the maximum in the critical density observed experimentally and in simulation models when it is plotted versus the carbon number. A quantitative agreement with experimental critical temperatures and densities was achieved with the PVr correlation, obtained from the PV by rescaling of the critical points predicted by the soft-SAFT equation to the experimental data. Hence, for practical use, fitted functions for the critical temperatures and densities predicted by the soft-SAFT equation up to a chain of a hundred carbons are provided. Our results validate simulation values when no experimental data are available, showing, in particular, excellent agreement with the critical properties recently predicted by Errington and Panagiotopoulos [99].

4.2   Critical properties of homopolymer fluids

*The soft-SAFT EOS is used to study the dependence of the critical properties on chain length for pure polymers. The critical constants of chains up to 10^6 monomer units are predicted. The main advantage of these calculations, versus others found in the literature, is the fact that the equation is able to accurately predict experimental data available only for short chains and, at the same time, it is able to predict the critical properties in the infinite chain length scaling regime, without any further assumptions. The equation gives quantitative agreement with experimental and Monte Carlo simulation data for normal alkanes. For very long chains, the equation predicts mean-field scaling behaviour, as expected. Moreover, taking advantage of the linearity of the molecular volumes and dispersive energies with the chain molecular weight, a value of 1/5 is found for the critical compressibility factor of an infinitely long n-alkane chain. It is demonstrated that this is not contradictory to Wertheim's theory.

4.2.1   Introduction

One of the major applications of SAFT has been the prediction of thermodynamic properties and phase behaviour of chainlike fluids, where it is very successful. Of great interest, both theoretically and from an application point of view, is the n-alkane series. Normal alkanes show great regularity in behaviour with respect to the carbon number, which makes them a suitable system to search for transferable parameters. Of course, these compounds are commonly found in the petrochemical industry. Although most of the simple macroscopic equations work for light n-alkanes, such equations are unable to predict the properties of heavier members of the series. Hence, several authors have calculated the phase equilibria of pure and binary mixtures of this series using the SAFT approach [48, 64, 101, 102, 105, 106, 118]. When using SAFT for experimental systems, the molecular parameters of the theory (segment size, dispersive energy, chain length, etc.) are obtained by fitting to available experimental data for the fluid of interest.

In the previous section, we reported predictions for the phase equilibria of pure and binary mixtures of heavy n-alkanes, using the soft-SAFT EOS [19,101], a modification of the original SAFT equation. We proposed a new set of transferable molecular parameters that provide a significant improvement over previous calculations [101],

---

especially for the heavy members of the series. Comparisons of soft-SAFT predictions with experimental and simulation data showed that the equation is able to capture the phase envelope in all cases, giving the same degree of accuracy as molecular simulations.

Once the success of the theory in quantitatively predicting the properties of heavy n-alkanes has been proved, our purpose is to compare the soft-SAFT results for the scaling of the critical properties of pure homopolymer fluids with experimental, theoretical and computer simulation results, either for pure polymers or polymer solutions.

For a long time there has been controversy about experimental results and theoretical estimates for the scaling exponents of the critical properties of flexible polymer fluids and dilute polymer solutions. The main discrepancy concerns the exponent x_c of the power law dependence of the critical mass density on the number of monomers n:

$$\rho(n) \propto n^{-x_c}. \tag{4.5}$$

It is well known that Flory-Huggins theory predicts $x_1 = 1/2$, whereas experimental [119–122] and computer simulation results [115,123,124] for high molecular weight polymers yield the value $x_1 = 0.38 \pm 0.01$. Moreover, theoretical results from renormalization group arguments [125, 126] confirm the classical mean-field value $x_1 = 1/2$, while the single-chain mean-field theoretical calculation due to Szleifer [127] finds $x_1 = 0.4$ for $n \leq 100$, in close agreement with the experimental value. A more detailed discussion of estimates for this exponent may be found elsewhere [128, 129].

Most of the theoretical calculations of critical constants of chain molecules have been obtained within the framework of lattice theories. Although the computational efficiency of these simple models permits calculations for very long chains, in some cases the models are too crude to quantitatively predict experimental data [130]. On the other hand, more sophisticated molecular simulations models, such as those recently proposed for alkanes [95,97,99] have proved to predict the phase equilibria and critical properties of these compounds in quantitative agreement with experimental data, but are computationally very demanding for very long chains. In particular, the critical constants for n-alkanes up to $n = 48$ (n-octatetracontane) were provided by Errington and Panagiotopoulos [99] from a united-atom model, using histogram reweighting grand canonical Monte Carlo methods, in quantitative agreement with available experimental data. To our knowledge, no accurate molecular simulation results for the critical properties of longer chains have been published using a detailed model, because of the rapidly increasing computational demands as chain length increases.

Recently, Yan and de Pablo [129]] reported simulation results for ultra-high molecular weight polymers (chains up to $16\,000$ sites in a simple cubic lattice model), showing a crossover in the critical density from experimental to mean-field scaling

behaviour. They claimed, as other authors [131] had suggested before, that the chain lengths involved in previous experiments and simulations were not long enough to reach the infinite chain length scaling regime. Furthermore, their simulation results also agreed with the leading term of the finite chain length corrections to the critical density deduced from renormalization group theory.

Regarding the critical temperature, all experimental and computer simulation results for long chains show a dependence on chain length consistent with the mean-field Shultz-Flory functional form,

$$\frac{1}{T_c(n)} - \frac{1}{T_c(\infty)} \propto \frac{1}{\sqrt{n}} + \frac{1}{2n}, \tag{4.6}$$

where $T_c(\infty)$ is the critical temperature for chains of infinite length.

Using a theoretical treatment, Vega and MacDowell [132] analysed the scaling behaviour of long chains as predicted by Wertheim's thermodynamic perturbation theory. They used a truncated virial expansion to describe the EOS near the critical point showing that, for very long chains, Wertheim's theory predicts a finite critical temperature, a critical compressibility factor of 1/3, and a vanishing critical pressure and density, with the scaling laws $n^{-3/2}$ and $n^{-1/2}$, respectively.

As mentioned above, among the molecular-based equations developed from statistical mechanics, the most successful one in quantitatively predicting experimental data for n-alkanes is the SAFT equation. Since the SAFT EOS is based on Wertheim's theory, it is expected that the equation would predict the same finite values and mean-field scaling behaviour for the critical properties as obtained by Vega and MacDowell [132]. However, they assumed a finite asymptotic critical temperature and a vanishing critical density for very long chains, whereas here we use just the soft-SAFT equation to obtain the chain length dependence of the critical properties from Wertheim's theory, in a predictive manner, i.e., without the need for any assumptions about the model.

We compare the soft-SAFT EOS results for the scaling of the critical properties of pure homopolymer fluids with available results for pure polymers or polymer solutions. Although not formally proved [128], the fact that the critical exponents are analogous for a pure polymer and a polymer + solvent system is virtually always assumed [116]. The main goal here is to estimate the critical properties for homopolymer systems ranging from short to very long chain lengths with the same tool, the soft-SAFT equation.

4.2.2 Theory

As mentioned in the previous section, predictions from the theory can be improved when additional microscopic information related to the fluid is introduced in the
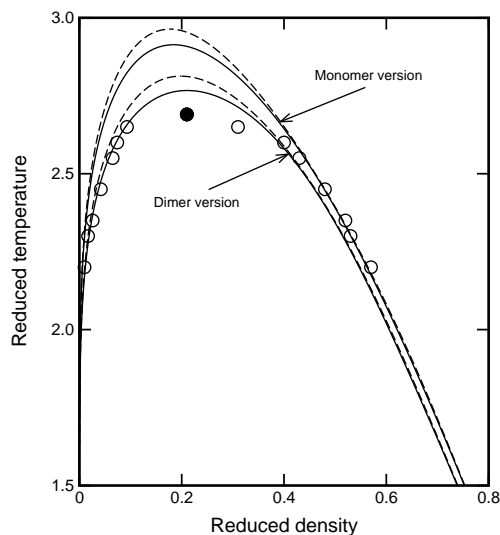
Figure 4.14: VLE of a pure chain of 8 LJ monomers. Circles are simulation data [133] (the filled circle is the estimated critical point) and lines correspond to soft-SAFT EOS predictions from the monomer and dimer versions. Calculations using the Johnson *et al.* EOS [45] (solid lines) and the Kolafa and Nezbeda EOS [46] (dashed lines) for a reference fluid of LJ monomers are also plotted.

equation. Blas and Vega [111] showed that the formation of the chains through a dimer reference fluid provides more accurate results than the monomer version of the theory. An overall improvement in the VLE predictions was observed for a wide range of chain lengths, especially for the vapour phase and near the critical point. This improvement over the original equation is due to the inclusion of additional structural information, given in terms of the pair radial distribution function g_{LJ} of dimers. As Müller *et al.* [61] showed some years ago, the theory is very sensitive to the approximations used to estimate this function. If this function is not accurate enough, like the one resulting from the Weeks-Chandler-Andersen theory, large discrepancies between simulation and theory can arise [61] in some points of the phase diagram.

As an example, we show in Figure 4.14 the VLE of a chain formed by 8 monomers. We check in this figure the performance of the theory versus molecular simulation results [133]. Lines are predictions from the equation using the monomer and dimer versions of the theory. The g_{LJ} functions for both versions are empirical expressions that fit extensive computer simulations of the LJ monomer and dimer fluids [53, 66]. A comparison with simulations for the predictions using the Johnson *et al.* EOS (solid

line) and the Kolafa and Nezbeda EOS (dashed line) for the reference fluid shows that the former is more accurate for the vapour phase.

The same figure shows that the improvement in the dimer version is significant in the vapour phase predictions, but the critical point continues to be overestimated in all cases, because of the inherent classical formulation of the equation. Since in this work we are interested in critical properties, we shall apply a simple rescaling of the VLE curve to the experimental critical point. The procedure is described in detail below in this section. As a result of this, both monomer and dimer versions of the equation, and both EOSs for the LJ fluid will provide identical results for the critical properties. Hence, to be consistent with previous works [118], we choose here the Johnson *et al.* EOS and the monomer reference fluid.

Thus we shall calculate here the chain contribution for a LJ fluid of tangent spheres, obtained through Wertheim's theory, in terms of the chain length m and the pair correlation function g_{LJ} of LJ monomers, evaluated at the bond length σ, as expressed in eq 2.7.

4.2.3 Molecular model

Polymer chains are described as fully flexible homonuclear molecules, modelled as m LJ spheres of equal diameter σ, and the same dispersive energy ϵ, bonded tangentially to form the chain. When fitting to experimental data, noninteger values of the chain length m are allowed in order to account for sphere overlap.

According to this model, three molecular parameters (chain length, monomer size and dispersive energy between two nonbonded monomers) are needed to describe, with the soft-SAFT EOS, all thermodynamic properties of each chain fluid.

Several authors have published different sets of molecular parameters for the n-alkane homologous series to be used with an LJ SAFT EOS [48,101]. They are usually obtained by fitting the experimental saturated liquid densities and vapour pressures. However, the accuracy in predicting the behaviour of compounds not included in the fitting procedure deteriorates in some cases. As we have mentioned in the last section, the new set of molecular parameters for the n-alkane series recently proposed by us [118], improves the accuracy of VLE predictions. Moreover, parameter values were in close agreement with those used in computer simulation models [95, 97, 99], showing the importance of fine-tuning the fitted molecular parameters to physically meaningful values.

In the last section it was observed that the chain length, volume and energy linearly increase with the n-alkane molecular weight, and hence, a correlation for these parameters was proposed [118]. In this work we take advantage of this fact and use similar correlations to calculate the critical properties of very long chains. In the

next subsection we explain how these parameters are used in order to compute critical properties of chains.

4.2.4   Calculation of critical properties

Figure 4.15 shows the VLE of n-hexane, to state in a clearer way how molecular parameters affect the equilibrium predictions. The solid line corresponds to the predictions of the equation when using a set of molecular parameters obtained by fitting experimental VLE data (crosses) for this substance. When one is interested in critical constants, and due to the fact that classical EOSs overestimate them, a simple rescaling of the molecular parameters to fit experimental critical points can be employed [118]. Although this simple mathematical method does not incorporate density fluctuations like, for instance, a crossover treatment [109, 134, 135], it provides very satisfactory results and avoids the need to fit additional parameters.

In order to achieve good agreement with experimental critical densities and temperatures (dashed line in Figure 4.15a), one needs to rescale both the size and the energy parameters. Unfortunately, as a consequence, predicted critical pressures using these rescaled parameters disagree with experimental data (dashed line in Figure 4.15b). Since these parameters are rescaled using experimental data from two properties among ρ_c, T_c and P_c, the property that is discarded is not quantitatively predicted, as shown in Figure 4.15. One may question how the critical compressibility factor can then be predicted accurately by the equation. It is straightforward to see that either the size or the energy parameter has to be rescaled twice, using two of the three possible pairs of sets of experimental data ($T_c - \rho_c$, $T_c - P_c$ and $\rho_c - P_c$). Hence, it is important to note that, in order to quantitatively predict the experimental critical compressibility factor, one cannot have a single set of rescaled molecular parameters. Therefore, two rescaled versions of the PVr correlation [118] are employed in this work: the PVr$^\rho$, rescaled to experimental T_c and ρ_c data, and the PVr^P, rescaled to T_c and P_c. The values of the chain length and dispersive energy are given, in both cases, by

$$
\begin{align}
m &= 0.0255 M_\text{w} + 0.628, \tag{4.7a} \\
m\epsilon/k_\text{B} &= 7.17 M_\text{w} + 58.1, \tag{4.7b}
\end{align}
$$

where units of ϵ/k_B and M_w, the molecular weight of the chain, are K and g/mol, respectively. For the PVr$^\rho$ and the PVr^P versions, molecular volumes in Å^3 are, respectively,

$$
\begin{align}
m\sigma^3 &= 1.34 M_\text{w} + 37.2, \tag{4.7c} \\
m\hat{\sigma}^3 &= 2.23 M_\text{w} + 1.75, \tag{4.7d}
\end{align}
$$
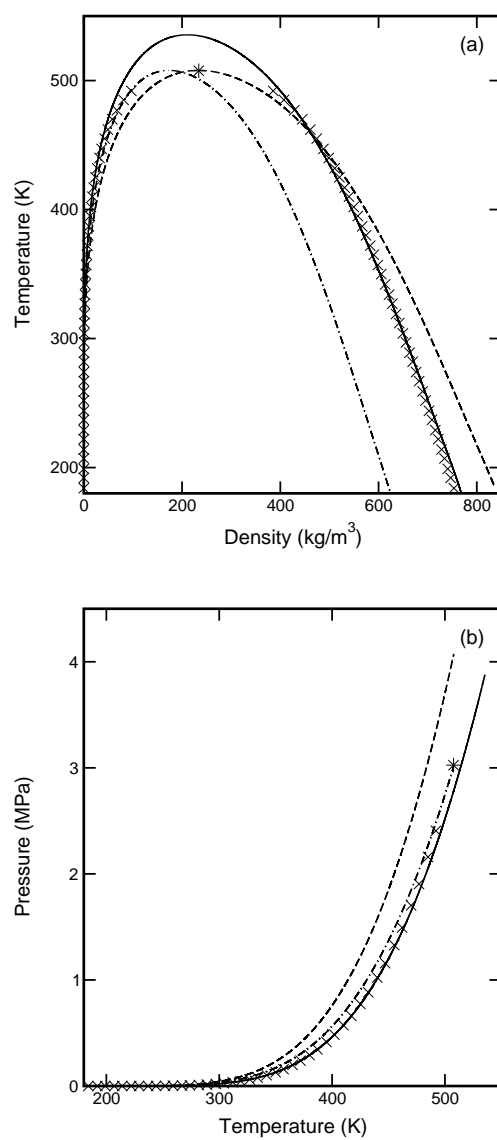
Figure 4.15: VLE of *n*-hexane: (a) coexisting densities, and (b) vapour pressures. Crosses represent experimental data [108]. Lines correspond to soft-SAFT EOS predictions with no rescaled molecular parameters [118] (solid), with rescaled parameters to the critical temperature and density (dashed) and with rescaled parameters to the critical temperature and pressure (dotdashed). The asterisk shows the location of the experimental critical point [110].

where the circumflex distinguishes the size parameter rescaled to T_c and P_c from that of the $T_c - \rho_c$ rescaling.

The soft-SAFT EOS, with molecular parameters from the PVr$^\rho$ correlation has proved to be able to predict [118] the critical properties of heavy n-alkanes up to 100 monomer units. Making use of the functional form of Wilding $et\ al.$ [115],

$$\Theta_c = \frac{1}{c_1 + c_2 n^{x_c}}, \qquad (4.8)$$

where Θ_c represents any of the critical properties (when Θ_c symbolizes the critical mass density, the right-hand side of eq 4.8 must be multiplied by the molecular weight), we found that critical mass densities, for $n \leq 100$, scale as $n^{-1/3}$ ($x_c = 4/3$ when Θ_c symbolizes the critical mole density). Since we are interested in the scaling behaviour of the critical properties for very long chains, we have used the same functional form to fit the soft-SAFT EOS predictions up to 10^6 monomer units. Note that when much longer chains are included in the fitting of this function, the critical exponent x_c increases. The critical exponents obtained, together with the ranges of fitting and AADs, are summarized in Table 4.3. For very long chains, the low limit of the range of fitting is an estimation of the chain length above which the long range regime holds. If one tries to include in the fitting lower values of n, deviations increase rapidly. Making the range narrower, the AAD and the critical exponent do not change significantly (less than 1%). Constants c_1 and c_2, which depend on the actual property, are of special interest to estimate critical parameters of n-alkanes of any molecular weight through eq 4.8, in a quick and simple way. However, since they are worthless for the forthcoming discussion, there are omitted in Table 4.3. The critical exponents, the scaling behaviour when the long range regime holds, and their connection to molecular parameter values will be discussed in the next subsection.

4.2.5 Results and discussion

Prior to discussing the scaling behaviour and critical exponents for the long range regime, we believe it is of interest to compare the predictions of the soft-SAFT equation for the critical parameters of n-alkanes with other methods available in the literature. To our best knowledge, n-octatetracontane (n-$C_{48}H_{98}$) is the longest chain length for which the vapour-liquid critical point has been obtained from simulations [99]. Furthermore, realistic predictions for the critical properties of heavy n-alkanes are very scarce. Jiang and Prausnitz [135] combined their crossover SAFT EOS with White's renormalization group theory, obtaining a simple theory that is able to describe the properties of chain fluids both outside and inside the critical regions. They used the so-called EOSCF-RG to predict the critical properties of n-alkanes up to $n = 36$. More recently, Chen and Mi [136] modified SAFT (from here

Table 4.3: Fitted critical exponents to the soft-SAFT predictions, according to the functional form of equation 4.8. The range of number of monomers and the absolute averaged deviations of the fitting are also shown.

Θ_c	x_c	Range of n	AAD (%)
ρ_c	1.333^a	$15 - 10^2$	0.14
T_c	-0.726	$2 - 10^2$	0.035
P_c	1.266	$7 - 10^6$	0.76
ρ_c	1.506^a	$350 - 10^6$	0.389
T_c	-0.472	$600 - 10^6$	0.003
P_c	1.494	$10^3 - 10^6$	1.14

[a]Exponent for the critical mole density.

on SAFT_{CM}) in order to calculate the properties near the critical points of nonpolar fluids. They considered the segment shape of chain molecules through a hard convex body EOS and radial distribution function, and excluded the dispersion energy between intramolecular segments. In their paper, calculated critical points up to a chain of 20 monomers are reported. On a different approach, a fitting of the recommended experimental values by Ambrose and Tsonopoulos [110], led Lemmon and Goodwin [137] to report correlations for the critical temperatures and pressures of the n-alkane series, as a function of the carbon number. Predictions for selected chains from these correlations and from the previously mentioned SAFT models, together with those from the best simulations we are aware of [99], are listed in Tables 4.4 and 4.5, together with experimental data and the soft-SAFT results.

Table 4.4 shows that critical temperatures for chains not longer than $n = 24$, where contrasted experimental data exist [110], are predicted accurately by all models. For heavier chains, in spite of the uncertainties of the experimental values, soft-SAFT EOS and the correlation from Lemmon and Goodwin overpredict the existing experimental data [114], whereas the EOSCF+RG equation reproduces them accurately. This last result was expected, since the EOSCF+RG fitted molecular parameters to these experimental critical temperatures and pressures. It should be mentioned that the soft-SAFT equation also uses experimental data to fit its molecular parameters, but only up to $n = 18$. For heavier chains, as for $n = 48$, for which simulation and soft-SAFT temperatures are in very close agreement, the results from the equation are pure predictions. Regarding critical pressures, apart from the fact that simulation results overestimate the experimental values, the rest of the models give good predictions for

Table 4.4: Comparison of critical temperatures and pressures predicted by the soft-SAFT EOS and other models available in the literature. Temperatures and pressures are given in K and MPa, respectively. Experimental data were taken from the compilation made by Ambrose and Tsonopoulos [110] ($n \leq 24$), and from Nikitin [114] ($n \geq 26$). Simulation results from Errington and Panagiotopoulos may be found in [99]. Predictions from the EOSCF+RG and SAFT$_{CM}$ models were obtained from [135] and [136], respectively. The semi-empirical correlation is given in [137].

n	Experimental		Simulation	
	T_c	P_c	T_c	P_c
12	658 ± 1	1.82 ± 0.1	657.1 ± 1.0	1.98 ± 0.03
16	723 ± 2	1.4 ± 0.2	719.5 ± 1.2	1.52 ± 0.03
20	768 ± 8	1.07 ± 0.2		
24	800 ± 8	0.87 ± 0.2	803.5 ± 1.2	1.03 ± 0.03
26	816 ± 12			
28	824 ± 12			
30	843 ± 12			
36	872 ± 12			
40				
48			939.0 ± 3.0	0.52 ± 0.03

n	soft-SAFT		EOSCF+RG		SAFT$_{CM}$		Correlation$_{LG}$	
	T_c	P_c	T_c	P_c	T_c	P_c	T_c	P_c
12	658.6	1.814	658.8	1.92	659.8	1.876	658.1	1.816
16	722.9	1.415	720.7	1.45	722.9	1.432	722.1	1.432
20	771.2	1.150	764.8	1.13	769.7	1.129	771.4	1.198
24	809.2	0.962	800.6	0.88			811.1	1.051
26	825.4	0.888					828.3	0.997
28	840.1	0.823	827.5	0.68			844.0	0.954
30	853.3	0.766	840.2	0.60			858.5	0.919
36	887.7	0.630	868.4	0.42			895.9	0.845
40	906.7	0.562					916.8	0.815
48	937.8	0.458					951.7	0.778

Table 4.5: Comparison of critical mass densities predicted by the soft-SAFT EOS and other models available in the literature. Densities are given in kg/m^3. Experimental data were taken from the compilation made by Ambrose and Tsonopoulos [110]. Simulation results from Errington and Panagiotopoulos may be found in [99]. Predictions from EOSCF+RG and $SAFT_{CM}$ models are taken from [135] and [136], respectively.

n	Experimental	Simulation	soft-SAFT	EOSCF+RG	$SAFT_{CM}$
12	226 ± 10	225.0 ± 1.4	227	257	240
16	219 ± 20	217.0 ± 1.6	217	260	231
20			209	257	204
24		202 ± 2	201	247	
26			197		
28			194	257	
30			191	249	
36			182	233	
40			177		
48		170 ± 7	169		

this property. For the heaviest chains, for which no experimental data are available, it seems that the correlation from Lemmon and Goodwin gives values that are too high compared with SAFT models. When extrapolated to longer chains, as pointed out by the authors, the correlation is assumed to provide only acceptable estimates, and new measurements are needed to verify this assumption.

Critical mass density values are listed in Table 4.5. It may be observed that, for the shortest chains, EOSCF+RG and $SAFT_{CM}$ overestimate experimental data, the former even showing an inconsistent trend as the carbon number increases. For this property, considering the uncertainties, soft-SAFT predictions coincide with the simulation values. In summary, a comparison of soft-SAFT predictions for the critical parameters of heavy n-alkanes with experimental data, and with the best available methods to obtain these properties, shows that our results are very accurate.

The critical properties as predicted by the soft-SAFT equation versus n are plotted in Figures 4.16-4.19, together with fitted equations according to the functional form of eq4.8. In all cases we show in the same graph a broad chain length range, including both short chains and the long chain length regime. We also include in these figures experimental data for n-alkanes up to $n = 18$ from the compilation by Ambrose and Tsonopoulos [110], and for $n = 16$ up to $n = 24$ from the review by Nikitin [114]. Simulation results from Errington and Panagiotopoulos [99] are also shown.

The mass critical density versus the carbon number is presented in Figure 4.16
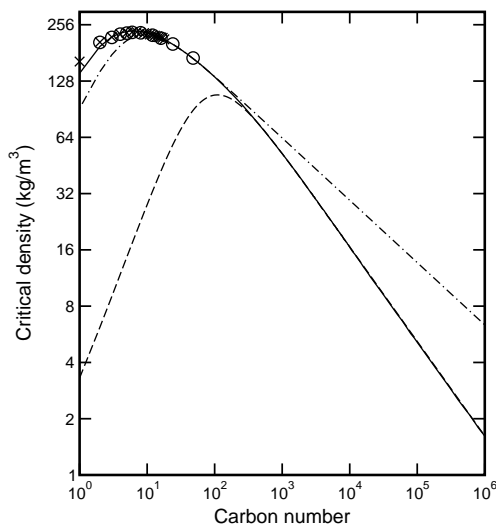
Figure 4.16: Mass critical density as a function of the number of monomer units. Crosses represent experimental data [110] and circles are molecular simulation results [99]. Predictions from the soft-SAFT EOS are represented as a solid line. The dashed and dot-dashed lines correspond to fitted equations according to the functional form of equation 4.8, with critical exponents shown in table 4.3.

in a log-log plot. The soft-SAFT EOS predictions are in excellent agreement with experimental and simulation results, capturing the maximum experimentally found for n-hexane, and predicting a dependence for $15 \leq n \leq 100$ that scales as $n^{-1/3}$ (see Table 4.3). In this range of chain length molecular details are important, and the apparent scaling exponents should depend to some extent on the system and the actual range of chain length considered. Nevertheless, the $n^{-1/3}$ scaling behaviour of the critical density for moderately long chain lengths agrees with experimental data of the polystyrene + methylcyclohexane system reported by Dobashi $et\ al.$ [138] (considering only chains up to 200 monomer units; a fit of the form $\Theta_c(n) = (b_1 + b_2 n^x)^{-1}$ for the experimental critical volume fractions Θ_c up to $n \simeq 200$ monomer units gives $x = 0.33$) and with Gibbs ensemble simulations performed on a lattice homopolymer model for various chain lengths up to $n = 128$ by Mackie $et\ al.$ [131]. It should be mentioned that this may be simply fortuitous; we do not have solid arguments to justify this coincidence.

Note that due to the intrinsic effects of using a correlation of molecular parameters for a series of chemical compounds, the anomalous critical properties of methane ($n = 1$) are not estimated accurately. For the long chain length regime, the soft-SAFT equation predicts a critical exponent $x_c = 1/2$ for the critical mass density, in agreement with mean-field theories. This scaling behaviour was expected since Vega and MacDowell have already shown that Wertheim's theory predicts mean-field scaling exponents in the infinite long chain regime. The unique assumption that underpinning our calculations for long chains is that the molecular volume and the dispersive energy between a monomer and a molecule continue to be proportional to the molecular weight. We are showing that, just by rescaling these parameters to experimental critical point data, soft-SAFT EOS is able to provide very accurate predictions for the critical properties of relatively short chain lengths, in spite of the classical formulation of the EOS. Hence,the effect of large correlation lengths on the Helmholtz free energy near the critical region is taken into account in some way with this rescaling. At this point, one may query whether the results for very long chains act in favour of the argument that a crossover to mean-field behaviour in the scaling of the critical properties of homopolymers exists. The answer should be negative because, for very long chains, molecular parameters cannot affect the scaling behaviour: the size and the energy parameters become constant and the chain length parameter is no longer relevant.

Fitted functions according to eq4.8 are plotted in Figure 4.16 as dashed and dot-dashed lines. It can be seen that the long chain length regime for this property holds above $n \simeq 350$, where the solid line becomes straight with a slope equal to $-1/2$ in a log-log scale.

The leading term of the finite chain length corrections to the critical density in the critical demixing of polymer solutions, derived from a renormalization group analysis, is given by

$$\phi_c \propto \left(\frac{\ln n}{n} \right)^{1/2}, \tag{4.9}$$

where ϕ_c is the polymer critical volume fraction. If we plot our results for ρ_c, for n greater than 10^3, versus the RHS in eq 4.9, a straight line is obtained. Hence, results for the vapour-liquid critical density of homopolymers also follow this finite chain length correction to mean-field theory, providing evidence in favour of a mean-field critical exponent, and of the analogy between the VLE of homopolymers and critical demixing of polymer solutions.

Figure 4.17 shows the critical temperature behaviour as a function of the number of monomer units in the chain. Quantitative agreement with experimental and computer simulation results for relatively short chains is obtained. Fitted functions according to eq4.8 are plotted as dashed and dot-dashed lines, showing that the long

chain length regime for this property holds down to $n \simeq 600$. For this regime, soft-SAFT EOS predictions show that $1/T_c(n)$ approaches the limiting temperature value $T_c(\infty) = 4.68$ with the leading term $n^{-1/2}$. Moreover, as predicted by Flory theory, results from the soft-SAFT equation lie on a straight line on the Shultz-Flory plot (eq 4.6), with an AAD of 2.66%. These results are in agreement with the work by Vega and MacDowell [132], where they used Wertheim's theory with a truncated virial expansion. These authors stated that Wertheim's theory overestimates the critical temperature of infinitely long chains by about 7% when $\partial \ln y(\sigma)/\partial \rho_R$ at $\rho_R = 0$ is calculated accurately. Fortuitously, when the derivative is calculated from the simulation results performed by Johnson *et al.* [45] (a less accurate value of the derivative) $T_c(\infty)$ is overestimated by only less than 2%. Also, all reported experimental and simulation results for polymer solutions agree with a scaling behaviour according to $n^{-1/2}$.

Critical pressures are plotted in Figure 4.18. The soft-SAFT EOS predicts a vanishing critical pressure that scales as $n^{-3/2}$ when the long chain scaling regime holds. Because the anomalous pressure value for $n = 1$ is overestimated when the PVr correlation is used, the maximum critical pressure experimentally found in ethane is not predicted, as expected. Apart from the value for methane, the experimental values are predicted with excellent accuracy, similar to that achieved by the simulation results of Errington and Panagiotopoulos [99]. The long chain length regime holds for values above $n = 1000$ (see Table 4.3), although in Figure 4.18, due to the large range of pressures shown, it seems to be reached at a lower number of monomers.

The critical compressibility factor values calculated from the soft-SAFT EOS critical density, temperature and pressure predictions, shown in Figures 4.16, 4.17 and 4.18, respectively, are presented in Figure 4.19 as a solid line. As expected, they are in excellent agreement with experimental data, showing the accuracy of soft-SAFT theory and the PVr correlation in predicting this critical property. The histogram reweighting Monte Carlo simulation results by Errington and Panagiotopoulos are not as accurate as the theoretical predictions, due to the slight overestimation of critical pressures for n-alkanes longer than n-butane.

The dot-double dashed line shown in Figure 4.19 corresponds to the predictions of the soft-SAFT equation when all the critical properties are calculated using the PVr$_\rho$ correlation (i.e., T_c and ρ_c are rescaled). When done in this way, the critical pressure is overestimated and the critical compressibility factor in the long chain regime becomes constant and equal to one third, as Wertheim's theory predicts [132]. Nevertheless, if one fits all three critical values, i.e., the two versions of the PVr correlation are used, Z_c reaches an asymptotic value of 1/5, as the solid line in Figure 4.19 shows. This seems to be contradictory to the well known fact that, under Wertheim's theory, virial coefficients do not scale correctly with the chain molecular weight in the long
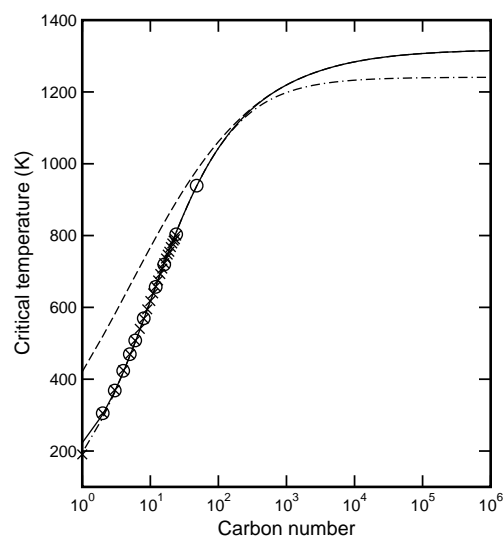
Figure 4.17: Critical temperature as a function of the number of monomer units. Crosses represent experimental data from Ambrose and Tsonopoulos [110] ($n \leq 24$) and from Nikitin [114] ($n \geq 26$). The remaining symbols are as in Figure 4.16.
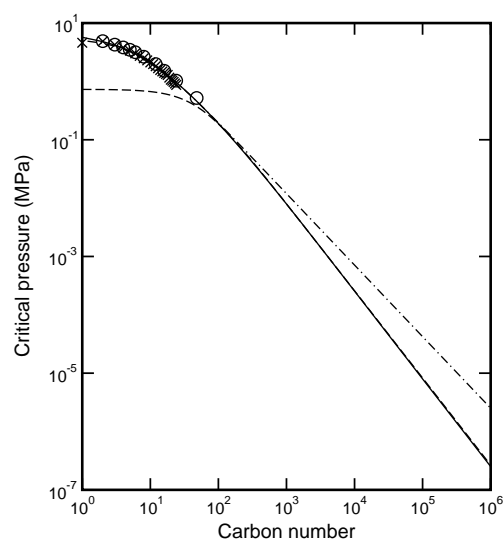
Figure 4.18: Critical pressure as a function of the number of monomer units. Symbols are as in Figure 4.16.
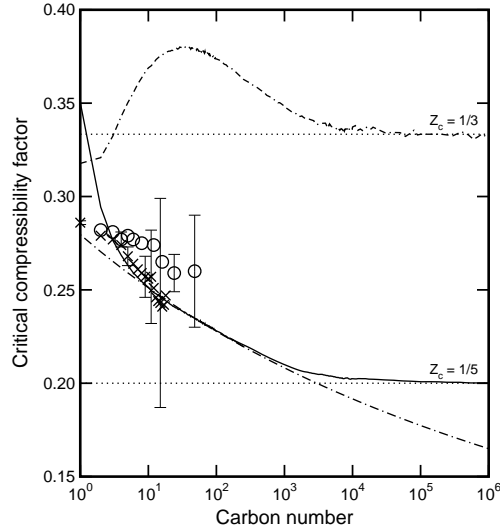
Figure 4.19: Critical compressibility factor as a function of the number of monomer units. The predictions from the soft-SAFT EOS are represented as a solid line, the dot-double dashed line corresponds to the soft-SAFT EOS results when using only the PVr$^\rho$ correlation of molecular parameters (see text), and the remaining symbols are as in Figure 4.16.

chain limit, and that the compressibility factor becomes 1/3 in this limit [132, 139]. This apparent contradiction can be explained in the following way. The use of two rescaled sets of molecular parameters implies that the compressibility factor $Zc(= P_c/[\rho_c k_B T_c])$ is not equal to the reduced compressibility factor Z_c^* ,

$$Z_c^* = \frac{P_c^*}{\rho_c^* T_c*} = \frac{P_c \hat{\sigma}^3/\epsilon}{\rho_c \sigma^3 k_B T_c/\epsilon}, \qquad (4.10)$$

because two different values of the size parameter are used. Note that Z_c approaches 1/3 as the chain length increases, for long chains [132]. Therefore,

$$\lim_{n \to \infty} Z_c(n) = \frac{1}{3} \frac{\sigma^3(n \to \infty)}{\hat{\sigma}^3(n \to \infty)} \simeq \frac{1}{5}, \qquad (4.11)$$

where the values of the size molecular parameters are calculated from eqs 4.7c-4.7d.

Lue *et al.* [139] stated that many fluid theories for chainlike molecules, like SAFT, yield a value for the critical compressibility factor in the limit of infinitely long chains that contradicts experimental trends. Although we agree with them, we think that the statement is somewhat risky since it is based on experimental data for very short

chains (up to 18 monomer units). Our results confirm that the soft-SAFT EOS predicts a reduced critical compressibility factor value of 1/3 in the long chain limit, consistent with Lue *et al.*'s statements. However, we have shown that if an appropriate rescaling of molecular parameters is performed (and using experimental data available only for very short chains), the equation yields a lower value, $Zc(\infty) = 1/5$. Whether this value coincides with the truly experimental one is a question for the future.

4.2.6 Conclusions

We have used the soft-SAFT EOS to predict the critical properties of pure short and long LJ chains up to 10^6 monomer units. The accuracy of the theory for predicting experimental data has been checked by direct comparison with experimental and simulation data for n-alkanes, available only for relatively short chains. In order to apply the equation to real systems, molecular parameters (chain length, monomer size and dispersive energy) must be fitted using experimental data, usually VLE data. The inability of the equation to predict critical properties accurately, due to its classical formulation, is overcome by a simple rescaling of these parameters to the experimental critical point. For the case of n-alkanes, a linear relationship between the rescaled fitted parameters and the molecular weight of the chain was observed. We have assumed that the proportionality of the molecular volume and dispersive energy with respect to molecular weight also holds for very long chains. This assumption allows us to predict the critical properties for longer chains, for which no simulation data are available. The physical meaning of the molecular parameters is a strong guarantee for successfully applying the equation to very long chains.

The theory quantitatively predicts available critical properties for relatively long chain lengths, and it shows a crossover to mean-field behaviour when the infinite chain length regime is reached, as may be inferred from Wertheim's theory. The mass critical density apparent scaling exponent changes from the value 1/3, found experimentally for short chains to 1/2 as predicted by the mean-field theories. It should be emphasized that the agreement with experimental data for short chains is due to the rescaling approach, since no crossover treatment for the critical region has been considered here. The critical temperatures follow the Shultz-Flory relationship, reaching an asymptotic value of $T_c(\infty) = 4.68$, and the critical pressures scale as $n^{-3/2}$.

We think that the success of the theory in predicting the critical point of short chains relies on the fact that the rescaling of the parameters takes into account in some way the effect of the long range fluctuations associated with this point. Since the scaling behaviour in the long chain regime does not depend on the molecular parameter values at all, because monomer size and dispersive energy become constant

and chain length is not longer important, classical exponents should be obtained for this regime.

Regarding the critical compressibility factor, the equation predicts a value of 1/5 for chains of infinite length. This is not contradictory to Wertheim's theory, which predicts an asymptotic value of 1/3, as explained in the previous subsection. The value of 1/5 is predicted using just experimental critical data for n-alkanes up to 18 monomer units and assuming that the volume and dispersive energy per molecule keep their proportionality to molecular weight for very long chains.

4.3 Solubility of hydrogen in heavy n-alkanes

*We present predictions on the solubility of hydrogen in several normal alkanes, ranging from decane and up to hexatetracontane. Optimized values for the chain length, LJ diameter and dispersive energy characterize the hydrogen molecule. The PV correlation is used for the n-alkanes. Two additional parameters, independent of the thermodynamic variables, were fitted to the experimental data of a single isopleth for each particular mixture. The agreement between the measured and predicted solubilities is excellent (overall AAD $<$ 1.5%) in all the thermodynamic range, and does not significantly worsen as the molecular weight of the compound increases.

4.3.1 Introduction

Hydrogen is a key compound in the production of fuels for the automotive industry and will acquire much more importance in the future, as the free carbon sources of energy tend to emerge for environmental reasons. Nowadays, hydrogen is mainly obtained from the catalytic steam reforming of nafta and natural gas, but renewable sources of energy seem to be promising for the near future. In many industrial processes where molecular hydrogen plays an important role, its solubility in different hydrocarbon solutions (e.g., fuels) is among the major factors required for design and optimal operation of these processes. It is also a key parameter in process models, such as the ones used in hydrogenation and hydrotreatment processes, where hydrogen solubility in selected liquid hydrocarbons is a good estimation of the hydrogen concentration in the liquid phase, a variable that is often related to kinetics.

It is well known that empirical and semiempirical models, like traditional cubic EOSs, have limited predictive capabilities, particularly outside the range where their parameters were fitted. On the contrary, parameters of molecular models based on statistical mechanics, like SAFT, have physical meaning and are independent of the thermodynamic conditions. Another important advantage of using a molecular-based theory, vs. simple mean-field approaches, is that one can explicitly consider intramolecular as well as intermolecular interactions among the chain molecules involved. Furthermore, the details of the applied intermolecular potential will be reflected in the accuracy of the thermodynamic properties calculated by using the theory. The goal of this work is to provide a reliable model for the prediction of vapour-liquid equilibria and the solubility of hydrogen in n-alkanes. To this end, calculations

---

*Section accepted for publication as an article in *AIChE J.*

Table 4.6: Molecular parameters for the pure compounds

	m	σ (Å)	ϵ/k_B (K)
H_2	0.4874	4.244	33.85
$n\text{-}C_{10}$	4.259	3.983	272.7
$n\text{-}C_{16}$	6.407	4.015	285.0
$n\text{-}C_{28}$	10.70	4.041	294.7
$n\text{-}C_{36}$	13.57	4.049	297.8
$n\text{-}C_{46}$	17.86	4.056	300.6

have been carried out for the following binary hydrogen + n-alkane systems: H_2 + $n\text{-}C_{10}$, H_2 + $n\text{-}C_{16}$, H_2 + $n\text{-}C_{28}$, H_2 + $n\text{-}C_{36}$, and H_2 + $n\text{-}C_{46}$.

4.3.2   Phase-equilibria calculations

Molecular parameters for pure H_2 have been calculated by fitting experimental pure hydrogen saturated liquid densities and vapour pressures [107]. Because of the type of model used, the m parameter is allowed to be a fractional number in order to account in some way for the nonsphericity of the molecule. In the next section we will show that this approach is not unrealistic for obtaining excellent results. For n-alkanes, we employ the PV correlation recently published by [118]. All values are given in Table 4.6. The PV correlation comes from the optimized parameters for the first eight members of the series, and it has been proven to provide very accurate results for vapour-liquid properties of pure heavy n-alkanes and their mixtures [118].

Figure 4.20 shows the coexisting vapour-liquid densities and vapour pressures of pure hydrogen. Crosses are experimental data [107]. The solid line corresponds to predictions from the equation, using the molecular parameters shown in Table 4.6. As can be observed in the figure, the parameters have been optimized for the subcritical region. Although EOSs with a classical formulation can accurately describe the phase behaviour of pure fluids and mixtures far from the critical point, they are unable to predict the near-critical region. This problem also can be explained as a difficulty in describing of the critical compressibility factor and critical exponents [136]. To overcome this limitation, a crossover treatment has been used recently in several works. See, for example, the work of [109]. An alternative approach is to rescale the molecular parameters to the critical point [117].

SAFT predictions in Figure 4.20 do not cover the temperature region below 16 K, because of the range of validity of the reference EOS for the LJ fluid: the temperature range covered by the molecular simulation data that this equation correlates
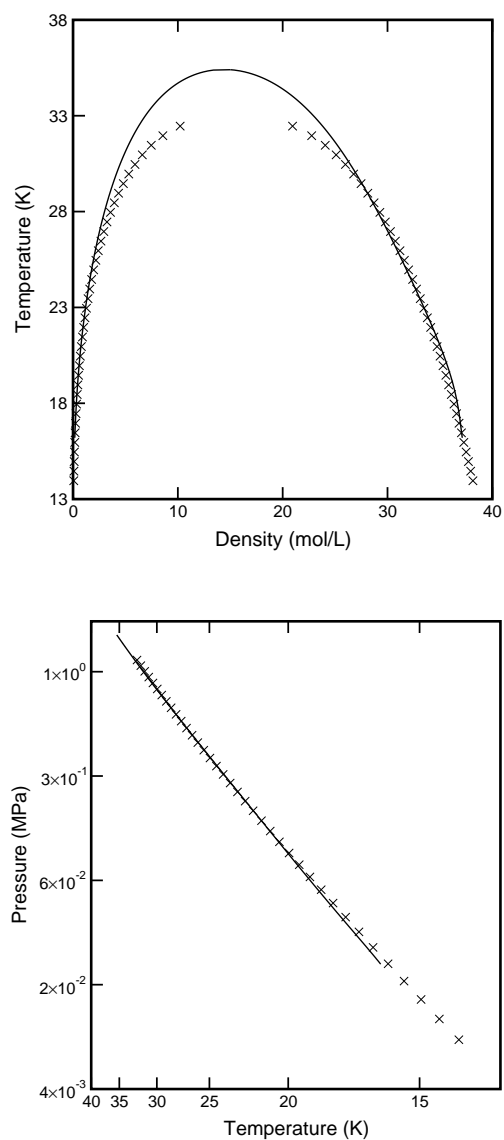
Figure 4.20: (a) Coexisting saturated densities of pure hydrogen. (b) Vapour pressures of pure hydrogen in a log-log plot. Symbols are experimental data from the NIST chemistry Webbook [107] and the line corresponds to predictions of SAFT with optimized parameters for the subcritical region.

Table 4.7: Size binary parameter for the mixtures

	η
n-C_{10}	0.8650
n-C_{16}	0.8777
n-C_{28}	0.8893
n-C_{36}	0.8918
n-C_{46}	0.8933

is approximately $0.7 \leq T^{\star} \leq 6.0$. Therefore, although some extrapolation is possible, as shown in these plots, consistent results are not guaranteed. For this reason, experimental data under 23.7 K ($T^{\star} = 0.7$) was not used in the optimization of the parameters for the hydrogen molecule.

Because of the asymmetry of the binary mixtures we are dealing with, the two cross-interaction binary parameters η and ξ should also be fitted using experimental data. The set that we use was published by Florusse *et al.* [140]. One of the main advantages of using such a molecular-based EOS is that parameters should not depend on the thermodynamic conditions. Hence, the procedure that we take is to use a *single set* of measured data, for example, along an isopleth, to adjust the size parameter while maintaining the energy parameter at a constant optimized value along the homologous series. Then we use the optimized values to predict equilibrium properties at any other thermodynamic condition. The fitted values of the cross-interaction size parameter are given in Table 4.7. The energy parameter was fixed at $5.000 \, 10^{-2}$. This number makes the hydrogen-alkane segment cross-interaction energy ϵ_{12} much lower than the interaction energy of the alkane-alkane and hydrogen-hydrogen segments, which is consistent with the low solubilities measured. Figure 4.21 shows the trend of the size parameter with respect to the carbon number of the normal alkane. This trend is the same as that of the size parameter σ of the n-alkane homologous series [118], and asymptotically tends to a constant value as the length of the chain increases, representing the effective value for the H_2-CH_2 group. Additionally, the alkane chain length times η varies linearly with the carbon number, which easily allows us to obtain, with confidence, the η values for other H_2 + n-alkane mixtures.

4.3.3 Results and discussion

We present predictions of the soft-SAFT EOS for the solubility of H_2 in n-decane, n-hexadecane, n-octacosane, n-hexatriacontane, and n-hexatetracontane. We also check the performance of the modified PR EOS, as found in the Hysys Plant 2.4.1
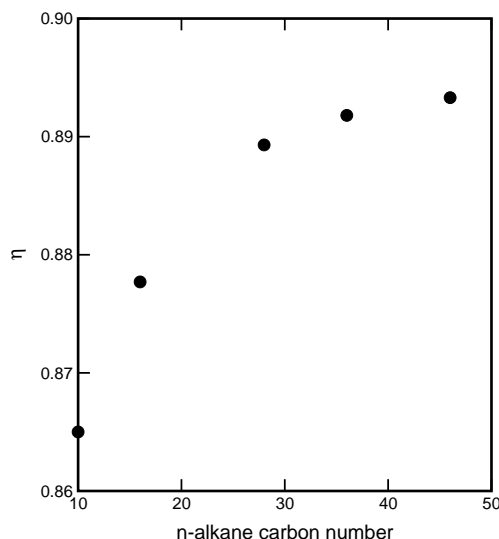
Figure 4.21: Size binary parameter as a function of the carbon number of the alkane in H_2 + n-alkane mixtures.

process-engineering simulator. Several reasons led us to choose this equation for comparison. On the one hand, PR is one of the most used equations in the process industry, and it has been proven to provide very good predictions for alkane binary systems (see [118], and references therein). On the other hand, we found it very appropriate to use a version embedded in a commercial package, since this is the path engineers usually take in order to use phase-equilibrium data for the design and optimization of chemical processes.

In Figure 4.22 the symbols represent primary experimental data (isopleths) [140]. The symbols in Figure 4.23 represent the solubility of H_2 in liquid n-decane for a number of isotherms, which have been calculated from the primary experimental data, as depicted in Figure 4.22. In both Figures the solid lines are the soft-SAFT predictions using the parameters of Tables 4.6 and 4.7. Excellent agreement is obtained, with an AAD of about 0.8%. Only about 12.5% of the measurements have been used to fit the cross-interaction parameters, but it is impossible to distinguish which of the isopleths in Figure 4.22 was chosen. Dot-dashed lines in this figure correspond to predictions using the PR EOS, which are shown for three selected isopleths. This EOS performs equally well as the soft-SAFT EOS, except at low temperatures, where it declines toward lower pressures.

Figures 4.24 and 4.25 show experimental data [140] and theoretical results for the
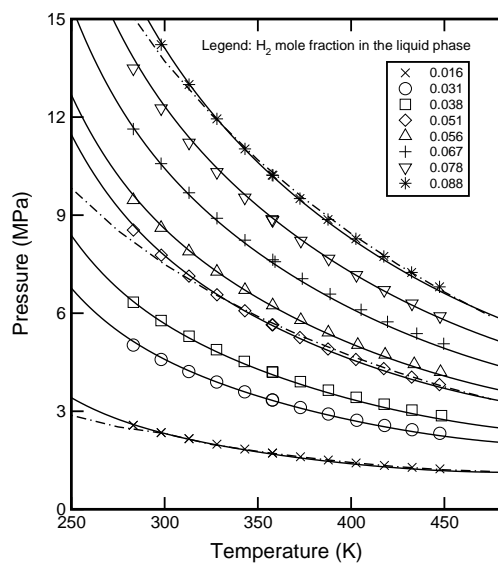
Figure 4.22: Isopleths of the H_2 + n-decane VLE. Symbols are used for experimental data [140]. Solid and dot-dashed lines show soft-SAFT and PR predictions, respectively.
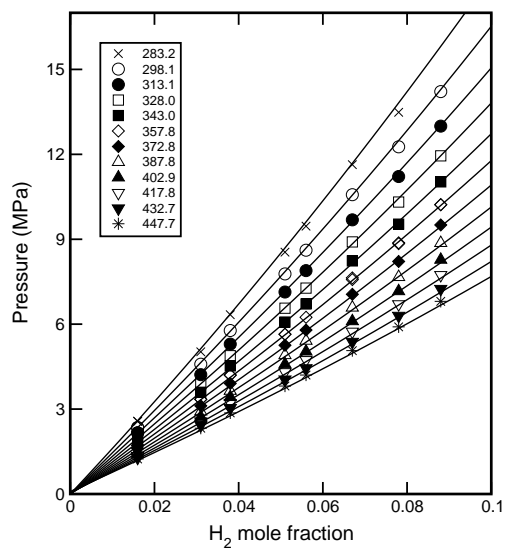
Figure 4.23: Solubility of hydrogen in n-decane, for selected isotherms. Symbols as in Figure 4.22. Temperatures are given in K.
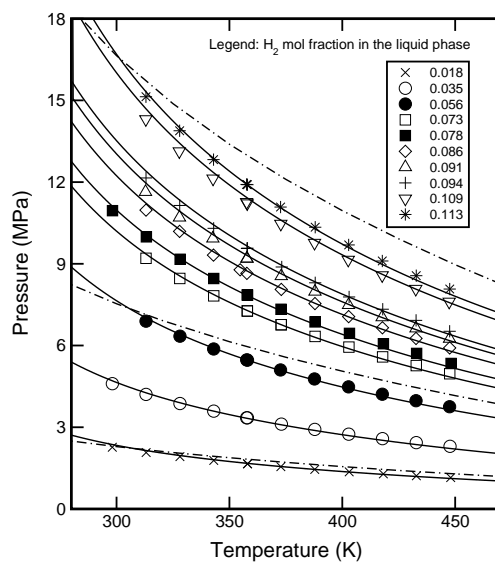
Figure 4.24: Isopleths of the H_2 + n-hexadecane VLE. Symbols as in Figure 4.22.
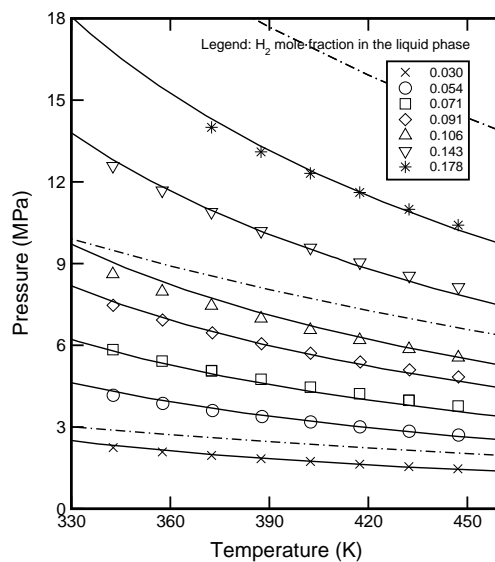
Figure 4.25: Isopleths of the H_2 + n-octacosane VLE. Symbols as in Figure 4.22. PR lines correspond to mole fraction values of 0.030, 0.091, and 0.178.

$H_2 + n\text{-}C_{16}$ and $H_2 + n\text{-}C_{28}$ mixtures, respectively. In these figures, the accuracy of the SAFT predictions is similar to that obtained for the lighter alkane (n-decane). On the other hand, the performance of the PR EOS rapidly deteriorates, and this is more noticeable at the largest mole fraction values of H_2 in the liquid phase.

In Figures 4.26 and 4.27 we check the performance of both the soft-SAFT and PR EOSs compared to experimental data from [141], which were measured up to much higher pressures and temperatures than were those we present in this study. The results are a very severe test for the performance of both EOSs in these systems. Data up to 25 MPa and 665 K are used for comparison. No fitting to these data was performed. Cross-interaction parameters for this mixture were optimized using the experimental data of a single isopleth selected from those shown in Figure 4.24, which are at rather lower pressures and temperatures. Predictions from the SAFT equation are excellent for the liquid phase (Figure 4.26). Poorer results were expected for the vapour phase (Figure 4.27), since no information of this phase was used in the optimization of cross-interaction parameters. However, the excellent accuracy of SAFT predictions for the H_2 solubility in the liquid phase, on which this study is focused, is remarkable.

PR solubility predictions are much less accurate, although vapour-phase compositions are captured better by PR than by SAFT. We are aware of the somewhat unfair comparison between both EOSs, because we did not fit any parameter of the PR equation. As mentioned before, our aim is to show the performance of the Hysys modified version of the PR EOS, with all parameters from the Hysys database. It has already been proven [142] that the fitting of the PR binary interaction parameter to *each* experimental isotherm will provide much better results. But the predictive capability of the EOS is not shown in this way. The performance of the PR equation depends strongly on the α function and the binary interaction parameter used. Although the effect of the binary parameter can be minimized through an optimized temperature-dependent α function [143], we believe that to fit parameters depending on temperature is an unavoidable requirement for obtaining accurate predictions using cubic EOSs. On the contrary, the soft-SAFT EOS does not have temperature-dependent parameters, and we only use data of a *single* experimental isopleth for the optimization of the binary interaction parameter of the mixture. In this way, we use SAFT in a fully predictive way at other thermodynamic conditions.

Figures 4.28 and 4.29 present experimental data [140], and model predictions for the binary systems $H_2 + n\text{-}C_{36}$ and $H_2 + n\text{-}C_{46}$, respectively. Due to the proximity to the triple point of the n-hexatetracontane, no thermodynamically consistent solutions for the SAFT EOS could be obtained below approximately 400 K. These stringent thermodynamic conditions lie far beyond the thermodynamic range of validity of the LJ reference EOS (see the section entitled Phase-equilibria calculations). The same
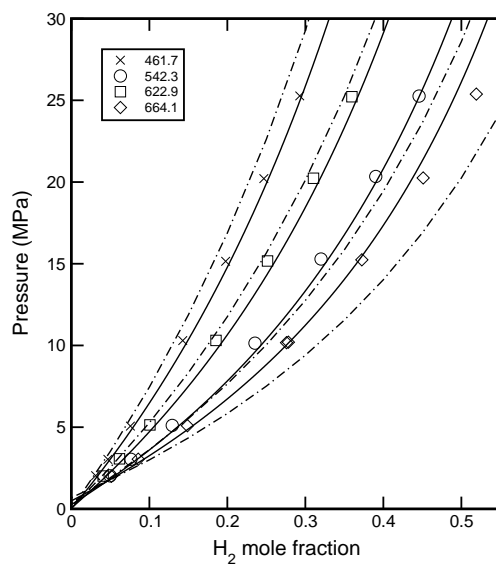
Figure 4.26: Solubility of H_2 in n-hexadecane, for selected isotherms (in K). Symbols as in Figure 4.22. Experimental data are taken from [141].
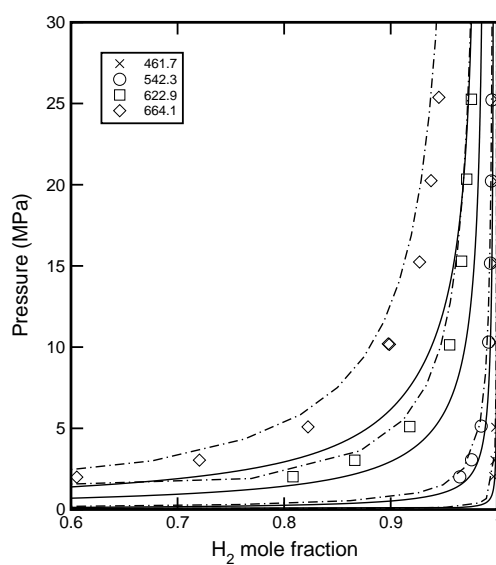
Figure 4.27: Equilibrium mole fraction of hydrogen in the vapour phase of the $H_2 + n$-hexadecane mixture, for selected isotherms (in K). Symbols as in Figure 4.22. Experimental data are taken from [141].
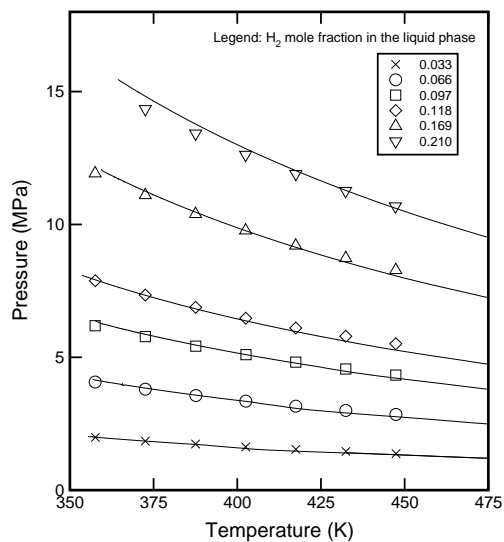
Figure 4.28: Isopleths of the H$_2$ + n-hexatriacontane VLE. Symbols as in Figure 4.22.
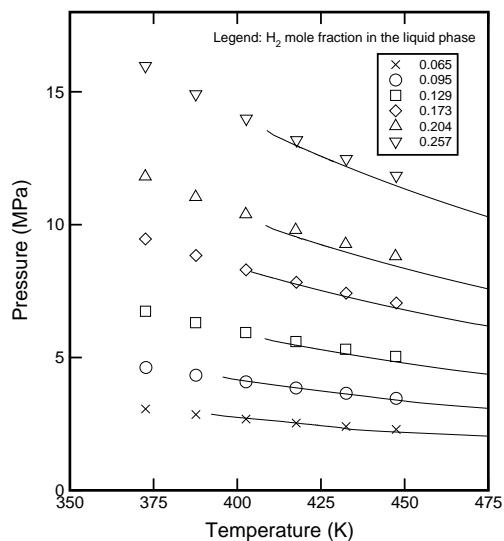
Figure 4.29: Isopleths of the H$_2$ + n-hexatetracontane VLE. Symbols as in Figure 4.22.

reasoning can be used for the $H_2 + n$-C_{36} mixture below approximately 360 K (Figure 4.28). Nevertheless, accuracies remain as low as for those mixtures with the lower chain-length alkanes, except for the highest solubilities of H_2, where deviations can increase up to an AAD of 2.5%. Consequently, the length of the alkane chain does not significantly influence the accuracy of the predictions, at least for the range of chain length studied here. The overall AAD of soft-SAFT predictions with respect to solubility measurements is less than 1.5%. PR predictions are not included in Figures 4.28 and 4.29, since the two heaviest alkanes are not available in the Hysys Plant library.

To summarize, the molecular model, in conjunction with the soft-SAFT theory, provides very reliable results for the solubility of H_2 in n-alkane systems in a wide range of pressures and temperatures. Furthermore, the accuracy of the predictions is independent of the thermodynamic conditions and the length of the alkane chain. It is also important to note that, to some extent, the success of the soft-SAFT theory relies on the physical meaning of the molecular parameters (e.g., segment size, dispersive energy, and chain length). Although their values are effective, their physical meaning is conserved, as we have already seen in Figure 4.21. As was recently discussed [118], parameters should be optimized by considering the experimental information range needed to later reproduce the thermodynamic features of interest. For $H_2 + n$-alkane mixtures, the experimental data from a single isopleth suffices to provide excellent predictions, provided that molecular parameters have been optimized following a meaningful trend.

4.3.4 Conclusions

SAFT modelling of the solubility of hydrogen in heavy n-alkanes has been presented. For the five selected mixtures studied ($H_2 + n$-C_{10}, $H_2 + n$-C_{16}, $H_2 + n$-C_{28}, $H_2 + n$-C_{36} and $H_2 + n$-C_{46}), the data covered a temperature range from about 280 K up to 450 K, and pressures raise up to 16 MPa. Optimized values for the VLE of the pure compounds are used to predict the behaviour of the mixtures. In addition, the size binary interaction parameter of the generalized Lorentz-Berthelot combining rules was fitted to experimental data of a single isopleth and used to quantitatively describe the same system in the whole range of experimental conditions, in a fully predictive manner.

The overall absolute averaged deviation of SAFT predictions with the experimental data is less than 1.5%. SAFT predictions are excellent over the entire thermodynamic range where data were measured. The accuracy is independent of the thermodynamic variables, and does not get significantly worse as the chain length of the n-alkane increases. Consequently, it is proven that for very asymmetric H_2

$+$ n-alkane systems, the soft-SAFT molecular model is able to provide very accurate and reliable results whenever optimized parameters remain meaningful, that is, follow physically meaningful trends.

4.4   Solubility of gases in n-perfluoroalkanes

A molecular model within a SAFT context for quantitatively predicting the solubility of xenon and oxygen in n-perfluoroalkanes is presented and discussed here. Optimized meaningful values of both molecular parameters for the pure perfluoroalkanes are also used to accurately predict vapour-liquid and liquid-liquid equilibria of n-alkane $+$ n-perfluoroalkane mixtures. Due to the high nonideality of the mixtures, the Lorentz-Berthelot cross-interaction parameters need to be adjusted using experimental data and ensuring coherent trends. An accurate description of the solubility of oxygen requires additional information to be included in the model. On the basis of *ab initio* arguments, we considered cross-association between oxygen and perfluoroalkane molecules, which allows solubilities to be described with a deviation below 5%, when compared to experimental data available in the literature.

4.4.1   Introduction

Perfluoroalkanes are completely fluorinated alkanes with particular physicochemical properties due to the high intramolecular and low intermolecular forces that characterize them. Nowadays, they are being used in a widely variety of fields ranging from industrial to biomedical applications. In industry, they are being used as substitutes for chlorinated solvents due to the fact that they are nontoxic and do not deplete stratospheric ozone [144]. Furthermore, fluorinated solvents are immiscible with both hydrocarbons and water [145], which facilitates their removal from the reaction medium by simple phase separation and filtration, and also recycling of the solvent. Due to their high solubility in CO_2, fluorocarbons are currently employed as CO_2-philic compounds in many chemical and analytical applications where supercritical or liquid CO_2 is used as a "green" alternative to conventional organic solvents [146]. For medical applications, perfluoroalkanes and other fluorinated liquids are used as oxygen carriers in artificial blood substitutes [147], due to the high solubility of oxygen in these compounds and their chemical and biological inertness. Liquid and gaseous perfluoroalkanes are also used as high-density intra-operative fluids for eye surgery [148]. They show high solubilities of xenon as well and, for that reason, they are being used as intravenous delivery media for laser-polarized xenon for in vivo magnetic resonance applications [149].

According to the exposed above, the study of the solubility of gases in liquids is still an actual issue due its importance in many industrial chemical processes,

---

*Section accepted for publication as an article in *J. Phys. Chem. B.*

environmental studies, and also the medical field. From the fundamental scientific point of view, it also plays an important role in the understanding of the interactions among molecules. It is in this context that we present this work. Empirical and semi-empirical models, like traditional cubic EOSs, have proved to have limited predictive capabilities, particularly outside the range where their parameters were fitted. On the other hand, molecular models based on statistical mechanics, like SAFT, use parameters with physical meaning and independent of the thermodynamic conditions. In addition, the use of these molecular based models allows one to explicitly consider intra-molecular and/or intermolecular interactions among the chain molecules involved, and to obtain additional information about the way molecules interact among themselves and with others when in solution.

There exist in the literature several works concerning the modelling of perfluorocarbon systems, including molecular simulations and EOS's. An effort has been devoted some years ago toward the development of accurate force fields for the linear perfluoroalkanes [150, 151]. These force fields have been applied to predictions of phase equilibria and critical properties of pure perfluoroalkanes, and the solubility of xenon in n-perfluorohexane [152]. On the other hand, the SAFT-VR approach, in addition to the aforementioned systems, has also been used for the prediction of phase equilibria of alkane + perfluoroalkane mixtures [153]. However, to our best knowledge, no modelling attempt of the solubility of oxygen in perfluoroalkanes within a SAFT context has been performed yet.

The goal of this work is to provide a reliable model based on the soft-SAFT EOS, for the prediction of the solubility of gases in perfluoroalkanes as well as the VLE and LLE for n-alkane + n-perfluoroalkanes mixtures. The EOS is first applied to the study of mixtures of molecules with similar size, which is the case of the n-alkane + n-perfluoroalkanes mixtures. The study of the nonsimilar gas + perfluoroalkanes systems will provide information about the behaviour of small inert molecules, such as xenon, and small noninert molecules, such as oxygen, in solution with perfluoroalkanes. We do not apply SAFT to oxygen + alkane mixtures because of the infeasibility of evaluating the model, since the existing experimental data are scarce and deviations among sources are significant [154–156].

4.4.2 Molecular model

Values for the molecular parameters of pure compounds are usually adjusted by minimizing deviations from the theory with respect to VLE experimental data. Nevertheless, whenever possible, it is worthy to use physical information in order to minimize the number of parameters to be optimized. In this manner, we set the m parameter of xenon to unity because it is spherical. Furthermore, experimental studies indicate that

Table 4.8: Optimized molecular parameters for the pure compounds.

	m	σ (Å)	ϵ/k_B (K)
O_2	1.168	3.198	111.5
Xe	1.000	3.953	222.6
CF_4	1.000	4.217	190.1
C_2F_6	1.392	4.342	204.5
C_3F_8	1.776	4.399	214.7
n-C_4F_{10}	2.134	4.433	223.0
n-C_5F_{12}	2.497	4.449	230.2
n-C_6F_{14}	2.832	4.479	236.6
n-C_7F_{16}	3.169	4.512	242.7
n-C_8F_{18}	3.522	4.521	245.1

C-C bond lengths for crystalline polytetrafluoroethylene and polyethylene are equivalent [150]. Hence, we set the values of the m parameter for n-perfluoalkanes equal to those optimized for the n-alkanes in section 4.1. The remaining molecular parameters of the nonassociating model for the pure compounds were calculated by fitting vapour pressures and saturated liquid densities to experimental data [107, 157–162] away from the critical region, and they are listed in Table 4.8. n-Perfluorooctane is the heaviest member of the series for which enough experimental data is available in the literature.

From the optimized parameters for the perfluoroalkanes, we provide a simple relationship of the molecular parameters with the carbon number in eqs 4.12a-4.12c. Units of σ and ϵ/k_B are Å and K, respectively.

$$m = 0.3580CN + 0.6794 \qquad (4.12a)$$

$$m\sigma^3 = 35.53CN + 42.27 \qquad (4.12b)$$

$$m\epsilon/k_B = 96.42CN + 92.25 \qquad (4.12c)$$

Parameters from these relationships deviate from the fitted parameters with an AAD equal to 0.8%. Eqs 4.12a-4.12c allow the transferability of parameters within the perfluoroalkane series.

One of the advantages of molecular theories compared to macroscopic models is that the formers need fewer parameters which are meaningful. To provide additional evidence of this, optimized size and energy parameters are plotted in Figure 4.30 with respect the carbon number CN of the n-perfluoroalkane chain. Since the model is homonuclear and the effect of the extreme CF_3 groups weakens as the chain length
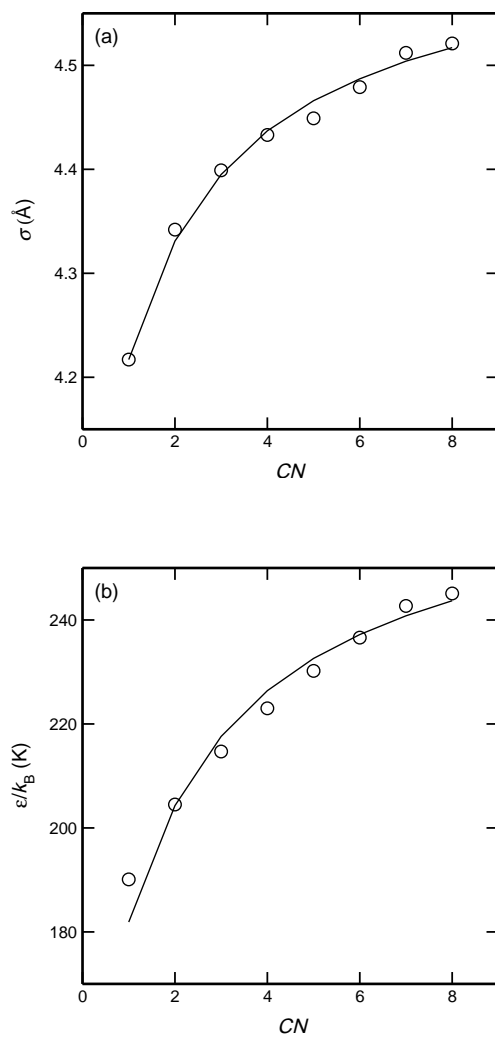
Figure 4.30: Molecular parameters for n-perfluoroalkanes: (a) segment diameter; (b) dispersive energy. Lines correspond to the values from the relationships of eqs 4.12a-4.12c.

increases, the LJ parameters should tend to an asymptotic value, as seen in Figure 4.30. Furthermore, molecular simulation united-atom models [150, 163] in which the LJ potential for the nonbonded interactions is used (without coulombic interactions) employ optimized values for the size parameter in the range $\sigma_{CF_2} = \sigma_{CF_3} = 4.65 \pm 0.05$ Å. These simulations give quantitative predictions for equilibrium properties of chains from n-perfluoropentane to n-perfluorohexadecane. The corresponding value from our model (equivalent to a chain of infinite number of carbons), straightforwardly calculated from eqs 4.12a-4.12c, is 4.63 Å. The similarity among the parameters from different theories acts in favor of the physical meaning of them.

4.4.3   Results and discussion

Once a molecular model in the SAFT framework is defined and appropriate values for the molecular parameters of pure compounds have been determined, we use the soft-SAFT EOS to predict the equilibrium properties of several mixtures of n-alkane + n-perfluoroalkane, and the solubility of xenon and oxygen in n-perfluoroalkanes from C_6 to C_9. Then, the accuracy of SAFT predictions will show the suitability of the molecular model for these perfluorocarbon systems.

In Figures 4.31a and 4.31b vapour-liquid coexisting densities and vapour pressures, respectively, of pure oxygen and pure xenon are shown. Symbols are experimental data taken from NIST Chemistry Webbook [107], whereas solid lines correspond to the soft-SAFT EOS. Subcritical equilibrium properties are accurately reproduced. Because of the classical formulation of the equation as it is used here, temperatures and pressures in the critical region are overpredicted. There exist ways to overcome this problem, either by fitting parameters to the critical point [117] or, in a more fundamental approach, including a crossover treatment [164]. Any of the methods will necessarily require of additional parameters or, at least, a new fitting to experimental data. Thus, because this work is focused on equilibrium properties far from the critical region, and also for consistency with previous works [117, 118], we use parameters fitted to subcritical VLE data.

Figures 4.32a and 4.32b present equilibrium liquid densities and vapour pressures, respectively, of pure n-perfluoroalkanes from n-perfluorohexane to n-perfluorooctane. Lines are soft-SAFT predictions using the parameters given in Table 4.8. Saturated liquid densities and vapour pressures are correlated with an AAD less than 0.5% and 7%, respectively. In the case of n-perfluorononane, since only experimental density data are available [160], we used the correlations of parameters for the n-perfluoroalkane series given by eqs 4.12a-4.12c. The agreement of the predicted density, with an AAD of 0.21%, is good, as for the rest of the perfluoroalkanes studied.

A more severe way to test the model and correctness of the parameters for the
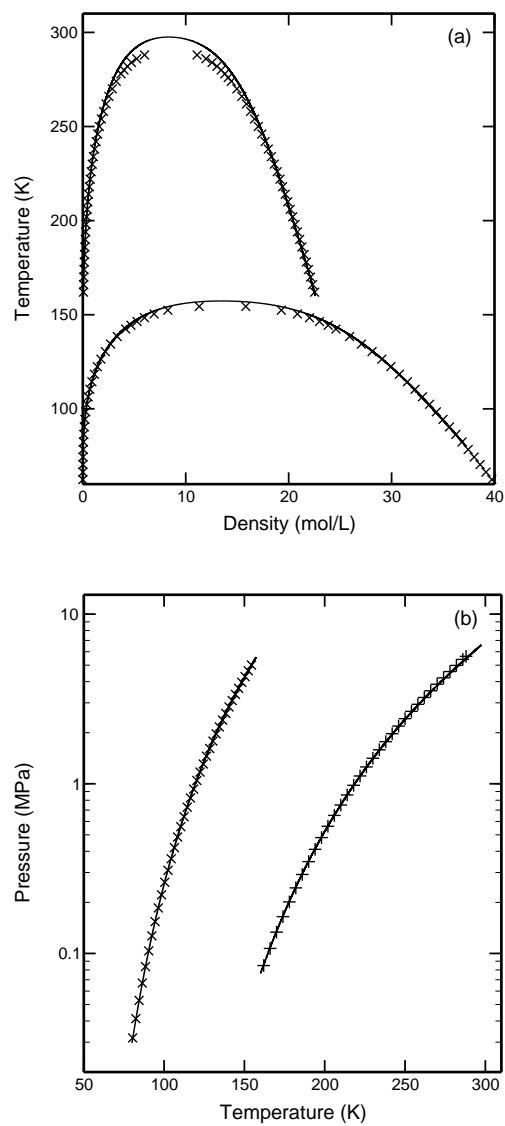
Figure 4.31: (a) Coexisting densities and (b) vapour pressures of pure oxygen (crosses) and xenon (plusses). Symbols are experimental data [107] and lines correspond to the soft-SAFT model with optimized parameters.
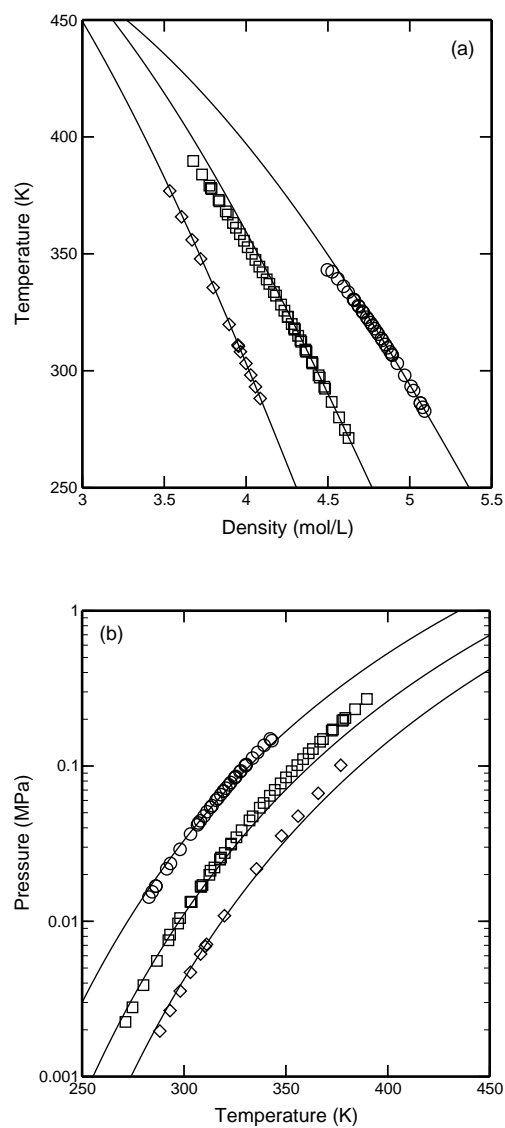
Figure 4.32: (a) Coexisting densities and (b) vapour pressures of n-perfluorohexane (circles), n-perfluoroheptane (squares) and n-perfluorooctane (diamonds). Symbols are experimental data (vapour pressures from reference [160] for C_6, [161] for C_7, [162] for C_8, and densities from [160]) and lines correspond to the soft-SAFT model with optimized parameters.
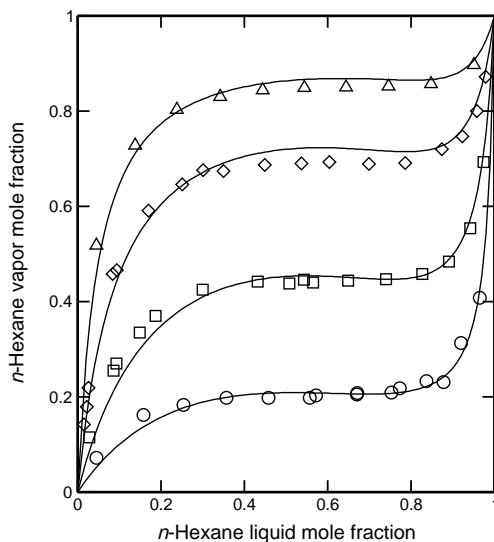
Figure 4.33: Vapour-phase mole fraction versus the liquid mole fraction for n-hexane + n-perfluoroalkane mixtures: $n = 5$ at 293.15 K (circles), $n = 6$ at 298.15 K (squares), $n = 7$ at 303.15 K (diamonds), and $n = 8$ at 313.15 K (triangles). Symbols represent experimental data [165] and lines correspond to the predictions from the soft-SAFT EOS.

perfluoroalkanes is to predict equilibrium curves of highly nonideal mixtures and compare them to experimental data. As a first case, we selected several n-alkane + n-perfluoroalkane mixtures of similar chain-length components, and make use of the fact that the molecular model and parameters for the normal alkanes have been broadly tested in previous works [118, 140], shown in sections 4.1 and 4.3.

Equilibrium diagrams of binary mixtures of n-perfluorohexane + n-alkane from (C_5-C_8) and of n-hexane + n-perfluoroalkane from (C_5-C_8) are presented in Figures 4.33-4.36. These binary n-alkane + n-perfluoroalkane mixtures belong to the type II phase behaviour in the classification of Scott and van Konynenburg [166] (characterized by a continuous vapour-liquid critical line and the presence of liquid-liquid phase separation) when the difference in chain length between the two components is not very large. Due to the nonideal interactions in these mixtures, the unlike energy parameter was treated as adjustable, and it was set at the optimum value $\xi = 0.9146$ for the correct prediction of the experimental azeotrope [165] of the n-hexane + n-perfluorohexane mixture at 298.15 K. Afterward, in a transferable manner, we used the same optimized value to predict the rest of the mixtures at different thermodynamic conditions. The unlike size parameter was not adjusted ($\eta = 1$), because we

verified that the simple Lorentz combination rule provided satisfactory results.

Figures 4.33 and 4.34 present composition diagrams of n-hexane + n-perfluoroalkane and n-perfluorohexane + n-alkane mixtures, respectively, and Figure 4.35 depicts vapour pressures of two of the systems shown in Figure 4.34. Very good agreement is obtained between soft-SAFT predictions and experimental data [165] in all cases, considering that the average uncertainty of the experimental compositions is 4%. The AADs of the SAFT predictions for compositions and pressures are less than 5% in all of the cases. At this point, it is worth mentioning that certain values of the binary parameters can originate s-shaped curves in the composition diagrams, wrongly predicting LLE. This is more likely to happen when one tries to reproduce vapour pressures with better accuracy than compositions. We could adjust the binary interaction parameters to completely avoid the appearance of s-shaped lines, but then deviations from experiments will largely increase. Therefore, because we want to retain this approximate model with the minimum parametrization, we should find a compromise. Consequently, although we tried to minimize the problem of s-shaped lines in Figures 4-6, we preferred to focus on the quantitative prediction of vapour-liquid equilibrium compositions. These systems have also been studied by McCabe *et al.* [153] using the SAFT-VR. Since they focused on the critical region, using rescaled parameters to the critical points of the pure components, the predictions that they provide for subcritical properties are fairly less accurate.

We also performed calculations of LLE properties for the systems for which experimental data are available [165], and they are presented in Figure 4.36. As a further verification of the transferability of parameters, we took the same values for the binary energy parameters used in the former VLE predictions, and hence no fitting to LLE data was done. Since the equation as it is used here does not correctly model the critical region, we expected SAFT to overpredict the UCST. However, although most of the experimental points are located in the critical region, it is observed that the shape of the curve is correct and the quantitative prediction of the low-temperature region is acceptable.

As a summary up to this point, the soft-SAFT model presented here allows the phase behaviour of n-alkane + n-perfluoroalkanes of similar chain length to be quantitatively predicted with the use of a single binary parameter. This parameter was adjusted using only the vapour-liquid equilibrium data near the azeotropic point of one mixture at a given temperature. This acts in favor of the transferability of the molecular parameters used.

It is known that xenon can be considered as the first member of the n-alkane series [167] in terms of phase-equilibria properties. Because of this similarity, our model for xenon with perfluoroalkanes should also provide satisfactory results, as it occurred with n-alkane + n-perfluoroalkane mixtures. Additionally, differences in size have
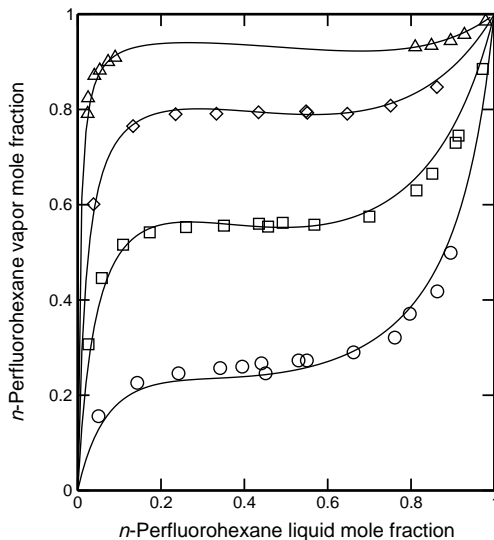
Figure 4.34: Vapour-phase mole fraction versus the liquid mole fraction for n-perfluorohexane + n-alkane mixtures: $n = 5$ at 293.65 K (circles), $n = 6$ at 298.15 K (squares), $n = 7$ at 317.65 K (diamonds) and $n = 8$ at 313.15 K (triangles). Symbols represent experimental data [165] and lines correspond to the predictions from the soft-SAFT EOS.

Table 4.9: Adjusted binary parameters for the solubility of xenon and oxygen in perfluoroalkanes, and AADs of the calculations by the soft-SAFT EOS with respect to experimental data.

	η	ξ	AAD (%)
Xe + n-C$_6$F$_{14}$	0.7970	0.8160	2.4
Xe + n-C$_7$F$_{16}$	0.8770	0.8160	2.0
Xe + n-C$_8$F$_{18}$	0.8880	0.8160	0.7
O$_2$ + n-C$_6$F$_{14}$	1.116	0.3200	4.5
O$_2$ + n-C$_7$F$_{16}$	1.381	0.8290	3.4
O$_2$ + n-C$_8$F$_{18}$	1.599	1.044	4.0
O$_2$ + n-C$_9$F$_{20}$	1.921	1.200	2.0
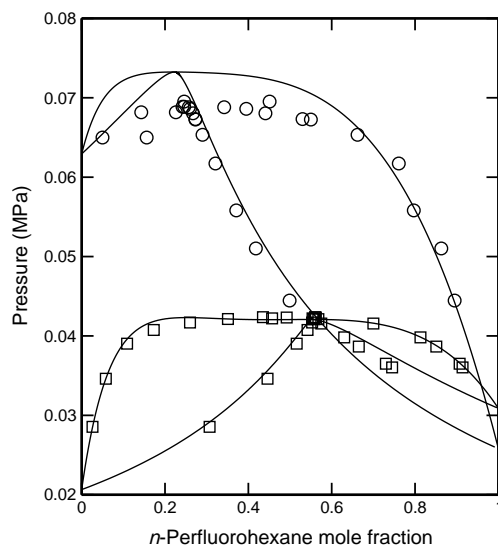
Figure 4.35: Vapour pressures of n-perfluorohexane + n-pentane and n-perfluorohexane + n-hexane. Thermodynamic conditions and symbols as in Figure 4.34.
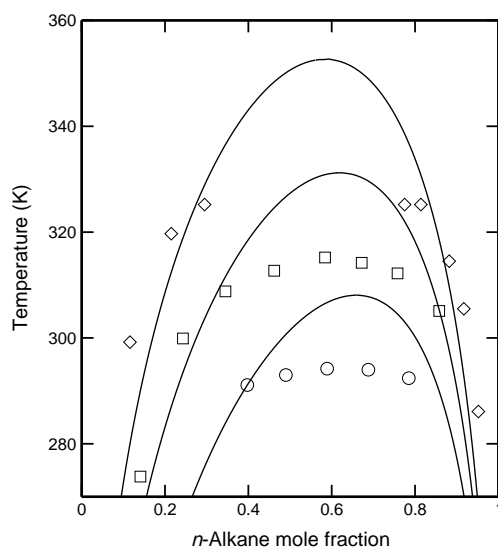
Figure 4.36: LLE of n-perfluoroalkane + n-alkane mixtures at 0.1 MPa: $n = 6$ (circles), $n = 7$ (squares) and $n = 8$ (diamonds). Symbols represent experimental data [165]. Solid lines correspond to the predictions from the soft-SAFT EOS.
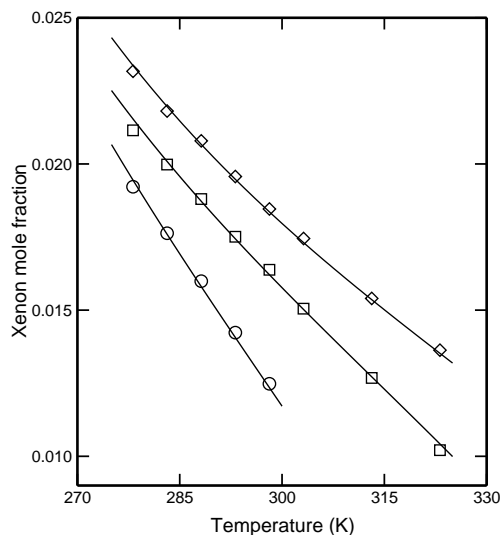
Figure 4.37: Solubility of xenon in linear perfluoroalkanes at 1 atm. Symbols represent experimental data [167] for *n*-perfluorohexane (circles), *n*-perfluoroheptane (squares) and *n*-perfluorooctane (diamonds) at 1 atm. Solid lines correspond to the predictions from the soft-SAFT EOS.

now a noticeable effect. We provide soft-SAFT predictions for the solubility of xenon in *n*-perfluorohexane, *n*-perfluoroheptane and *n*-perfluorooctane at 1 atm, which are presented in Figure 4.37. The experimental data shown in this plot were calculated from the Ostwald coefficients reported in the literature [168]. Binary interaction parameters were adjusted for each mixture, and they are listed in Table 4.9. Note that the energy binary parameter is set constant for all of the mixtures with xenon, as we did with the *n*-alkanes + *n*-perfluoroalkanes mixtures. Although the agreement is excellent (see also Table 4.9 for AADs), the predictive capability of the model and parameters cannot be tested for these mixtures at other conditions because, to our best knowledge, there is no additional experimental solubility data available in the literature.

In principle, given that the soft-SAFT model without considering association has proved to provide reliable quantitative predictions for the xenon + *n*-perfluoroalkane and *n*-alkane + *n*-perfluoroalkane systems, one could expect a similar achievement for the solubility of oxygen in linear perfluoroalkanes. However, the comparison with our measurements, calculated from the Ostwald coefficients measured by Dias [169] and presented in Figure 4.38, shows that the soft-SAFT model without association
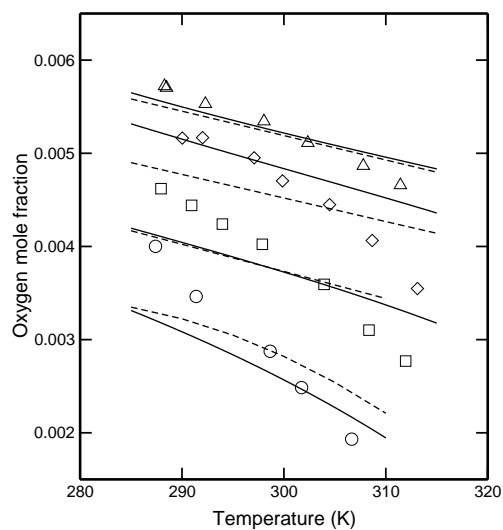
Figure 4.38: Solubility of oxygen in linear perfluoroalkanes at 1 atm. Symbols represent experimental data [169] for n-perfluorohexane (circles), n-perfluoroheptane (squares), n-perfluorooctane (diamonds) and n-perfluorononane (triangles). Lines correspond to the PR (dashed) and the soft-SAFT equations with the nonassociating model (solid).
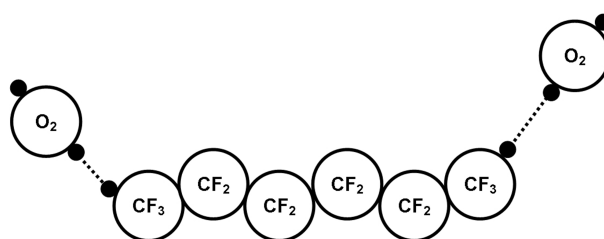
Figure 4.39: Two-dimensional sketch of the cross association model for the solubility of oxygen in n-perfluoroalkanes.
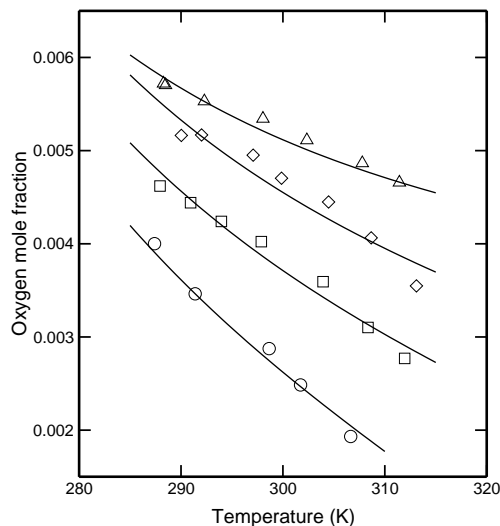
Figure 4.40: Solubility of oxygen in linear perfluoroalkanes at 1 atm. Symbols as in Figure 4.40. Lines correspond to the soft-SAFT EOS with the cross-associating model.

inevitably predicts a much weaker dependence on temperature, regardless of the values of the binary interaction parameters. We also observed that the PR EOS does not provide a good trend either, as can be seen in Figure 4.38 as a dashed line (one binary parameter of the EOS was fitted to the experimental data [169]). Since van der Waals interactions seemed to be correctly captured in the previous cases, one should think that additional interactions exist in this mixture, which are not considered by the model.

According to Mack and Oberhammer [170], *ab initio* calculations of the interaction potentials for the complex $CF_4 - O_2$ provide evidence that an interaction between the oxygen and the positive carbon nucleus in CF_4 occurs, forming a very strong complex. Admitting that the same interactions can be found between oxygen and higher order perfluoroalkanes, and that they may significantly affect equilibrium properties, the soft-SAFT model should account for this in some way. Therefore, we proposed to add the free energy of cross-association between oxygen and perfluoroalkane molecules to the total energy of the system. Consequently, both molecular oxygen and perfluoroalkanes were modelled as associating molecules with two association sites on each, as drawn in Figure 4.39. In the case of oxygen, sites represent the two lone pairs of electrons and, in the case of perfluoroalkanes, the two ends of the molecule where the carbon atoms are more exposed (less screened by the fluorine atoms).
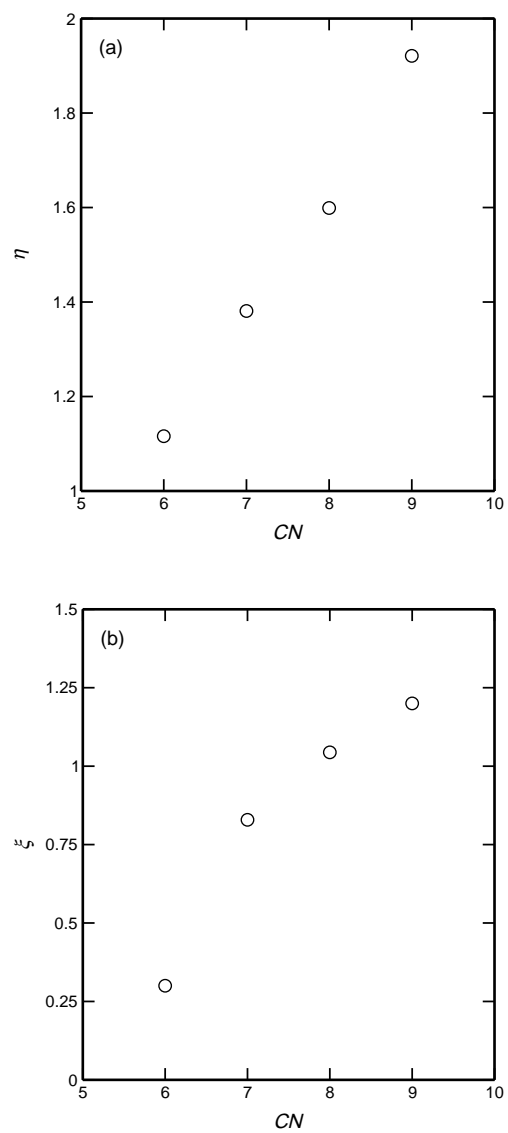
Figure 4.41: (a) Size and (b) energy binary parameters for the solubility of oxygen as a function of the carbon number of the n-perfluoroalkane.

The magnitude of the site-site interaction between oxygen and perfluoroalkane molecules in the SAFT model depends on the two cross-association parameters, $\varepsilon = 2000$ K and $k = 8000$ Å^3, which were set constant for all mixtures. These values provide the proper solubility dependence with temperature, which was impossible to reproduce without the association model. Binary interaction parameters were then fitted for each mixture to experimental data, and they are listed in Table 4.9. Predictions of the soft-SAFT EOS with the associating model for the solubility of oxygen in perfluoroalkanes at 1 atm are shown in Figure 4.40 as solid lines, with the same experimental data shown in Figure 4.40. As can be observed, the soft-SAFT model that includes cross-association satisfactorily reproduces oxygen solubilities in perfluorocarbon chains, compared to experimental data, having an AAD below 5%. Furthermore, binary interaction parameters have a sound trend with respect to the carbon number of the perfluoroalkane chain, as seen in Figure 4.41. Since size and energy parameters for pure perfluoroalkanes increase and tend to a constant value as the chain length increases, the same behaviour is expected for the binary parameters. However, note that, for the size binary parameter, the curvature is still not observed for this chain-length range.

4.4.4   Conclusions

A SAFT model and parameters for the solubility of xenon and oxygen in n-perfluoroalkanes are provided. It turns out that cross-association between oxygen and perfluoroalkanes has to be considered in order to capture the correct temperature dependence of the solubilities. As explained in the last section, this is supported by *ab initio* calculations reported in the literature, which suggest that strong interactions exist between molecular oxygen and the carbon atoms of the perfluorocarbon chains.

Predictions of the solubility of xenon and the VLE and LLE of n-alkane + n-perfluoroalkane mixtures with a nonassociating model are also given. Size and energy molecular parameters for the pure n-perfluoroalkanes were optimized by fitting to experimental vapour pressures and saturated liquid densities. The chain-length parameter was taken from the values optimized for the n-alkane series. Comparison of these optimized values to those from other models and the fact that they correlate as a function of the carbon number of the chain gives proof of their physical meaning and transferability.

Due to the high nonideality of the mixtures considered in this section, temperature independent binary interaction parameters need to be optimized. For n-alkane + n-perfluoroalkane mixtures of similar length, a unique optimized value of the binary energy parameter is used to describe VLE and LLE equilibrium properties in a broad range of temperatures with an AAD lower than 5% in most of the cases. Solubilities of

xenon are predicted with a global AAD less than 2%. For the solubility of oxygen, the AAD of predictions of the soft-SAFT model compared to experimental measurements is below 5%. Unique values for the two cross-association parameters were set and the optimized binary interaction parameters present an appropriate trend with respect to the perfluoroalkane chain length. We emphasize that a great advantage of using SAFT is that it is possible to systematically improve the model to provide reliable and accurate predictions, provided that parameters remain meaningful.

4.5   VLE of CO_2 with n-alkanes and 1-alkanols

The soft-SAFT EOS is used to quantitatively describe VLE and critical properties of carbon dioxide with n-alkanes and 1-alkanols. Two square-well sites account for the self-association capability of the 1-alkanols. Optimized values for the chain length, LJ diameter and dispersive energy, and association energy and volume, are provided for the 1-alkanol series. The two Lorentz-Berthelot parameters need to be adjusted for each binary mixture. As in previous sections, we use a simple rescaling of the molecular parameters to quantitatively describe the critical properties of the mixtures. Although satisfactory, the quantitative agreement with experimental data of VLE predictions needs improvement. We believe that, for a better description of the fluid phase equilibria of these mixtures, the effect of the quadrupolar moment of CO_2 needs to be included in the model.

4.5.1   Introduction

In many supercritical fluid applications, carbon dioxide is widely used as the near-critical solvent. Although it has many advantages, its poor solvency with respect to polar compounds may be an inconvenience. Nevertheless, this is overcome, in most cases, by using alkanols as co-solvents, added to enhance the solubility of polar compounds in carbon dioxide. Since solutes are molecules usually much more complex and larger than the solvent, very asymmetric mixtures are normally found in industrial applications.

It is known that complex multiphase equilibria may occur in CO_2 + n-alkane + 1-alkanol systems, especially close to the critical point of the solvent. Even more, for small changes in temperature, pressure or composition, a variety of unexpected phenomena can be encountered. Therefore, to understand, anticipate and control these phenomena, a fundamental understanding regarding the fluid phase behaviour of such mixtures is needed.

A systematic experimental research on the fluid phase behaviour of ternary mixtures containing near-critical carbon dioxide has been recently carried out by Peters and Gauter [171]. On the theoretical side, accurate and reliable models are needed to describe the phase behaviour of these systems. Following the modelling approach, our mid-term aim is to apply the soft-SAFT equation to model fluid phase equilibria and critical behaviour of CO_2 binary and ternary mixtures. Here, as a first step, and to test the performance and accuracy of the equation for these systems, we selected several mixtures: CO_2 + n-decane, CO_2 + 1-propanol, and CO_2 + 1-pentanol.

Previous work on this issue has been reported by Passarello *et al.* [172], who applied the original SAFT equation to the homologous series CO_2 + n-alkanes from

n-C$_3$ to n-C$_{44}$. Galindo and Blas [173] studied the global fluid phase behaviour in these mixtures using the SAFT-VR EOS.

4.5.2 Molecular model

Following the work shown on previous sections, we model CO$_2$ and 1-alkanols as homonuclear chainlike molecules of equal diameter σ and the same dispersive energy ϵ. The hydroxyl group in alkanols is mimicked by two square-well sites embedded off-centre in one of the LJ segments, with volume k and association energy ε.

Molecular parameters for n-decane are taken from the PV correlation for the n-alkane series (eqs 4.1a-4.1c). For CO$_2$ and 1-alkanols, they have been calculated by fitting experimental saturated liquid densities and vapour pressures, as usually. Experimental saturated liquid densities and vapour pressures were correlated with AADs of less than 3% and 5%, respectively. Parameter values are given in Table 4.10. Since the length of the chain should not affect the strength of association bonds, we set the parameters of the association sites at constant values, except for methanol and ethanol, which do not much differ from a spherical shape. The representation of the size and energy parameters for the 1-alkanols as a function of the carbon number, as can be seen in Figure 4.42, shows coherent trends. From the optimized parameters shown in Table 4.10, simple relationships of the molecular parameters with the carbon number are given in equations 4.12a-4.12c. Units of σ and $\epsilon/k_{\rm B}$ are Å and K, respectively.

$$m = 0.2348CN + 1.263 \tag{4.13a}$$
$$m\sigma^3 = 25.64CN + 32.22 \tag{4.13b}$$
$$m\epsilon/k_{\rm B} = 91.37CN + 229.8 \tag{4.13c}$$

Because of the asymmetry of the binary mixtures we are dealing with, the two binary parameters η and ξ should be also fitted to experimental data. As explained in chapter 2 (see eqs 2.5-2.6), they are factors in the geometric mean of the size and energy parameters between CO$_2$ and n-alkane or 1-alkanol segments (the Lorentz-Berthelot combining rule).

4.5.3 Results and discussion

Figures 4.43a and 4.43b show the vapour-liquid coexisting densities and vapour pressures of carbon dioxide, respectively. Circles are experimental data. The solid line corresponds to predictions from the equation, using fitted molecular parameters (non-rescaled). The dashed line is the curve obtained when molecular parameters are
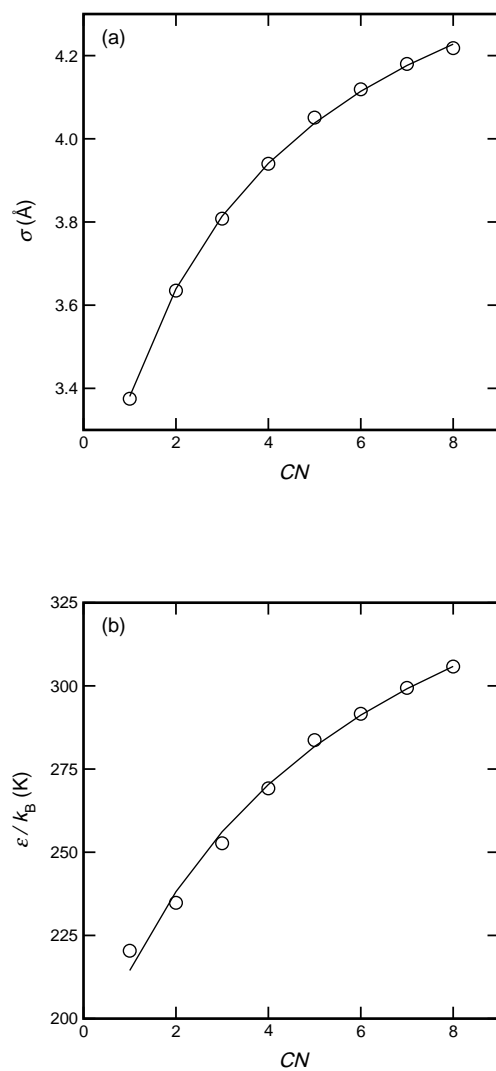
Figure 4.42: Molecular parameters for 1-alkanols: (a) segment diameter; (b) dispersive energy. Lines correspond to the values from the relationships of eqs 4.13a-4.13c.
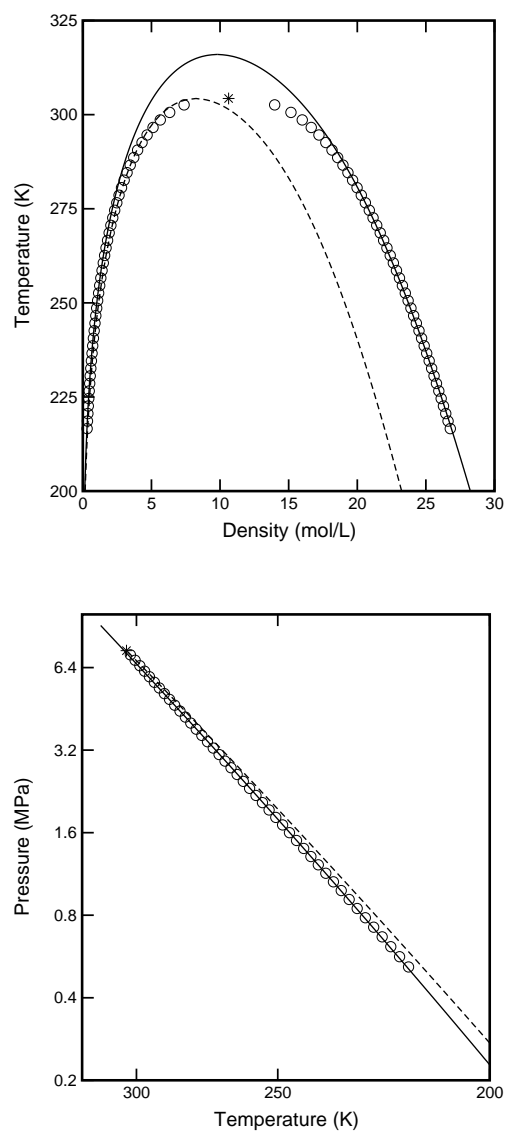
Figure 4.43: (a) Coexisting densities and (b) vapour pressures of CO$_2$. Circles are experimental vapour-liquid data, whereas the star indicates the location of the experimental critical point. Solid and dashed lines correspond to soft-SAFT with nonrescaled and rescaled parameters.

Table 4.10: Molecular parameters for the pure compounds

	m	σ (Å)	ϵ/k_B (K)	ε/k_B (K)	$k(\mathring{A}^3)$
CO_2	2.681	2.534	153.4	0	0
methanol	1.491	3.375	220.4	3213	4847
ethanol	1.740	3.635	234.8	3387	2641
1-propanol	1.971	3.808	252.7	3450	2250
1-butanol	2.210	3.940	269.2	3450	2250
1-pentanol	2.420	4.051	283.7	3450	2250
1-hexanol	2.676	4.119	291.6	3450	2250
1-heptanol	2.900	4.180	299.4	3450	2250
1-octanol	3.148	4.218	305.8	3450	2250

rescaled to fit the experimental critical temperature and pressure ($\sigma = 2.684$ and $\epsilon = 147.7$). Because of the disagreement between the theoretical and the experimental critical compressibility factor, as explained in preceding sections, the critical density is necessarily off.

Figure 4.44 presents equilibrium pressures for the mixture CO_2 + n-decane in a broad range of temperatures. The binary parameter values η and ξ were fitted to the experimental data out of the critical region of the isotherm at 344.3 K. The overall absolute averaged deviation for the pressure is 13%, but in two isotherms (277.6 and 462.6) this deviation increases up to a 19%. Similar deviations were obtained by Passarello *et al.* using the original SAFT equation for the same mixture, and with unique size, energy and binary parameter values for the whole series of n-alkanes. Therefore, we believe that the effect of the quadrupolar moment of the CO_2 plays a more important role than the type of reference fluid and the number of optimized parameters. In Figure 4.45 the critical line for this mixture is shown. As expected, the nonrescaled molecular parameters overestimate experimental critical pressures and temperatures. When the rescaled parameters are used, predictions improve up to an AAD of 4.8% for the critical pressures. Note that no fitting is performed in the mixture in this case: once the molecular parameters of the pure fluids are rescaled, the equation is used to predict the critical properties for the whole range of compositions.

In Figure 4.46 the critical line for the CO_2 + 1-propanol mixture is shown, using the rescaled parameters, and no fitting to experimental mixture data. The overall deviation is about 8%.

In Figure 4.47 isotherms for the CO_2 + 1-pentanol mixture are plotted. In this case, η and ξ were fitted to the experimental data at 325.9 K. The critical region is overestimated, as expected, but this can be overcome by using the rescaled param-
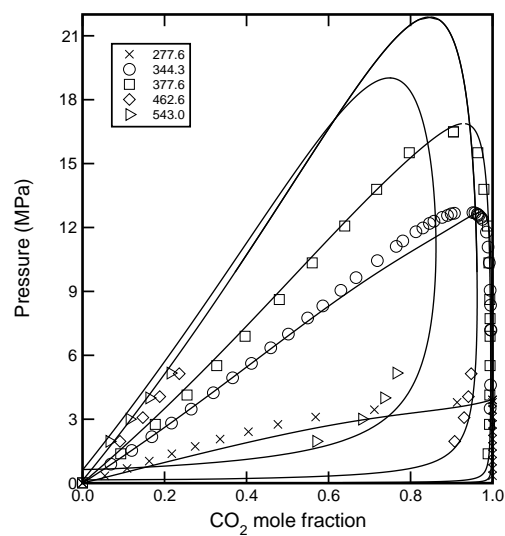
Figure 4.44: Isotherms in the CO$_2$ + n-decane mixture. Predictions from the soft-SAFT EOS (lines) and experimental data [172, 174] (symbols). Temperatures are given in K.
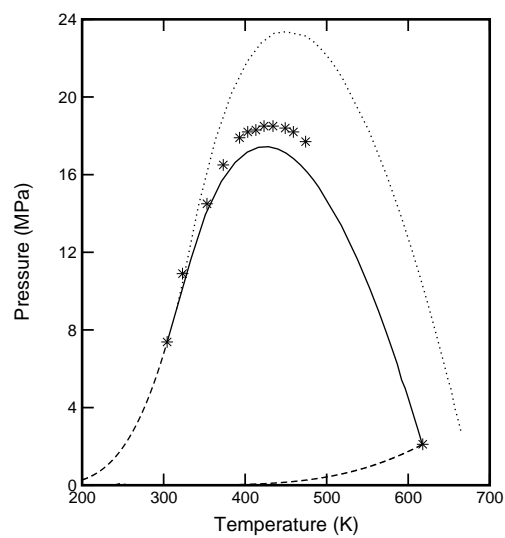
Figure 4.45: Critical line of the CO$_2$ + n-decane mixture. Predictions from the soft-SAFT EOS with nonrescaled (dotted line), rescaled parameters (solid line), and experimental data [175] (stars).
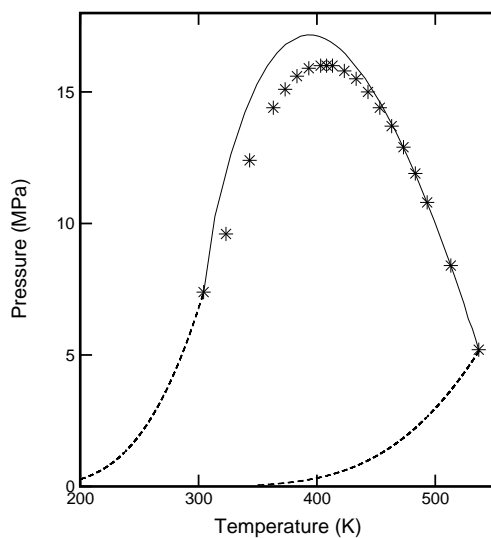
Figure 4.46: Critical line of the CO_2 + 1-propanol mixture. Predictions from the soft-SAFT EOS (lines) and experimental data [176] (symbols).
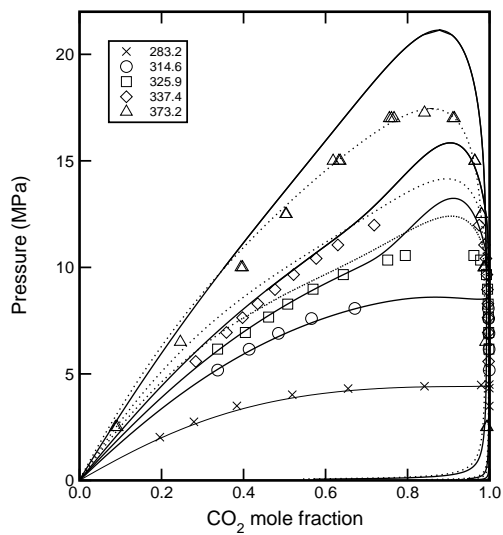
Figure 4.47: Isotherms in the CO_2 + 1-pentanol mixture. Predictions from the soft-SAFT EOS (lines) and experimental data (symbols) [177, 178]. Dotted lines are predictions of the critical region using rescaled molecular parameters. Temperatures are given in K.

eters, (see dotted line in the figure). The overall deviation for the pressure is below 5% (in the subcritical region), and discarding the highest temperature isotherm, this value decreases to 2.6%. Although the range of experimental data available is narrower, compared to the CO$_2$ + *n*-decane mixture, the pressure deviation in any of the isotherms of the CO$_2$ + 1-pentanol mixture is much lower than any of those corresponding to the CO$_2$ + *n*-decane mixture. We think that, in associating mixtures, the effect of the association forces on the equilibrium properties is larger than the effect of the quadrupolar moment of the CO$_2$.

4.5.4 Conclusions

Soft-SAFT predictions for the vapour-liquid equilibria and critical properties of CO$_2$ + *n*-decane, CO$_2$ + 1-propanol and CO$_2$ + 1-pentanol mixtures are reported here. Good agreement with experimental data is achieved for the CO$_2$ + 1-alkanol mixtures. In the CO$_2$ + *n*-decane mixture, pure predictions for the critical line are not as good agreement as for vapour-liquid equilibrium properties. We believe that this is caused by the effect of the quadrupolar moment of CO$_2$. For a significant improvement of the description of CO$_2$ + *n*-alkane mixtures, we believe that the effect of multipolar forces has to be included in the molecular model.

Chapter 5

Bulk and interfacial properties studied by molecular simulation

*We present canonical molecular dynamics (MD) and Gibbs ensemble Monte Carlo (GEMC) results for the vapour-liquid orthobaric densities of methane and propane. Computational advantages and drawbacks of both simulation methods are discussed and future work is outlined on the application of these techniques to the calculation of transport and interfacial properties. n-Alkanes are described through the TraPPE-UA force field. We study the effect of the truncation of interactions in the Lennard-Jones potential on the accuracy of the orthobaric liquid densities for these inhomogeneous systems along the phase diagram. We observed that a cut-off of at least 5.5 times the Lennard-Jones diameter is needed to obtain accurate results for saturated liquid densities.

5.1   Introduction

Molecular simulations are undoubtedly becoming a standard and powerful tool in science and engineering, increasingly providing answers to a broad range of fundamental and industrial problems. Of particular importance in many technological

---

applications in the chemical and petrochemical industries is knowledge of the phase behaviour of hydrocarbons. Since the pioneering work of Siepmann *et al.* [179], much effort has been devoted in the recent years to the development of accurate force fields for hydrocarbons using molecular simulations. Among the recently proposed models for n-alkanes with the united-atom approach the most accurate ones are: the NERD force field developed by de Pablo and co-workers [95], the TraPPE-UA model proposed by the group of Siepmann [97] and the model proposed by Errington and Panagiotopoulos (which we shall denote EP) [99]. The TraPPE-UA and the NERD models reproduce well the critical parameters and the saturated liquid densities of n-alkanes over a wide range of chain lengths, although they are less accurate for the saturated vapour densities and vapour pressures. On the other hand, the EP model is able to describe more accurately the vapour pressures and critical properties. All these models have been used to predict, with no additional fitting, the phase diagram of binary mixtures of n-alkanes, including short and long chains, finding, in general, good agreement with experimental data.

All the simulations mentioned above were performed using the Gibbs Ensemble Monte Carlo (GEMC) technique, with additional algorithms to improve the sampling of the phase space, or to increase the acceptance probability for insertion/deletion. Due to its simplicity, speed and accuracy in predicting the equilibrium properties of both phases in a single simulation, GEMC [180] has become the standard method to compute phase-equilibria properties through molecular simulations. However, it should be mentioned that the molecular dynamics (MD) method was employed long before for phase-equilibria predictions of simple fluids, as already reported in the pioneering work of Ladd and Woodcock [181], and on that of Holcomb *et al.* [182,183], some years later. The simulations were performed putting in physical contact two bulk phases previously equilibrated through NVT MD simulations. Nevertheless, as Ladd and Woodcock mentioned in their paper, at that time there were severe limitations on running these simulations, i.e. the total number of molecules one could deal with was very small, and also the total simulation time was very limited. Nowadays, increasing computer power makes direct simulations of the interface by Monte Carlo (MC) or canonical MD increasingly more attractive, since both of the limitations previously mentioned can be overcome. A clear advantage of them over the GEMC method is that they yield microscopic information on the interfacial region and thermodynamic properties such as the surface tension, in addition to phase-equilibrium properties in both phases. Moreover, MD can provide dynamical properties in the same simulation run, such as the residence time of molecules at the interface and the self-diffusion coefficient in both phases and at the interface.

A main drawback of these MD and MC approaches is the difficulty to stabilize the interface when the density difference between the coexisting phases is small, as

occurs in the near critical region, a consequence of the finite-size effect of the simulations. We should note the GEMC method also faces the same problems near the critical point. Additionally, MC methods encounter problems when simulating dense systems, where low acceptance probabilities may cause obtaining results to be impractical. Although this limitation has been overcome to a large degree by making use of the configurational-bias techniques, it is still very costly to obtain LLE equilibria of mixtures by MC simulations. On the other hand, as pointed out by Gelb and Müller [184], MD has an advantage when simulating systems at very high densities, since it does not require insertion into the dense phase, and it is particularly suitable for the study of multicomponent systems or more complex molecules.

This chapter is part of an ongoing work in calculating several equilibrium and dynamical properties of some industrial relevant fluids. Our mid-term goal is to employ the MD technique for the computation of thermodynamic and structural properties, which, in addition to providing vapour-liquid equilibrium data, will allow us to simultaneously investigate the dynamics of the interface formation, to compute transport coefficients and to study the structure of the interface, as well as the surface tension. In particular, simulation results for the surface tension will allow a direct comparison and testing of theoretical calculations. Here, as a first step on this work, we check the accuracy and performance of our program on providing the coexistence densities of some fluids, as compared to experimental data.

Accurate results for the vapour-liquid phase equilibria and surface tension of chlorine and hexane were obtained by Alejandre *et al.* [185] through MD simulations. They outlined the advantages and drawbacks of MD and GEMC methods for chain molecules and addressed the two major difficulties associated with the truncation of interactions in inhomogeneous systems: (1) truncation of the forces in MD results in a shift of the truncated potential used in MC, i.e. the models are, a priori, different, and this has a significant influence in phase-equilibrium calculations and (2) truncation of the interactions have a considerable effect on phase-equilibrium properties. Both effects were quantified later by Trokhymchuk and Alejandre [186] for the monatomic LJ fluid. The effect of the potential truncation on the chemical potential and other thermodynamic properties of the LJ fluid has also been addressed in a recent paper by Shi and Johnson [187]. They used the GCMC method combined with histogram reweighting techniques, arriving to similar conclusions as reference [186] regarding the influence of the cut-off on the phase-equilibria properties.

Transport properties were also computed using MD by Rivera *et al.* [188] for nitrogen and butane mixtures. They parameterised the NERD force field for nitrogen with the GEMC technique and employed MD simulations to compute diffusion coefficients, surface tension and shear viscosity of the mixture, as a function of the temperature. They approximated the full potential by truncating the interactions at a large cut-off

and did not apply long-range corrections to the configurational energy in the MD calculations. The importance of the cut-off value used is seen in Figure 1 of their paper where, for a value of 4.3σ, the full potential is not reached, leading to lower saturated liquid densities for pure nitrogen.

In more recent works, Goujon *et al.* [189, 190] investigated vapour-liquid equilibrium properties of *n*-pentane by direct MC simulations, implementing a method for incorporating long-range corrections in inhomogeneous fluids. Comparison to experimental data showed the importance of the cut-off (and the long-range corrections) in these calculations. Goujon *et al.* also determined the surface tension of *n*-pentane as a function of temperature through calculation of the pressure tensor. A conclusion from their work is that the deviations between the calculated surface tension and those obtained from a generalized equation for the surface tension, from the triple point to the critical point, decrease as the cut-off is increased. However, little dependence on the cut-off radius is observed if long-range corrections are applied. They suggested simulations using the MD technique to compare with the thermodynamic equilibrium properties obtained by direct MC simulations.

It is clear that molecular simulations are also very useful to test and refine molecular models in a systematic way, since they provide exact data for a given potential model. However, computational limitations may still affect the accuracy of simulation results for complex systems, as can occur with multibranched, highly polar, or long polymer molecules, and for multicomponent or multiphase systems. Such limitations are nearly always driven by three factors: system size, truncation of interactions and equilibration time. Nowadays, system size is rarely a factor when dealing with simple systems, since large numbers of small molecules are easily simulated, even on todays PCs. Truncation of the pair potential may or may not be a significant source of error. For example, many pair potentials in the field of biological simulation are parameterised with a cut-off assumed; hence, using a cut-off in calculations with these potentials is only problematic if the cut-off used is different from that used to parameterise the potential. Generally, however, potentials are parameterised using long-range corrections (i.e. essentially no cut-off). In simulating coexistence by MD, the question of a cut-off becomes quite important, since the incorporation of a long-range correction is nontrivial (see, for example, reference [191]). A straight solution is to use a cut-off as large as is necessary to ensure the results are essentially independent of cut-off and not attempt to apply a long-range correction for the nonuniform fluid. Trokhymchuk and Alejandre [186] studied the influence of the cut-off on phase-equilibrium properties for the LJ fluid from MD simulations. Less is known about the influence of truncation in the case of chainlike molecules such as the alkanes.

While the cut-off used is an important determinant of actual computer time used for simulating a given system (execution time will increase at least linearly and at

worst quadratically in the cut-off), for most simulations, the equilibration time, measured as the longest relaxation time in the system, is generally the primary determinant of the computational cost of a simulation. For MD, the time to form and stabilize the interface can be long, especially in the case of large molecules that diffuse slowly and have long internal relaxation times. The time required for collection of statistics is also driven by the longest relaxation time in the system, since to obtain reliable statistical measurements of the properties of interest, typically one must collect averages over several relaxation times.

This work is focused on the prediction of orthobaric densities of methane and propane by both MD and GEMC. We study the influence of the truncation of interactions on the accuracy of coexistence densities, and obtain additional properties, such as density profiles, and the time dependence of selected properties by MD.

5.2   Molecular model

The TraPPE-UA force field describes n-alkanes as united-atom (UA) cores interacting through a Lennard-Jones 12-6 potential when they belong to different molecules or are separated by more than three bonds within the same molecule,

$$u_{\mathrm{LJ}}(r_{ij}) = 4\epsilon_{ij} \left[\left(\frac{\sigma_{ij}}{r_{ij}} \right)^{12} - \left(\frac{\sigma_{ij}}{r_{ij}} \right)^{6} \right], \tag{5.1}$$

where ϵ_{ij} is the energy parameter of the interaction, σ_{ij} is the Lennard-Jones (LJ) core diameter and r_{ij} is the distance between interaction sites i and j. In MD, we truncate interactions using a cut-and-shifted potential, which corresponds to truncated forces. The LJ parameters for the interaction sites of the TraPPE-UA model were fitted by Martin and Siepmann [97] to critical temperatures and saturated liquid densities. They are summarized in Table 5.1. United-atom cores are connected by bonds at an equilibrium distance of 1.54 Å. The TraPPE-UA model also accounts for intramolecular forces, which, apart from the nonbonded LJ interactions, include bond angle bending and the torsion of dihedral angles. Dihedral angles apply for molecules with more than three carbons, i.e., from butane on. Bond angle bending is governed by the harmonic potential

$$u_{\mathrm{bend}} = \frac{k_\theta}{2}(\theta - \theta_0)^2, \tag{5.2}$$

with the force constant $k_\theta/k_{\mathrm{B}} = 62\,500$ K rad^{-2}, where k_{B} is the Boltzmann's constant. The equilibrium angle between three consecutive united-atom cores is set at $114°$.

Table 5.1: Interaction potential parameters of the TraPPE-UA model.

	ϵ/k_{B} (K)	σ (Å)
CH_4	148	3.73
CH_3 (n-alkane)	98	3.75
CH_2	46	3.95

5.3   Simulation details

In the canonical MD technique we use here, a fixed number of molecules is initially placed in a simple cubic lattice and the fluid then melted to an established liquid density. Once the system is equilibrated, the box is suddenly enlarged in one of its dimensions forming a rectangular parallelepiped, thereby fixing a constant equilibrium global density that lies between the corresponding coexisting densities at the simulation temperature, and thus allowing the interface and the vapour phase to form. Finite size effects play an important role in the MD technique, mainly because of the high energy cost of forming the interfaces. The energy barrier can be sometimes so high that the system does not have enough energy to cross it. Hence, system sizes need to be much larger than those normally used in GEMC simulations. For example, for propane we could not stabilize the interfaces with less than approximately 2000 molecules. As a guide, the number of molecules [186] should be larger than 1000 and the shortest dimension of the box should measure not less than 10σ, even for simple LJ spheres.

We have used the reversible multi-time step RESPA algorithm [192] to integrate the equations of motion with a large time step of 5 fs and a small time step of 0.5 fs. The canonical ensemble is generated by the Nosé-Hoover thermostat. Instead of using a constrained integration algorithm, such as RATTLE [193], we included a bond stretching potential [194]

$$u_{\mathrm{stret}} = \frac{k_l}{2}(l - l_0)^2,\tag{5.3}$$

which is a harmonic function around an equilibrium bond length $l_0 = 1.54$ Å and with a large spring constant $k_l/k_{\mathrm{B}} = 452\,900$ K Å^{-2}. This effectively maintains the bonds at the fixed length l_0 and has a negligible effect on the phase diagram [194]. Neighbour lists with a cut-off skin of 0.3σ are used in the calculation of nonbonded forces. The choice of skin width means that the recalculation of the neighbour list takes places only when the maximum displacement inside the interaction cut-off plus the cut-off skin exceeds 0.15σ. After $50\,000$ time steps the box is suddenly enlarged in one Cartesian direction to form a parallepiped with a side ratio of 2.5, allowing

Table 5.2: Summary of MD simulation details. Note that $L_x = L_y$ and L_z was set to 2.5 L_x.

	T (K)	N	ρ (mol/L)	$L_x/\sigma_{\mathrm{CH_2}}$
Methane	110	2197	11.0	13.67
	130	2197	11.0	13.67
	150	2197	11.0	13.67
	170	2197	11.0	13.67
Propane	200	2197	7.0	15.01
	217	2197	6.0	15.80
	249	2197	6.0	15.80
	281	3375	6.0	18.23

the interface to form. Properties are continuously monitored in block averages of 500 fs. Density profiles are determined by dividing the simulation box into 500 slabs, and calculating the density in each slab with respect to the centre of mass of the system, every 5000 time steps. By monitoring the Hamiltonian and the density profile we can check the equilibration of the interfaces. After equilibrating the system, further averaging for at least 125 000 time steps is performed.

There are two important practical aspects to consider when enlarging the simulation box on these MD simulations. On one hand, the volume of the box should be chosen such that the overall density in the box is close to the line of rectilinear diameters. In this way, liquid and vapour volumes in the box become similar and both vapour-liquid interfaces are almost equally distant between them by the liquid and the vapour sides. On the other hand, and related to the latter, the number of molecules must be large enough to satisfy the condition that the distance between both interfaces is larger than twice the cut-off radius. This avoids the situation in which a molecule simultaneously interacts with others located at both interfaces. Consequently, the larger the cut-off radius is, the larger the number of molecules to be simulated. Table 5.2 summarizes the initial conditions for the MD simulations, where the global density in the box is included.

We have also performed GEMC simulations, in combination with the configurational-bias Monte Carlo method (CBMC), to check the computational time needed to reproduce the simulation data published by Martin and Siepmann [97] and to compare to the MD simulation run at equivalent thermodynamic conditions. Since GEMC and CBMC are well established in the literature, only the details concerning our implementation are discussed here. We perform five types of MC moves: swapping of volume and swapping of particles between the two boxes, and three moves

related to individual molecules: translation of the centre of mass, rotation about the centre of mass, and change of the internal conformation of the chain by means of a configurational-bias re-growth (for molecules with more than two united-atom cores). Fixed probabilities are set to select the type of move to be attempted: 3 and 34% for the exchange of volume and the exchange of particles, respectively, and a probability of 21% for each one of the remaining moves. The maximum displacements for the translation, rotation and volume changes are adjusted independently in each box to achieve a 50% acceptance rate. For the modification of the conformation of a molecule with the CBMC technique, a molecule and the number of atoms to be re-grown are randomly selected. The number of trial orientations is equal to 10, while 50 random trial positions were used to increase the molecule exchange acceptance rate when inserting the first interaction site.

In the propane GEMC simulations, we truncated the interactions at $3.5\sigma_{CH_2}$ and analytic tail corrections were applied. A system size of 400 molecules of propane at 200 K was equilibrated for at least 5000 cycles (one cycle is N MC moves, where N is the number of molecules). The production length consisted of 25 000 cycles. The run required 39 h of CPU time on a 1.3GHz PC. A MD simulation at the same temperature with 2197 molecules (sufficient to stabilize the interfaces) and a cut-off $r_c = 5.5\sigma_{CH_2}$, which was run for 750 ps (125 000 time steps) after equilibration, needed slightly more than 140 h of CPU time on the same computer, which is equivalent to that used by Goujon *et al.* [189, 190] for the direct simulation of the interface with the NVT MC methodology. We set $r_c = 5.5\sigma_{CH_2}$ to approximate the full potential and to avoid dealing with long-range corrections in inhomogeneous media.

5.4　Results and discussion

We present here phase coexisting densities of methane and propane obtained by MD and GEMC, focusing on the importance of the cut-off radius used in the simulations. Additional properties for propane calculated from MD simulations, such as the density profiles, time dependence of the density of the centre of mass and the temperature, and the influence of the number of molecules on the density profiles are also presented and discussed here.

As has already been shown by Trokhymchuk and Alejandre [186], spherically truncated and spherically truncated and shifted potentials do not significantly differ from the full LJ potential when interactions are truncated beyond 5.5σ. We have quantified the effect of the cut-off in the vapour-liquid equilibria of methane, modelled as a spherical LJ fluid. Results calculated in this work by MD are shown in Figure 5.1, compared to GEMC simulations, also obtained in this work, and to experimental val-
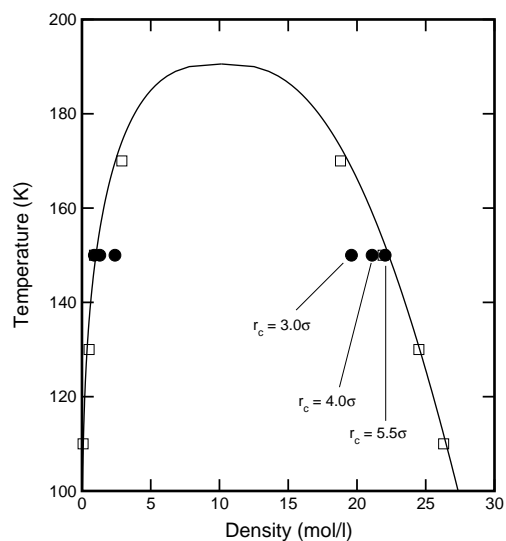
Figure 5.1: Coexistence curve of methane from MD (circles) and GEMC (squares) calculations compared to experimental data [107] (line).
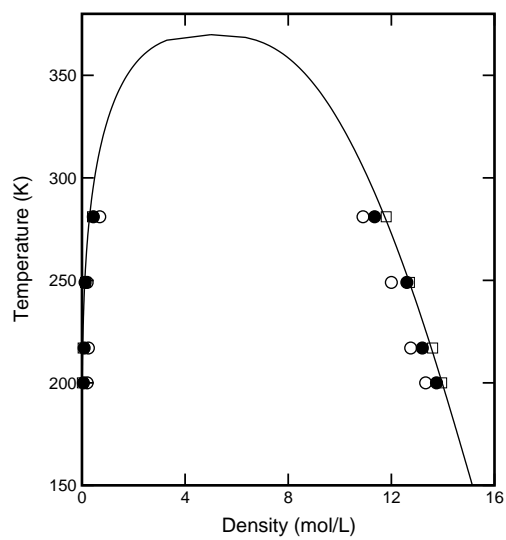
Figure 5.2: Coexisting densities of propane obtained by MD simulations at two values of r_c: 4.5 (open circles) and $5.5\sigma_{CH_2}$ (filled circles). Comparison to GEMC results (squares) and experiments [107] (line). GEMC data are from reference [97], except at 200 K (this work).

Table 5.3: MD predictions of the coexisting densities for propane with a cut-off equal to 5.5 σ_{CH_2}, compared to GEMC results reported by Martin and Siepmann [97] and to experimental data [107]. Densities are given in mol/L.

T (K)	MD (this work)		GEMC		Experimental	
	ρ_L	ρ_V	ρ_L	ρ_V	ρ_L	ρ_V
200	13.75	0.054	13.95^a	0.0169^a	13.97	0.0122
217	13.20	0.084	13.6	0.045	13.55	0.0295
249	12.60	0.12	12.7	0.14	12.70	0.108
281	11.35	0.32	11.8	0.41	11.74	0.295

[a] This work.

ues [107]. Error bars in the simulation data are smaller than the symbol size. We have used three different cut-off values for an intermediate temperature (150 K), $r_c = 3.0$, 4.0 and 5.5 σ_{CH_4}. It is clearly seen from the figure that using a small cut-off radius effectively makes the molecules less attractive and that the larger value ($5.5\sigma_{CH_4}$) provides an adequate representation of the full potential, giving quantitative agreement with experimental data. For the case of the GEMC simulations, long-range corrections are applied (it is straightforward in this case) and, hence, no point is made on the value of the cut-off radius in these simulations.

Figure 5.2 shows the coexisting densities of propane, a nonspherical molecule. We present MD results for two values of the cut-off, 4.5 and $5.5\sigma_{CH_2}$, compared to GEMC simulations and to experimental data taken from the literature [20]. As for the case of methane, a clear dependence of the coexisting densities on the potential cut-off is observed. It should be noted that for the MD simulations of propane, a larger number of molecules compared to methane was needed to equilibrate the interface, especially close to the critical point. For instance, for the case of $T = 281$ K, the stable two-phase equilibrium interface was obtained with 3375 molecules. This is essentially due to the larger fluctuations observed at these conditions. Simulations at lower temperatures needed less molecules and reached equilibrium faster.

The MD simulation results for propane at a cut-off value of $5.5\sigma_{CH_2}$ are also presented in Table 5.3, compared to GEMC simulation results from this work for the case of $T = 200$ K, and from the work of Martin and Siepmann [97] for the rest of the temperatures, and to experimental data [107]. The overall deviation of the MD predicted saturated liquid densities from the experimental values is 2.1%. Relative deviations in the equilibrium vapour densities are very large, mainly because of poor statistics due to the smaller number of molecules in the vapour phase in the
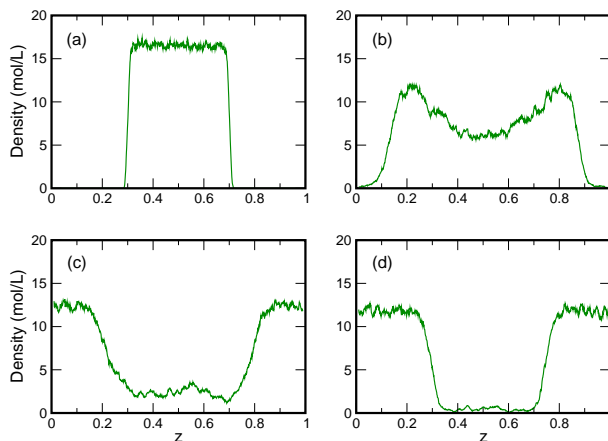
Figure 5.3: Time evolution of the density profile for propane at 281 K along the longest axis z of the simulation box. z is dimensionless. (a) Profile at the time step at which the enlargement of the simulation box takes place; (b) and (c) Transition profiles; (d) Profile at the equilibrium state.

simulations (see Figure 5.4). This is more noticeable at low temperatures. A question may remain on how the liquid phase changes by considering a larger cut-off. It is possible that the quantitative agreement with experimental data improves in that case. In fact, a detailed study on the dependency of the cut-off for each member of the n-alkanes series is needed, in principle, following this approach. As mentioned already, a larger cut-off implies a larger number of molecules in the simulation, making some of them very lengthy, as the chain length increases. However, since for the case of propane the overall deviations from the experimental data is 2.1% (in the range of the experimental error), and it is out of the scope of this work to quantify the exact value of the cut-off for each member following this procedure, we think that a cut-off of $5.5\sigma_{CH_2}$ suffices in this case. If one is interested in obtaining the VLE of the whole series through MD simulations, it is clear than long-range corrections can not be avoided in that case.

Once vapour-liquid equilibria for propane was reached, the differences in computing time between MD and GEMC quantified, and the importance of the cut-off value in the absence of long-range corrections evaluated, we calculated density profiles and time dependent properties. As we have mentioned already, a clear advantage of performing MD simulations versus GEMC simulations is the fact that these and other properties can be obtained, including interfacial and transport properties.

Figure 5.3 presents the evolution of the density profile of propane at 281 K. The density in the direction perpendicular to the planes of the interfaces is plotted versus the value of z, the position along that direction with respect to the position the centre of mass of the whole system. Therefore, although the centre of mass of the system may move, it always lies at $z = 0.5$ in our plots. The density profile at the time step when the box is suddenly enlarged keeping a slab of liquid in its centre surrounded by two void spaces, is shown in Figure 5.3a, while Figures 5.3b-d show different times after the enlargement. In this particular case, somewhat unusual, the profile inverts its shape so that the liquid and vapour phases swap their position in the box. A possible explanation could be that the evaporation rate of the molecules from the liquid to the vapour phase initiated by the enlargement of the box is high enough to invert the position of the phases.

Figure 5.4 shows a snapshot of a particular equilibrium configuration of 2197 propane molecules at 249 K in a $15.80 \times 15.80 \times 39.51$ Å simulation box, as obtained from MD simulations, where the two phases and the interfaces are clearly observed. A significant number of molecules are at the vapour-liquid interface, which becomes more evident at higher temperatures, where the percentage can exceed 50% of the total number of molecules.

The time evolution of the temperature and density at the centre of mass of propane at 249 K are shown in Figure 5.5. Three different regimes are observable in these graphics: the equilibration of the liquid before the sudden enlargement of the box, the instant at which the enlargement takes place, and the time evolution of the system after it. A study of these properties is useful as a test of when and how fast equilibrium is reached, depending on the thermodynamic conditions and on the simulation parameters.

Additional properties, such as the pressure tensor and from it the surface tension, can be obtained by MD. It would be very interesting to use this technique to investigate the formation of the interface itself, the orientation of the molecules around it, and the transport properties governing these phenomena. The calculation of these properties and their comparison with experimental data will be matter of future work.

5.5   Conclusions

We have presented some preliminary simulation results for vapour-liquid equilibria properties of methane and propane, which are modelled according to the TraPPE-UA model for n-alkanes. The influence of the cut-off radius on the coexisting orthobaric densities was studied by MD, and results compared to those obtained by GEMC simulations, and to experimental data. In order to study the influence of the cut-off
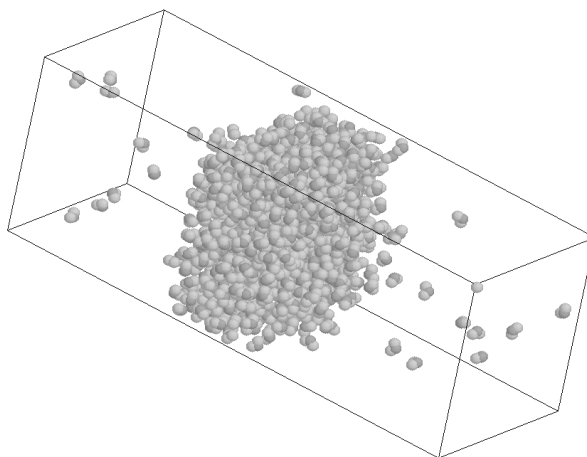
Figure 5.4: Snapshot of the simulation box of propane at equilibrium at 217 K. The dimensions of the box are a $15.80 \times 15.80 \times 39.51$ Å.
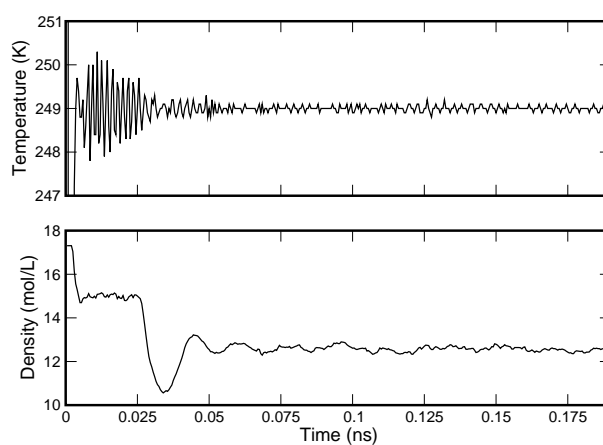
Figure 5.5: Time evolution of the temperature and density of the centre of mass of a simulation of propane at 249 K.

value on the coexisting densities, no long-range corrections were applied in the MD simulations. MD results showed that a cut-off of at least 5.5 times the Lennard-Jones diameter is needed to obtain an accuracy of about 2% when compared to experimental saturated liquid densities and to GEMC simulations with effectively infinite range (finite range cut-off with long-range correction). An alternative approach is to include long-range corrections in these inhomogeneous fluids.

Chapter 6

Interfacial properties described by the soft-SAFT+DGT approach

The soft-SAFT equation coupled with the density gradient theory is applied to the prediction of interfacial tensions of pure fluids and mixtures. The approach is able to accurately describe interfacial tensions in the whole thermodynamic range for pure systems. For mixtures, important deviations may occur when critical points are involved, because of the classical nature of the soft-SAFT EOS.

6.1   Introduction

Interfacial phenomena in fluids play a crucial role in many aspects of our daily lives. The formation of micelles by amphiphilic surfactant molecules in aqueous solutions (like soaps and cosmetics), the nature of the lipid bilayers that form cell membranes, the stability of colloids in emulsions (such as milk and paintings), to mention just a few examples, all depend on the type and magnitude of the relevant molecular interactions that occur at the interfaces in these inhomogeneous systems. In fact, it is the interplay between bulk and interface contributions to the free energy of a system which leads to the broad variety of known interfacial phenomena.

The behaviour at interfaces between fluids is also central to important technological processes. Reservoir engineering applications, surfactant technology, production of food and chemicals with emulsion or suspension processes, development of detergents, all require of a good understanding of the interfacial phenomena, to tackle problems

during production or with the stability of the products. Particularly, adsorption processes within the interface can cause a hindrance of mass transport across the phase boundary. Knowledge of interfacial tensions is needed for the understanding and control of all these processes. For instance, the optimization of the nonthermal secondary and tertiary oil extraction from depleted reservoirs by miscible displacement needs reliable interfacial tension predictions for alkane mixtures pressurized by a soluble gas (methane, nitrogen or, most commonly, carbon dioxide) [195].

Experimental interfacial tension data is readily available for common pure fluids, like the light alkanes, but this is not the case for heavier chains, for which data at low temperatures and in the near critical region are scarce. The situation is worst when dealing with mixtures. For this reason, accurate predictive methods are needed.

Many attempts have been made in the last century to relate the interfacial tension of pure fluids to other physical properties such as density, refractive index, critical constants, compressibility and sound velocity, from theoretical or empirical viewpoints. However, most of these theories have parameters with an unclear physical meaning, and their predictive capability and applicability to mixtures is limited. An example is the the parachor method [196,197], which is the one traditionally used in industry. It employs empirical relationships that combine the interfacial tension and the difference of densities between phases by means of a temperature-independent parameter, the parachor. The main advantage lays in its simplicity, but it is an approximate method that significantly depends on the chosen scaling exponent for the interfacial tension [198].

Other frequently used methods for the estimation of interfacial tensions are the corresponding states principle [199,200] and the density gradient theory [73,76–78]. An approach based on the corresponding states principle may provide very accurate predictions, but its predictive power strongly depends on the reference fluid chosen and the empirical equations used to describe its thermodynamic properties. Queimada *et al.* [201] recently presented two predictive corresponding states approaches for the surface tension of the *n*-alkanes, which provide very accurate results.

The density gradient theory, based on van der Waals work [74,75], and rediscovered by Cahn and Hilliard [73], relates an equation of state to interfacial properties. The physical background has been presented in chapter 3. As explained in that chapter, the theory explicitly considers the local free energy density within the interface, hence providing a route to obtain density profiles across the interface and the interfacial thickness, which cannot be calculated by empirical methods. The van der Waals' theory for inhomogeneous fluids was originally developed to hold only in the critical region [73,75]. However, it appeared that the theory also gives good results close to the triple point [86].

There has recently been a significant effort towards the investigation of the appli-

cability of the van Cahn-Hilliard density gradient theory for fluids. Several authors have applied the DGT to different equation of state models, mostly the PR and SAFT equations. Cornelisse *et al.* [202] computed interfacial tensions for carbon dioxide, *n*-butane, *n*-decane, and their binary and ternary mixtures with the modified PR EOS of Chou and Prausnitz. They obtained good agreement in general, but the scaling behaviour did not agree with experiments, due to the classical formulation of the EOS. In a later work [203], the same authors provided a temperature-dependent model for the influence parameter that provided critical exponents closer to experimental values, thus improving the description of equilibrium densities and interfacial tensions near the critical point. Miqueu *et al.* [83] employed recently the DGT and the PR EOS with volume corrections to the calculation of interfacial tensions of hydrocarbons, gases and refrigerants. From their results, they stated that the temperature dependence of the influence parameter needs to be retained. They provided a simple correlation to account for this temperature dependence. Contrarily, Kahn and Enders neglected the temperature dependence of the influence parameter and used the PR EOS, the Sanchez-Lacombe and the original SAFT EOS models to compute interfacial tensions for hexane, benzene, methanol and water. They showed that predictions strongly depend on the choice of the model. Although SAFT has a significant advantage for associating substances, Kahn and Enders obtained that, for nonpolar molecules, the PR EOS seems to perform better than the original SAFT regarding the description of interfacial properties.

As discussed extensively in chapter 5, computer simulation is a powerful tool for the calculation of interfacial properties. However, the additional complications due to the appropriate treatment of long-range contributions, and the intensive use of computer time, make it difficult nowadays to use molecular simulations for the extensive computation of interfacial properties of real complex fluids.

The most widespread theory of inhomogeneous fluid systems is the density functional method. It expresses the thermodynamic properties of the system as a functional of the single particle density, and the interfacial density profile is obtained by numerically solving the condition that the functional be a minimum at equilibrium. In this sense, the DGT is also a density functional theory (DFT). A good description of density functional approaches can be found in the book by Evans [204]. Chapman first suggested the use of Wertheim's TPT within a density functional approach [40], and Segura *et al.* [205] proposed a perturbation DFT for inhomogeneous associating fluids. Recently, the SAFT equation has been incorporated within DFT by Blas, Jackson and collaborators [206, 207]. They studied the effect of the association and range of attractive interactions on the vapour-liquid interface. The main advantage of their SAFT-DFT method is that it does not use any empirical parameter for the prediction of interfacial properties, hence being truly molecular and predictive. How-

ever, this may turn out to be a difficulty when predicting interfacial properties of systems for which the free energy functional is not accurately known.

In this work the soft-SAFT equation is incorporated within the Cahn-Hilliard DGT approach for the quantitative prediction of vapour-liquid interfacial tensions of n-alkanes, 1-alkanols, carbon dioxide and mixtures of them. We aim to provide accurate predictions far from and close to the critical region, contrary to the works existing in the literature [84, 85, 202] that employ a DGT approach, in which the description of interfacial tensions near the critical point is rather poor.

6.2   Soft-SAFT+DGT model

The physical and mathematical descriptions of the soft-SAFT and DGT approaches have been presented in Chapters 2 and 3. However, we shall emphasize here that for the computation of interfacial properties of planar interfaces, apart from the molecular parameters for the pure compounds required by the soft-SAFT model, we need to specify a value for the influence parameter, which we treat in an empirical way. As previously commented on, several temperature-dependent expressions for the influence parameter have been used [83, 202, 203] in order to improve the accuracy of the interfacial tensions, particularly near the critical point. In our approach, we assume that its temperature dependence is negligible, hence avoiding the need of additional parameters. This assumption has been proved to be reasonable [84, 85, 87].

It is known that the interfacial tension scales as $\gamma = (T_c - T)^x$. Experiments give a scaling exponent $x = 1.26$, while the classical scaling result is $x = 1.5$. The soft-SAFT+DGT model does not capture the correct scaling of the interfacial tension, due to its classical formulation. Instead of implementing an approach that provides a nonclassical behaviour, such as a modification of the influence parameter [87, 203], or a crossover treatment of the soft-SAFT EOS, we choose a simpler way: we use molecular parameters rescaled to the experimental critical point. For details about the procedure, the reader is referred to Section 4.2. We want to stress that a rescaling of molecular parameters will not change the classical scaling behaviour of the interfacial tension given by our approach, but will impose the condition of null interfacial tension at the experimental critical point, thus providing a better description of the critical region.

The rescaling method is a simple and good way to treat pure systems. This is because the reduced (nondimensional) thermodynamic properties in the soft-SAFT approach do not depend on the size and energy parameters σ and ϵ. The rescaling method, which only changes the values of these two parameters, does not affect the reduced properties of a pure system. In fact, both parameters can be viewed as

Table 6.1: Optimized influence parameter for the compounds studied.

	$10^{19}c$ (J m^5 mol^{-2})		$10^{19}c$ (J m^5 mol^{-2})
methane	0.2992	methanol	0.4283
ethane	0.8148	ethanol	1.033
propane	1.675	1-propanol	1.890
n-butane	2.922	1-butanol	3.032
n-pentane	4.474	1-pentanol	4.064
n-hexane	6.536	1-hexanol	5.696
n-heptane	8.722	1-octanol	9.579
n-octane	11.47	carbon dioxide	0.3125

scaling factors needed for the description of real systems. However, the situation is different when dealing with mixtures, for which the reduced properties also depend on the ratios σ_i/σ_j and ϵ_i/ϵ_j. Whenever component i and component j have different critical points, a rescaling of the parameters will modify these ratios, thus changing the properties of the mixture. Accordingly, we expect that the interfacial properties of mixtures will deviate from experimental values. A more detailed discussion on this issue will be given in the results and discussion section below.

The previously optimized molecular parameters for the n-alkanes (Table 4.1), 1-alkanols and carbon dioxide (Table 4.10) have been rescaled to the experimental vapour-liquid critical temperatures and pressures [110, 208]. As a consequence, the predicted critical density will be off. However, interfacial tensions are typically given as a function of temperature or pressure.

Once molecular parameters are available, the influence parameter has been optimized for each pure compound employing interfacial tension experimental data [209, 210] from the triple point to the critical point. The fitted values are given in Table 6.1 and Figure 6.1.

The trends of the influence parameter for the n-alkane and 1-alkanol series with respect to the carbon number of the chain, presented in Figure 6.1, are physically reasonable. The values can be correlated by the following parabolic functions,

$$10^{19}c_{\ n-alkane} = 0.1488 - 2.999 \times 10^{-2}CN + 0.1804\,CN^2, \qquad (6.1a)$$
$$10^{19}c_{\ 1-alkanol} = 0.1377 + 0.2059\,CN + 0.1212\,CN^2, \qquad (6.1b)$$

which can be used to obtain the influence parameter for longer chains. The influence parameter is given in J m^5 mol^{-2}.
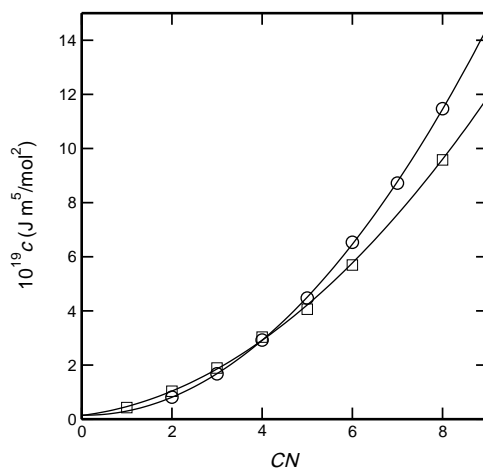
Figure 6.1: Optimized influence parameter for the light members of the n-alkane (circles) and 1-alkanol (squares) series versus the carbon number. Lines correspond to the values obtained from correlations 6.1a and 6.1b.

6.3   Results and discussion

We present results of the soft-SAFT+DGT approach for interfacial tensions of the first eight members of the 1-alkane and 1-alkanol series, and for carbon dioxide, in Figures 6.2a, 6.3 and 6.4, respectively. The experimental data shown in these figures have been used to fit the influence parameter. As expected, the theory correlates experimental data with a good accuracy in all the thermodynamic range for all these systems. If nonrescaled parameters were used, the critical temperature would be overestimated and this would cause the shape of the curve in the vicinity of the critical point to change, lowering the global accuracy. It has to be noted that the good description in the critical region here is not linked to nonclassical effects. Although this can not be observed in the plots presented, the classical scaling exponent $x = 1.5$ is recovered very near to the critical point.

Using eq 6.1a, the influence parameter for heavier alkanes is obtained, and then used to predict interfacial tensions of n-decane, n-dodecane, n-hexadecane and n-eicosane, which are depicted in Figure 6.2b. The agreement is very good, thus showing the suitability of the approach. It would be desirable to compare soft-SAFT+DGT predictions with experimental data for longer 1-alkane and 1-alkanol chains. However,
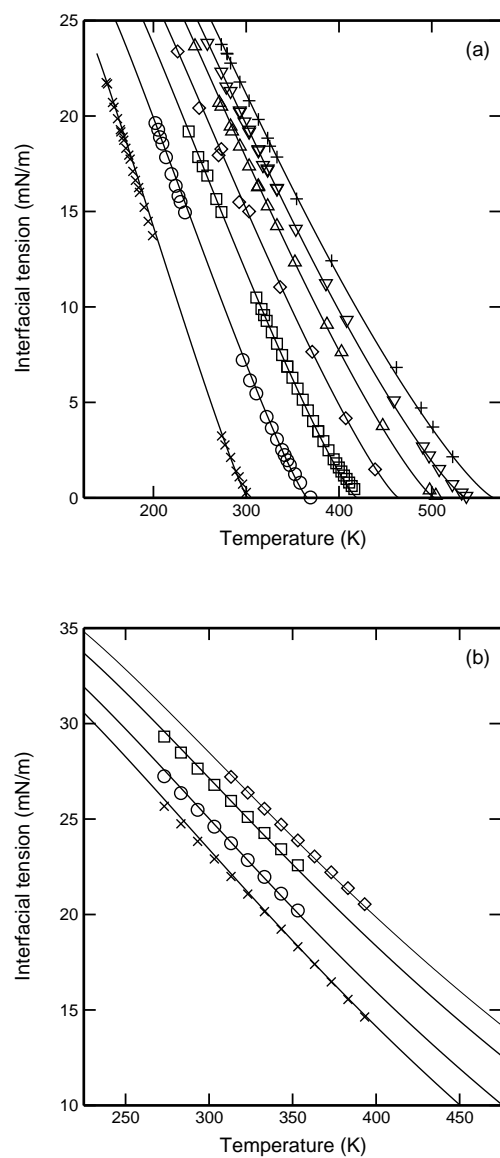
Figure 6.2: Vapour-liquid interfacial tensions of n-alkanes: (a) from ethane to n-octane (from left to right); (b) n-C_{10}, n-C_{12}, n-C_{16} and n-C_{20} (from left to right). Symbols are experimental data [209, 211] and lines correspond to the soft-SAFT+DGT approach.
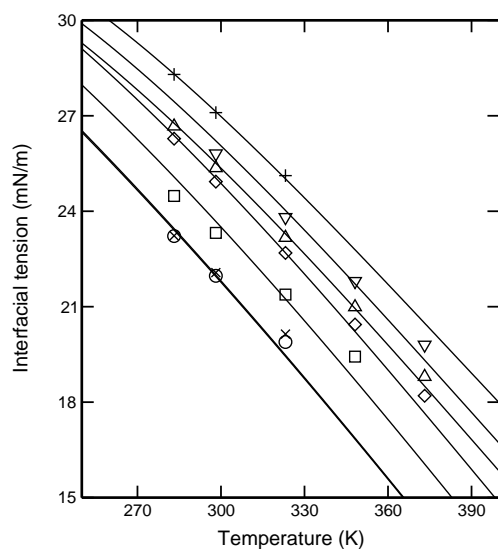
Figure 6.3: Vapour-liquid interfacial tensions of 1-alkanols from methanol to 1-octanol (from left to right), except 1-heptanol. Symbols are experimental data [210] and lines correspond to the soft-SAFT+DGT approach. Note that lines for methanol (crosses) and ethanol (circles) superpose.
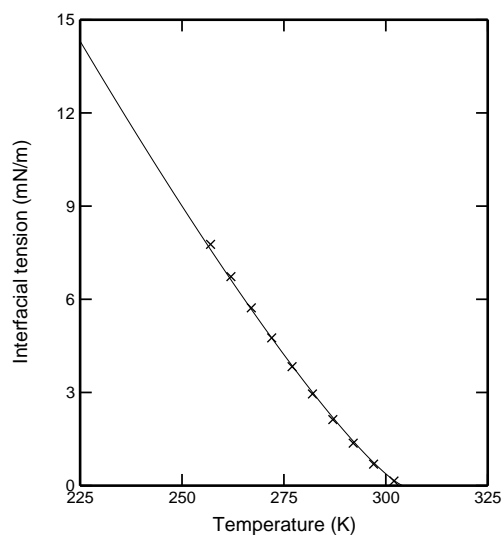
Figure 6.4: Vapour-liquid interfacial tensions of carbon dioxide. Crosses are experimental data [210] and lines correspond to the soft-SAFT+DGT approach.
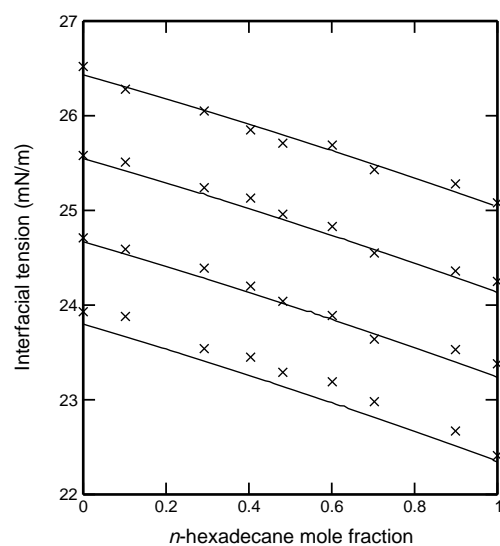
Figure 6.5: Predictions for the vapour-liquid interfacial tensions of the n-hexadecane $+$ n-eicosane mixture at 323.15, 333.15, 343.15 and 353.15 K (from top to bottom). Crosses are experimental data [212] and lines correspond to the soft-SAFT+DGT approach.
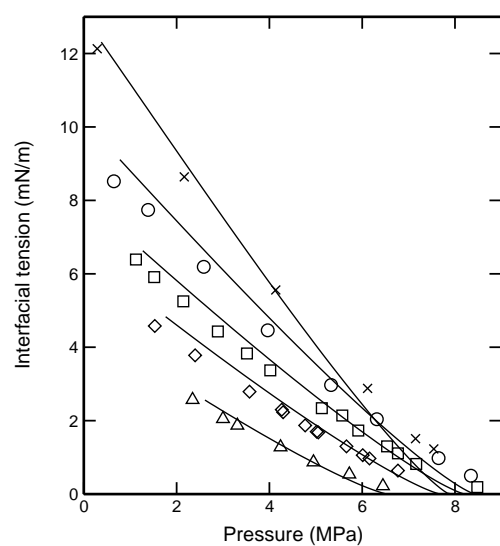
Figure 6.6: Predictions for the vapour-liquid interfacial tensions of the methane $+$ propane mixture at 258.15 (crosses), 283.15 (circles), 303.15 (squares), 318.15 (diamonds) and 338.15 K (triangles). Symbols are experimental data [197] and lines correspond to the soft-SAFT+DGT approach.

measurements of interfacial tensions are scarce or unavailable for all but the most common industrially used compounds. Reliable data is not always available and conflicting datasets can be found even for volatile systems, like carbon dioxide [209].

We have seen that pure systems can be predicted by the soft-SAFT+DGT approach with an accuracy comparable to empirical correlations [209]. Nevertheless, the application of the theory to mixtures, for which empirical equations usually fail, is more interesting. Predictions are shown for the systems n-hexadecane + n-eicosane, methane + propane, and carbon dioxide + n-butane, for which experimental data at several isotherms are available. The simple geometric mean for the cross parameter c_{ij} (eq 3.7 with $\beta = 1$) is employed.

Figure 6.5 shows predictions for the interfacial tensions of four isotherms of the mixture n-hexadecane + n-eicosane. There is no fitting to mixture data ($\eta = \xi = \beta = 1$). Considering the scatter of the experimental data, predictions are in good agreement. Deviations observed in the interfacial tension of the pure components are due to the fact that experimental data come from different sources. A comparison of literature values has been made in reference [211].

Figure 6.6 presents an interfacial tension-pressure plot for the methane + propane mixture. Contrarily to the previous case, one component is supercritical at the thermodynamic conditions shown. This makes the interfacial tension vanish at the critical point of the mixture. In this situation, inaccuracies in the prediction of the critical point can be largely reflected in the accuracy of the description of interfacial tensions. This can be observed in Figure 6.6, and more easily in Figure 6.7, where only data at 303.15 K is shown. Squares and the solid line are the same as those in the previous figure. It is seen that the critical point is underestimated, and that interfacial tensions far from the critical point are higher than the experimental values. Similar deviations in the interfacial tension are also noticeable if they are represented versus composition. These poor predictions are due to a bad description of the bulk properties, which are plotted in Figures 6.8 and 6.9. Note that the solid line in Figures 6.6-6.9 corresponds to the soft-SAFT predictions using rescaled parameters for both pure components with no fitting to mixture data. As a consequence, an incorrect shape of the equilibrium curve is obtained, and subcritical properties largely deviate (see also Figure 4.15).

We tried to improve the description of bulk properties in the mixture methane + propane by fitting the energy binary parameter ξ to the experimental data. Two options were tested: to fit the mixture critical point, and to describe coexisting densities better. The corresponding results for the bulk properties and the interfacial tension are shown in Figures 6.6-6.9 as dashed and dot-dashed lines, respectively. None of these fittings improved the description of interfacial tensions, in spite of the fact that the dashed line reproduces the critical point and almost captures the correct shape.
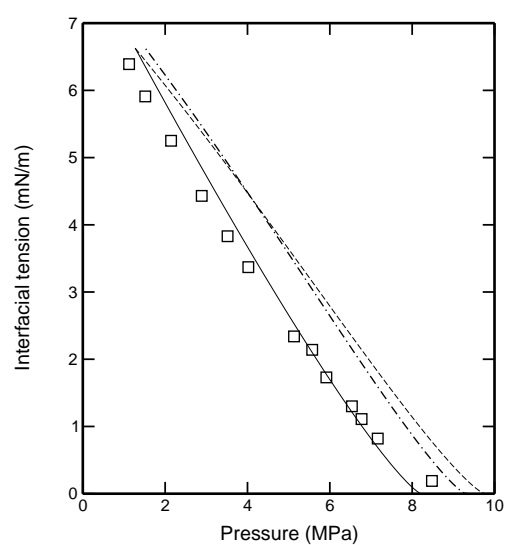
Figure 6.7: Vapour-liquid interfacial tensions of the methane + propane mixture at 303.15 K. Squares are the same experimental data shown in Figure 6.6. The solid line, also shown in the previous figure, corresponds to SAFT+DGT predictions using simple Lorentz-Berthelot rules. The dashed line is obtained when the energy binary parameter is adjusted to reproduce the critical point of the mixture. The dot-dashed line shows predictions when this parameter is adjusted to better describe coexisting densities.

Inaccuracies in the prediction of mixture critical points may cause larger deviations than those just shown. As an example, interfacial tensions at various temperatures as predicted by the soft-SAFT+DGT approach for the carbon dioxide + n-butane mixture are plotted in Figure 6.10. We have chosen this mixture because it has been also studied by Cornelisse [87] and Miqueu [198] with the DGT (coupled with a volume-corrected Peng-Robinson EOS) and parachor methods, providing quantitative agreement with $\beta = 1$. However, the soft-SAFT+DGT predictions have large deviations, although they are qualitatively correct. A $P - T$ projection of the critical line of the mixture is shown in Figure 6.11, as predicted by the soft-SAFT EOS with rescaled parameters. As can be seen in this figure, deviations in the critical pressure are reflected in Figure 6.10. The maximum in the critical line makes isotherms at 319.3 and 344.3 K intersect.

To summarize, the use of rescaled parameters, which is a good option for pure systems and binary mixtures of compounds at subcritical conditions, provides an unrealistic description for bulk properties of mixtures with supercritical components, and may cause important deviations in the predicted interfacial tensions. We want to emphasize that this is not a failure of the DGT, but a consequence of the classical nature of the soft-SAFT EOS. Although the use of nonscaled molecular parameters could provide better results in some cases, we believe that a crossover treatment of the SAFT equation will provide significant improvements in the prediction of interfacial properties.

6.4 Conclusions

The application of the soft-SAFT+DGT approach to real systems has been found to be a successful predictive method. We found that, within this approach, the use of rescaled molecular parameters and a constant influence parameter provides accurate interfacial properties for pure systems in the whole thermodynamic range. The influence parameter for the n-alkane and 1-alkanol series has been found to have a semi-parabolic dependence of the carbon number of the chain. Taking advantage of this, we have reported accurate predictions for the interfacial tensions of heavy n-alkanes.

When dealing with mixtures, the presence of a critical point can cause important deviations in the predicted interfacial tensions, mainly when rescaled parameters are employed. This is due to the classical formulation of the soft-SAFT EOS, which can be corrected by means of crossover functions.
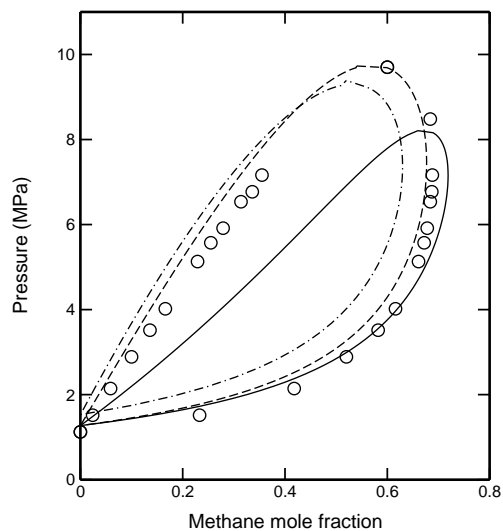
Figure 6.8: Pressure-composition diagram for the methane + propane mixture at 303.15 K. Circles represent experimental data [197] and lines, defined in Figure 6.7, are predictions using parameters for the pure compounds rescaled to the experimental critical point.
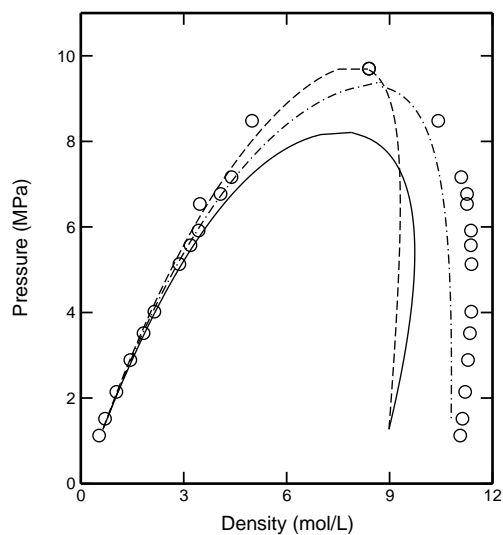
Figure 6.9: Pressure-density diagram for the methane + propane mixture at 303.15 K. See Figure 6.8 for details.
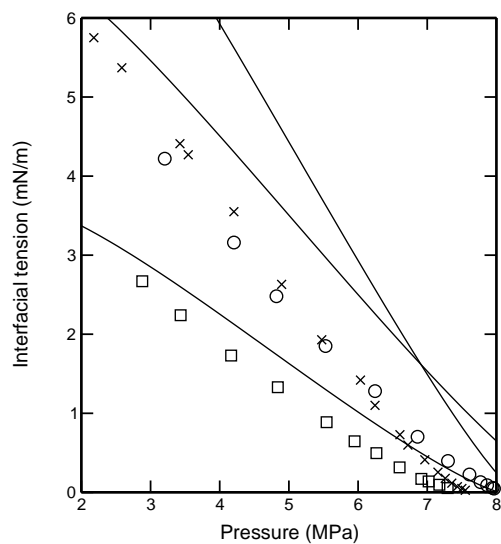
Figure 6.10: Vapour-liquid interfacial tensions of the carbon dioxide + n-butane mixture at 319.3 (crosses), 344.3 (circles) and 377.6 K (squares). Symbols represent experimental data [213] and lines are predictions from the soft-SAFT+DGT approach.
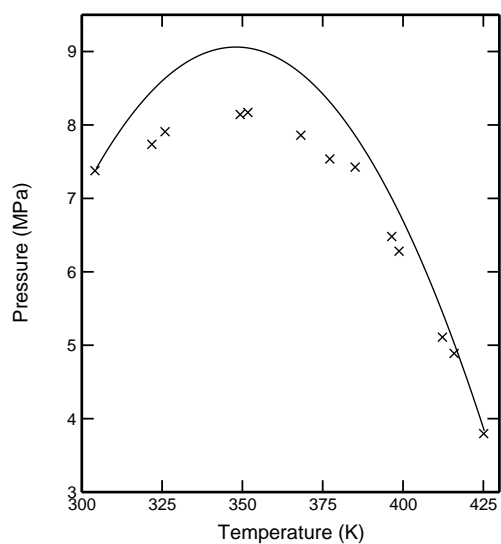
Figure 6.11: Critical line of the carbon dioxide + n-butane mixture. Crosses are experimental data [214] and the line corresponds to the predictions of the soft-SAFT EOS using parameters for the pure compounds rescaled to the experimental critical points.

Chapter 7

Conclusions

This thesis work has been devoted to the development of tools from molecular modelling and their application in the modern molecular thermodynamics area. The Statistical Associating Fluid Theory, the density gradient theory, and molecular simulations, both Monte Carlo and molecular dynamics, have been employed to study the behaviour of bulk and interfacial properties of chain fluids at thermodynamic equilibrium. The real systems treated include pure n-alkanes, n-alkanols, n-perfluoroalkanes, hydrogen, oxygen, xenon, carbon dioxide and a number of mixtures of them.

The soft-SAFT equation of state has been used to study a number of systems: first, a set of transferable and physically meaningful parameters for the n-alkane series was proposed, which linearly correlate with the carbon number of the chain. They allowed to accurately predict the phase envelope of pure heavy n-alkanes and asymmetric binary mixtures of them. It was shown that the soft-SAFT equation also captures the maximum in the critical density observed experimentally. This correlation of molecular parameters for the n-alkane series allowed the study of the critical behaviour of homopolymers. The equation quantitatively predicts available critical properties for relatively long chain lengths, and it shows a crossover to mean-field behaviour when the infinite chain length regime is reached. Moreover, assuming that the volume and dispersive energy per molecule keep their proportionality to molecular weight for very long chains, it was found that the equation predicts a value of 1/5 for the critical compressibility factor of chains of infinite length.

The solubility of hydrogen in long n-alkanes was another successful application of the soft-SAFT equation. It was proven that the soft-SAFT model is able to provide very accurate and reliable results for these very asymmetric systems. The extension of the equation to cross-associating systems allowed a correct description of the solubility of oxygen in n-perfluoroalkanes. It was shown again the importance of physically

meaningful parameters, by showing reasonable trends and comparing parameter values to those from other models when possible. The study of carbon dioxide binary mixtures allowed to conclude that, for an accurate description of these systems, the effect of the quadrupole of the carbon dioxide has to be included in the SAFT model.

The soft-SAFT equation has been coupled with the Cahn-Hilliard density gradient theory for the calculation of properties of planar interfaces. It was shown that the interfacial tension for pure compounds can be accurately predicted with this approach. The influence parameter for the n-alkane and 1-alkanol series shows a parabolic dependence with respect to the carbon number of the chain. Although interfacial properties of subcritical mixtures can be accurately predicted with this approach, problems arise when a critical point is involved. In this case, we believe that a crossover SAFT will greatly improve the description of interfacial properties.

Although most of the work was directed towards the development of a reliable and accurate tool based on SAFT for the prediction of the thermodynamic behaviour of complex fluids, molecular simulations were also used for the computation of bulk and interfacial properties of methane and propane. In particular, a molecular dynamics code was extended for the computation of interfacial density profiles. The influence of the cut-off radius on the coexisting densities was also studied, showing that a cut-off radius of 5.5 times the Lennard-Jones diameter is needed to obtain an accuracy of about 2% when compared to experimental saturated liquid densities.

This work has demonstrated that the keys of an appropriate use of molecular modelling tools are the selection of a suitable specific model representative of the structure and relevant interactions of the real system, and the use of parameters that should show physical trends (within a chemical series) and be transferable (within a chemical series and to other compounds) whenever possible.

The versatility of SAFT and molecular simulations leads to many possible ways of improving molecular models. A few topics are briefly commented below, which could be a natural continuation of this work:

- Combination of the soft-SAFT equation and a renormalization group theory that account for the contributions of long-wavelength fluctuations. A crossover SAFT will give nonclassical critical exponents and an accurate representation close and far from the critical point, which can not be achieved by rescaling molecular parameters to fit experimental critical points. Other versions of the SAFT equation have already followed this path.

- Implementation of multipolar expansion terms into the soft-SAFT equation will allow to account for the effects of electrostatic interactions between molecules. In particular, the inclusion of a quadrupole-quadrupole term is expected to improve the phase-equilibria quantitative prediction of CO_2-based mixtures.

- Quantitative study of the effect of the number and location of association sites on the thermodynamics of freely-jointed Lennard-Jones associating chains by Monte Carlo simulations, and comparison with the predictions of SAFT. In the first level of approximation, SAFT ignores where the sites are placed, and simulations will help on the suitability of this approach for the description of thermodynamic properties of models with specific locations of the sites.

- Extension of the soft-SAFT EOS for the description of the thermodynamic behaviour of near-critical CO_2 + n-alkane + 1-alkanol ternary mixtures, used as model systems in supercritical fluid technology. This kind of mixtures can present interesting fluid behaviour such as miscibility windows and two-phase holes. A SAFT model for these systems would be very useful both from the fundamental and technological points of view.

- Calculation of second-derivatives of the free energy with the soft-SAFT EOS, such as heat capacities or compressibilities. The description of these sensitive properties is a severe test for the quality of equations of state.

Bibliography

[1] Dirac, P. A. M. Quantum mechanics of many-electron systems. *Proc. Roy. Soc. (London)* **123**, 714 (1929).

[2] Mathias, P. M.; Cheng, H.; Cook, S. J.; Klotz, H. C.; Parekh, V. S. Molecular modeling in engineering design and materials development. *Fluid Phase Equilib.* **116**, 225 (1996).

[3] Prausnitz, J. M. Molecular thermodynamics: opportunities and responsibilities. *Fluid Phase Equilib.* **116**, 12 (1996).

[4] Whiting, W. B. Effect of uncertainties in thermodynamic data and models on process calculations. *J. Chem. Eng. Data* **41**, 935 (1996).

[5] Macchietto, S.; Maduabeuke, G.; Szczepanski, R. Exact determination of process sensitivity to physical properties. *Fluid Phase Equilib.* **29**, 59 (1986).

[6] Kister, H. Z. Can we believe the simulation results? *Chem. Eng. Prog.* **98**, 52 (2002).

[7] Horowitz, B. A. Hardware, software, nowhere. *Chem. Eng. Prog.* **94**, 69 (1998).

[8] Chapman, W. G.; Gubbins, K. E.; Jackson, G.; Radosz, M. SAFT-equation-of-state solution model for associating fluids. *Fluid Phase Equilib.* **52**, 31 (1989).

[9] Chapman, W. G.; Gubbins, K. E.; Jackson, G.; Radosz, M. New reference equation of state for associating liquids. *Ind. Eng. Chem. Res.* **29**, 1709 (1990).

[10] Huang, S. H.; Radosz, M. Equation of state for small, large, polydisperse, and associating molecules. *Ind. Eng. Chem. Res.* **29**, 2284 (1990).

[11] Huang, S. H.; Radosz, M. Equation of state for small, large, polydisperse, and associating molecules - Extension to fluid mixtures. *Ind. Eng. Chem. Res.* **30**, 1994 (1991).

[12] Wertheim, M. S. Fluids with highly directional attractive forces. 1. Statistical thermodynamics. *J. Stat. Phys.* **35**, 19 (1984).

[13] Wertheim, M. S. Fluids with highly directional attractive forces. 2. Thermodynamic perturbation-theory and integral-equations. *J. Stat. Phys.* **35**, 35 (1984).

[14] Wertheim, M. S. Fluids with highly directional attractive forces. 3. Multiple attraction sites. *J. Stat. Phys.* **42**, 459 (1986).

[15] Wertheim, M. S. Fluids with highly directional attractive forces. 4. Equilibrium polymerization. *J. Stat. Phys.* **42**, 477 (1986).

[16] Müller, E. A.; Gubbins, K. E. Molecular-based equations of state for associating fluids: a review of SAFT and related approaches. *Ind. Eng. Chem. Res.* **40**, 2193 (2001).

[17] Gil-Villegas, A.; Galindo, A.; Whitehead, P. J.; Mills, S. J.; Jackson, G.; Burgess, A. N. Statistical associating fluid theory for chain molecules with attractive potentials of variable range. *J. Chem. Phys.* **106**, 4168 (1997).

[18] Gross, J.; Sadowski, G. Perturbed-chain SAFT: an equation of state based on a perturbation theory for chain molecules. *Ind. Eng. Chem. Res.* **40**, 1244 (2001).

[19] Blas, F. J.; Vega, L. F. Thermodynamic behaviour of homonuclear and heteronuclear Lennard-Jones chains with association sites from simulation and theory. *Molec. Phys.* **92**, 135 (1997).

[20] Economou, I. Statistical Associating Fluid Theory: a successful model for the calculation of thermodynamic and phase equilibrium properties of complex fluid mixtures. *Ind. Eng. Chem. Res.* **41**, 953 (2002).

[21] Pericaud, P.; Galindo, A.; Jackson, G. Recent advances in the use of the SAFT approach in describing electrolytes, interfaces, liquid crystals and polymers. *Fluid Phase Equilib.* **194-197**, 87 (2002).

[22] Frenkel, D.; Smit, B. *Understanding molecular simulation: from algorithms to applications.* Academic Press, 2nd edition, 2001.

[23] Jackson, G. Theory of closed-loop liquid liquid immiscibility in mixtures of molecules with directional attractive forces. *Mol. Phys.* **72**, 1365 (1991).

[24] Dolezalek, F. Zur Theorie der binären Gemische und konzentrierten Lösungen. *Z. Phys. Chem.* **64**, 727 (1908).

[25] Guggenheim, E. A. *Mixtures.* Oxford University Press, 1952.

[26] Wilson, G. M. Vapor-liquid equilibrium. XI: A new expression for the excess free energy of mixing. *J. Am. Chem. Soc.* **86**, 127 (1964).

[27] Abrams, D.; Prausnitz, J. M. Statistical thermodynamics of liquid mixtures: A new expression for the excess Gibbs energy of partly or completely miscible systems. *AIChE J.* **21**, 116 (1975).

[28] Andersen, H. C. Clusters expansions for hydrogen-bonded fluids. 1. Molecular association in dilute gases. *J. Chem. Phys.* **59**, 4714 (1973).

[29] Andersen, H. C. Clusters expansions for hydrogen-bonded fluids. 2. Dense liquids. *J. Chem. Phys.* **61**, 4985 (1974).

[30] Cummings, P. T.; Stell, G. Statistical mechanical models of chemical reactions: analytical solution of models of $A + B \Leftrightarrow AB$ in the Percus-Yevick approximation. *Molec. Phys.* **51**, 253 (1984).

[31] Cummings, P. T.; Blum, L. Analytic solution of the molecular Ornstein-Zernike equation for non-spherical molecules. Spheres with anisotropic surface adhesion. *J. Chem. Phys.* **84**, 1833 (1986).

[32] Chapman, W. G.; Gubbins, K. E.; Joslin, C. G.; Gray, C. G. Mixtures of polar and associating molecules. *Pure Appl. Chem.* **59**, 53 (1987).

[33] Chapman, W. G.; Gubbins, K. E.; Joslin, C. G.; Gray, C. G. Theory and simulation of associate liquid mixtures. *Fluid Phase Equilib.* **29**, 337 (1986).

[34] Joslin, C. G.; Gray, C. G.; Chapman, W. G.; Gubbins, K. E. Theory and simulation of associating liquid mixtures. II. *Molec. Phys.* **62**, 843 (1987).

[35] Jackson, G.; Chapman, W. G.; Gubbins, K. E. Phase equilibria of associating fluids. Spherical molecules with multiple bonding sites. *Molec. Phys.* **65**, 1 (1988).

[36] Wertheim, M. S. Thermodynamic perturbation theory of polymerization. *J. Chem. Phys.* **87**, 7323 (1987).

[37] Chapman, W. G.; Jackson, G.; Gubbins, K. E. Phase equilibria of associating fluids. Chain molecules with multiple bonding sites. *Molec. Phys.* **65**, 1057 (1988).

[38] Chapman, W. G. Prediction of the thermodynamic properties of associating Lennard-Jones fluids: Theory and simulation. *J. Chem. Phys.* **93**, 4299 (1990).

[39] Blas, F. J.; Vega, L. F. Thermodynamic properties and phase equilibria of branched chain fluids using first- and second-order Wertheim's thermodynamic perturbation theory. *J. Chem. Phys.* **115**, 3906 (2001).

[40] Chapman, W. G. *Theory and simulation of associating liquid mixtures*. Ph. D. thesis, Cornell Univerity, Ithaca, NY, 1988.

[41] Banaszak, M.; Chiew, Y. C.; Radosz, M. Thermodynamic perturbation theory. Sticky chains and square-well chains. *Phys. Rev. E* **48**, 3760 (1993).

[42] Sadowski, G. A square-well based equation of state taking into account the connectivity in chain molecules. *Fluid Phase Equilib.* **149**, 75 (1998).

[43] Tavares, F. W.; Chang, J.; Sandler, S. I. A completely analytic equation of state for the square-well chain fluid of variable well width. *Fluid Phase Equilib.* **140**, 129 (1997).

[44] Davies, L. A.; Gil-Villegas, A.; Jackson, G. An analytical equation of state for chain molecules formed from Yukawa segments. *J. Chem. Phys.* **111**, 8659 (1999).

[45] Johnson, J. K.; Zollweg, J. A.; Gubbins, K. E. The Lennard-Jones equation of state revisited. *Molec. Phys.* **78**, 591 (1993).

[46] Kolafa, J.; Nezbeda, I. The Lennard-Jones fluid - an accurate analytic and theoretically-based equation of state. *Fluid Phase Equilib.* **100**, 1 (1994).

[47] Müller, E. A.; Gubbins, K. E. An equation of state for water from a simplified intermolecular potential. *Ind. Eng. Chem. Res.* **34**, 3662 (1995).

[48] Kraska, T.; Gubbins, K. E. Phase equilibria calculations with a modified SAFT equation of state. 1. Pure alkanes, alkanols, and water. *Ind. Eng. Chem. Res.* **35**, 4727 (1996).

[49] Economou, I. G.; Tsonopoulos, C. Associating models and mixing rules in equations of state for water/hydrocarbon mixtures. *Chem. Eng. Sci.* **52**, 511 (1997).

[50] Rowlinson, J. S.; Swinton, F. L. *Liquid and Liquid Mixtures.* Butterworth Scientific, London, 1982.

[51] Díaz Peña, M.; Pando, C.; Renuncio, J. A. R. Combination rules for intermolecular potential parameters. I. Rules based on approximations for the long-range dispersion energy. *J. Chem. Phys.* **76**, 325 (1982).

[52] Müller, E. A.; Gubbins, K. E. Simulation of hard triatomic and tetratomic molecules. A test of associating fluid theories. *Molec. Phys.* **80**, 957 (1993).

[53] Johnson, J. K.; Müller, E. A.; Gubbins, K. E. Equation of state for Lennard-Jones chains. *J. Phys. Chem.* **98**, 6413 (1994).

[54] Honnell, K. G.; Hall, C. K. A new equation of state for athermal chains. *J. Chem. Phys.* **90**, 1841 (1989).

[55] Chang, J.; Sandler, S. I. An equation of state for the hard-sphere chain fluid: theory and Monte Carlo simulation. *Chem. Eng. Sci.* **49**, 2777 (1994).

[56] Ghonasgi, D.; Chapman, W. G. A New equation of state for hard chain molecules. *J. Chem. Phys.* **100**, 6633 (1994).

[57] Flory, P. J. *Principles of polymer chemistry.* Cornell University Press, Ithaca, NY, 1953.

[58] Müller, E. A.; Vega, L. F.; Gubbins, K. E. Theory and simulation of associating fluids: Lennard-Jones chains with association sites. *Molec. Phys.* **83**, 1209 (1994).

[59] Walsh, J. M.; Gubbins, K. E. The liquid structure and thermodynamic properties of Lennard-Jones spheres with association sites. *Molec. Phys.* **80**, 65 (1993).

[60] Johnson, J. K.; Gubbins, K. E. Phase equilibria for associating Lennard-Jones fluids from theory and simulation. *Molec. Phys.* **77**, 1033 (1992).

[61] Müller, E. A.; Gubbins, K. E.; Tsangaris, D. M.; de Pablo, J. J. Comment on the accuracy of Wertheim's theory of associating fluids. *J. Chem. Phys.* **103**, 3868 (1995).

[62] Weeks, J. D.; Chandler, D.; Andersen H. C. Role of repulsive forces in determining the equilibrium structure of simple liquids. *J. Chem. Phys.* **54**, 5237 (1971).

[63] Ghonasgi, D.; Chapman, W. G. Prediction of the properties of model polymer-solutions and blends. *AIChE J.* **40**, 878 (1994).

[64] Kraska, T.; Gubbins, K. E. Phase equilibria calculations with a modified SAFT equation of state. 2. Binary mixtures of *n*-alkanes, 1-alkanols, and water. *Ind. Eng. Chem. Res.* **35**, 4738 (1996).

[65] Delhommelle, J.; Boutin, A.; Tavitian, B.; Mackie, A. D.; Fuchs, A. H. Vapour-liquid coexistence curves of the united-atom and anisotropic united-atom force fields for alkane mixtures. *Molec. Phys.* **96**, 1517 (1999).

[66] Johnson, J. K. Perturbation theory and computer simulations for linear and ring model polymers. *J. Chem. Phys.* **104**, 1729 (1996).

[67] Fotouh, K.; Shukla, K. A comparative study of numerical methods for calculating phase equilibria in fluid mixtures form an equation of state. *Chem. Eng. Sci.* **51**, 3763 (1996).

[68] Xu, G.; Brennecke, J. F.; Stadtherr, M. A. Reliable computation of phase stability and equilibrium from the SAFT equation of state. *Ind. Eng. Chem. Res.* **41**, 938 (2002).

[69] Sadus, R. J. *High-pressure phase behaviour of multicomponent fluid mixtures.* Elsevier, Amsterdam, 1992.

[70] Powell, M. J. D. *A fortran subroutine for solving systems of nonlinear algebraic equations.* Numerical methods for nonlinear algebraic equations; Rabinowitz, P. (editor); Gordon & Breach, New York, 1970.

[71] More, J. J. *The Levenberg-Marquardt algorithm: Implementation and theory.* Numerical Analysis; Watson, G. A. (editor); Springer-Verlag, New York, 1977.

[72] More, J.; Garbow, B.; Hillstrom, K. *User guide for minpack: Technical Report ANL-80-74.* Argonne National Laboratory, Argonne, IL, 1980.

[73] Cahn, J. W.; Hilliard, J. E. Free energy of a nonuniform system. I. Interfacial free energy. *J. Chem. Phys.* **28**, 258 (1958).

[74] van der Waals, J. D. Thermodynamische theorie der kapillarität unter voraussetzung stetiger dichteänderung. *Z. Phys. Chem.* **13**, 657 (1894).

[75] van der Waals, J. D. The thermodynamic theory of capillarity under the hypothesis of a continuous density variation. *J. Stat. Phys.* **20**, 197 (1976).

[76] Carey, B. S.; Striven, L. E.; Davis, H. T. Semiempirical theory of surface tensions of pure normal alkanes and alcohols. *AIChE J.* **24**, 1076 (1978).

[77] Carey, B. S.; Striven, L. E.; Davis, H. T. On gradient theories of fluid interfacial stress and structure. *J. Chem. Phys.* **69**, 5040 (1978).

[78] Carey, B. S.; Striven, L. E.; Davis, H. T. Semiempirical theory of surface tension of binary systems. *AIChE J.* **26**, 705 (1980).

[79] Rowlinson, J. S.; Widom, B. *Molecular theory of capillarity*, volume 8th. Oxford University Press, Oxford, UK, international series of monographs on chemistry edition, 1989.

[80] Bongiorno, V.; Davis, H. T. Modified van der Waals theory of fluid interfaces. *Phys. Rev. A* **12**, 2213 (1975).

[81] Yang, A. J. M.; Fleming, P. D.; Gibbs, J. H. A molecular theory of interfacial phenomena in multicomponent systems. *J. Chem. Phys.* **64**, 3732 (1976).

[82] Bongiorno, V.; Scriven, L. E.; Davis, H. T. Molecular theory of fluid interfaces. *J. Colloid Interface Sc.* **57**, 462 (1976).

[83] Miqueu, C.; Mendiboure, B.; Graciaa, A., Lachaise, J. Modelling of the surface tension of pure components with the gradient theory of fluid interfaces: a simple and accurate expression for the influence parameters. *Fluid Phase Equilib.* **207**, 225 (2003).

[84] Kahl, H.; Enders, S. Calculation of surface properties of pure fluids using density gradient theory and SAFT-EOS. *Fluid Phase Equilib.* **172**, 27 (2000).

[85] Kahl, H.; Enders, S. Interfacial properties of binary mixtures. *Phys. Chem. Chem. Phys.* **4**, 931 (2002).

[86] Davis, H. T.; Striven, L. E. Stress and structure in fluid phase interfaces. *Adv. Chem. Phys.* **49**, 357 (1982).

[87] Cornelisse, P. M. W. *The Gradient theory applied. Simultaneous modelling of interfacial tension and phase behaviour.* Ph. D. thesis, Delft University of Technology, The Netherlands, 1997.

[88] McCoy, B. F.; Davis, H. T. Free-energy theory of inhomogeneous fluids. *Phys. Rev. A* **20**, 1201 (1979).

[89] Poser, C. I.; Sanchez, I. C. Interfacial tension theory of low and high molecular weight liquid mixtures. *Macromolecules* **14**, 361 (1981).

[90] Anselme, M. J.; Gude, M.; Teja, A. S. The critical temperatures and densities of the n-alkanes from pentane to octadecane. *Fluid Phase Equilib.* **57**, 317 (1990).

[91] Siepmann, J. I.; Karaborni, S.; Smit, B. Vapor-liquid-equilibria of model alkanes. *J. Am. Chem. Soc.* **115**, 6454 (1993).

[92] Smit, B.; Karaborni, S.; Siepmann, J. I. Computer simulations of vapor-liquid-phase equilibria of n-alkanes. *J. Chem. Phys.* **102**, 2126 (1995).

[93] Toxvaerd, S. Molecular-dynamics calculation of the equation of state of alkanes. *J. Chem. Phys.* **93**, 4290 (1990).

[94] Mackie, A. D.; Hernandez-Cobos, J.; Vega, L. F. Liquid vapor equilibria for an ab initio model for water. *J. Chem. Phys.* **111**, 2103 (1999).

[95] Nath, S. K.; Escobedo, F. A.; de Pablo, J. J. On the simulation of vapor-liquid equilibria for alkanes. *J. Chem. Phys.* **108**, 9905 (1998). A misprint in Table 2 for the coexistence densities of n-hexadecane has been observed. We thank the authors for providing us the correct data.

[96] Nath, S. K.; Escobedo, F. A.; de Pablo, J. J.; Patramai, I. Simulation of vapor-liquid equilibria for alkane mixtures. *Ind. Eng. Chem. Res.* **37**, 3195 (1998).

[97] Martin, M. G.; Siepmann, J. I. Transferable potentials for phase equilibria. 1. United-atom description of n-alkanes. *J. Phys. Chem. B* **102**, 2569 (1998).

[98] Chen, B.; Siepmann, J. I. Transferable potentials for phase equilibria. 3. Explicit-hydrogen description of normal alkanes. *J. Phys. Chem. B* **103**, 5370 (1999).

[99] Errington, J. R.; Panagiotopoulos, A. Z. A new intermolecular potential model for the *n*-alkane homologous series. *J. Phys. Chem. B* **103**, 6314 (1999).

[100] Vega, C.; MacDowell, L. G. Understanding the critical properties of chain molecules. *Molec. Phys.* **88**, 1575 (1986).

[101] Blas, F. J.; Vega, L. F. Prediction of binary and ternary diagrams using the statistical associating fluid theory (SAFT) equation of state. *Ind. Eng. Chem. Res.* **37**, 660 (1998).

[102] Blas, F. J.; Vega, L. F. Critical behavior and partial miscibility phenomena in binary mixtures of hydrocarbons by the statistical associating fluid theory. *J. Chem. Phys.* **109**, 7405 (1998).

[103] Fu, Y. H.; Sandler, S. I. A simplified SAFT equation of state for associating compounds and mixtures. *Ind. Eng. Chem. Res.* **34**, 1897 (1995).

[104] Galindo, A.; Whitehead, P. J.; Jackson, G.; Burgess, A. N. Predicting the high-pressure phase equilibria of water plus *n*-alkanes using a simplified SAFT theory with transferable intermolecular interaction parameters. *J. Phys. Chem.* **100**, 6781 (1996).

[105] McCabe, C.; Jackson, G. SAFT-VR modelling of the phase equilibrium of long-chain *n*-alkanes. *Phys. Chem. Chem. Phys.* **1**, 2057 (1999).

[106] Vega, L. F.; Blas, F. J. Tricritical phenomena in chain-like mixtures from a molecular-based equation of state. *Fluid Phase Equilib.* **171**, 91 (2000).

[107] NIST Chemistry Webbook. http://webbook.nist.gov/chemistry.

[108] Smith, B. D.; Srivastava, R. *Thermodynamic data for pure compounds: part A hydrocarbons and ketones.* Elsevier, Amsterdam, The Netherlands, 1986.

[109] Kiselev, S. B.; Ely, J. F. Crossover SAFT equation of state: application for normal alkanes. *Ind. Eng. Chem. Res.* **38**, 4993 (1999).

[110] Ambrose, D.; Tsonopoulos, C. Vapor-liquid critical properties of elements and compounds. 2. Normal-alkanes. *J. Chem. Eng. Data* **40**, 531 (1995).

[111] Blas, F. J.; Contreras, O. R.; Mackie, A. D.; Vega, L. F. Improved vapor-liquid equilibria predictions for Lennard-Jones chains from the statistical associating fluid dimer theory: comparison with Monte Carlo simulations. *J. Chem. Phys.* **115**, 4355 (2001).

[112] Gmehling, J.; Onken, U.; Arlt, W. *Vapor-liquid equilibrium data collection.* DECHEMA, Frankfurt/Main, Germany, 2nd edition, 1997-2001.

[113] Peters, C. J.; de Roo, J. L.; Lichtenthaler, R. N. Measurements and calculations of phase-equilibria of binary-mixtures of ethane + eicosane. 1. Vapor + liquid equilibria. *Fluid Phase Equilib.* **34**, 287 (1987).

[114] Nikitin, E. D. The critical properties of thermally unstable substances: measurement methods, some results and correlations. *High Temp.* **2**, 305 (1998).

[115] Wilding, N. B.; Müller, M.; Binder, K. Chain length dependence of the polymer-solvent critical point parameters. *J. Chem. Phys.* **105**, 802 (1996).

[116] MacDowell, L. G.; Müller, M.; Vega, C.; Binder, K. Equation of state and critical behavior of polymer models: a quantitative comparison between Wertheim's thermodynamic perturbation theory and computer simulations. *J. Chem. Phys.* **113**, 419 (2000).

[117] Pàmies, J. C.; Vega, L. F. Critical properties of homopolymer fluids studied by a Lennard-Jones statistical associating fluid theory. *Molec. Phys.* **100**, 2519 (2002).

[118] Pàmies, J. C.; Vega, L. F. Vapor-liquid equilibria and critical behavior of heavy *n*-alkanes using transferable parameters from the soft-SAFT equation of state. *Ind. Eng. Chem. Res.* **40**, 2532 (2001).

[119] Shinozaki, K.; Van Tan, T.; Saito, Y.; Nose, T. Interfacial-tension of demixed polymer-solutions near the critical-temperature-polystyrene+methylcyclohexane. *Polymer* **23**, 728 (1982).

[120] Perzynski, R.; Delsanti, M.; Adam, M. Experimental-study of polymer interactions in a bad solvent. *J. Phys. (France)* **48**, 115 (1987).

[121] Chu, B.; Wang, Z. An extended universal coexistence curve for polymer solutions. *Macromolecules* **21**, 2283 (1988).

[122] Xia, K. Q.; Franck, C.; Widom, B. Interfacial tensions of phase-separated polymer solutions. *J. Chem. Phys.* **97**, 1446 (1992).

[123] Panagiotopoulos, A. Z.; Wong, V. Phase equilibria of lattice polymers from histogram reweighting Monte Carlo simulations. *Macromolecules* **31**, 912 (1998).

[124] Frauenkron, H.; Grassberger, P. Critical unmixing of polymer solutions. *J. Chem. Phys.* **107**, 9599 (1997).

[125] Duplantier, B. Lagrangian tricritical theory of polymer-chain solutions near the theta-point. *J. Phys. (France)* **43**, 991 (1982).

[126] Duplantier, B. Geometry of polymer-chains near the theta-point and dimensional regularization. *J. Chem. Phys.* **86**, 4233 (1987).

[127] Szleifer, I. A new mean-field theory for dilute polymer solutions: Phase diagram, conformational behavior and interfacial properties. *J. Chem. Phys.* **92**, 6940 (1990).

[128] Chatterjee, A. P.; Schweizer, K. S. Analytic integral equation theory for the critical properties of homopolymer fluids. *J. Chem. Phys.* **108**, 3813 (1998).

[129] Yan, Q.; de Pablo, J. J. Critical behavior of lattice polymers studied by Monte Carlo simulations. *J. Chem. Phys.* **113**, 5954 (2000).

[130] Panagiotopoulos, A. Z. On the equivalence of continuum and lattice models for fluids. *J. Chem. Phys.* **112**, 7132 (2000).

[131] Mackie, A. D.; Panagiotopoulos, A. Z.; Kumar, S. Monte Carlo simulations of phase equilibria for a lattice homopolymer model. *J. Chem. Phys.* **102**, 1014 (1995).

[132] Vega, C.; MacDowell, L. G. Critical temperature of infinitely long chains from Wertheim's perturbation theory. *Molec. Phys.* **98**, 1295 (2000).

[133] Escobedo, F. A.; de Pablo, J. J. Simulation and prediction of vapour-liquid equilibria for chain molecules. *Molec. Phys.* **87**, 347 (1996).

[134] Jiang, J.; Prausnitz, J. M. Phase equilibria for chain-fluid mixtures near to and far from the critical region. *AIChE J.* **46**, 2525 (2000).

[135] Jiang, J.; Prausnitz, J. M. Equation of state for thermodynamic properties of chain fluids near-to and far-from the vaporliquid critical region. *J. Chem. Phys.* **111**, 5964 (2000).

[136] Chen, J.; Mi, J. Equation of state extended from SAFT with improved results for non-polar fluids across the critical point. *Fluid Phase Equilib.* **186**, 165 (2001).

[137] Lemmon, E. W.; Goodwin, A. R. H. Critical properties and vapor pressure equation for alkanes C_nH_{2n+2}: Normal alkanes with $n \leq 36$ and isomers for $n = 4$ through $n = 9$. *J. Phys. Chem. Ref. Data* **29**, 1 (2000).

[138] Dobashi, T.; Nakata, M.; Kaneko, M. Coexistence curve of polystyrene in methylcyclohexane. I. Range of simple scaling and critical exponents. *J. Chem. Phys.* **72**, 6685 (1980).

[139] Lue, L.; Friend, D. G.; Elliot, J. R. Critical compressibility factors for chain molecules. *Molec. Phys.* **98**, 1473 (2000).

[140] Florusse, L. J.; Pàmies, J. C.; Vega, L. F.; Peters, C. J.; Meijer H. Solubility of hydrogen in heavy *n*-alkanes: experiments and SAFT modeling. *AIChE J.* (2003). Article in press.

[141] Lin, H.; Sebastian, H. M.; Chao K. Gas-liquid equilibrium in hydrogen + *n*-hexadecane and methane + *n*-hexadecane at elevated temperatures and pressures. *J. Chem. Eng. Data* **25**, 252 (1980).

[142] Park, J.; Robinson, Jr.; R. L.; Gasem, K. A. M. Solubilities of hydrogen in heavy normal paraffins at temperatures from 323.2 to 423.2 K and pressures to 17.4 MPa. *J. Chem. Eng. Data* **40**, 241 (1995).

[143] Twu, C. H.; Coon, J. E.; Harvey, A. H.; Cunningham, J. R. An approach for the application of a cubic equation of state to hydrogen-hydrocarbon systems. *Ind. Eng. Chem. Res.* **35**, 905 (1996).

[144] Chechik, V.; Crooks, R. M. Dendrimer-encapsulated Pd nanoparticles as fluorous phase-soluble catalysts. *J. Am. Chem. Soc.* **122**, 1243 (2000).

[145] Banks, R. E.; Smart, B. E.; Tatlow, J. C. *Organofluorine chemistry: principles and commercial applications*, chapter Fluorinated textile finishes and surfactants, pages 321–336. Kluwer Academic/Plenum, New York, 1994.

[146] Raveendran, P.; Wallen, S. Exploring CO_2-philicity: Effects of stepwise fluorination. *J. Phys. Chem. B* **107**, 1473 (2003).

[147] Banks, R. E.; Smart, B. E.; Tatlow, J. C. *Organofluorine chemistry: principles and commercial applications*, chapter Properties and biomedical applications of perfluoro-chemicals and their emulsions, page 555. Kluwer Academic/Plenum, New York, 1994.

[148] Miller, J. H. Jr.; Googe, J. M. Jr.; Hoskins, J. C. Combined macular hole and cataract surgery. *Am. J. Ophthalmol.* **123**, 705 (1997).

[149] Wolber, J.; Rowland, I.; Leach, M.; Bifone, A. Perfluorocarbon emulsions as intra-venous delivery media for hyperpolarized xemon. *Magnetic Resonance in Medicine* **41**, 442 (1999).

[150] Cui, S. T.; Siepmann, J. I.; Cochran, H. D.; Cummings, P. T. Intermolecular potentials and vapor-liquid phase equilibria of perfluorinated alkanes. *Fluid Phase Equilib.* **146**, 51 (1998).

[151] Watkins, E. K.; Jorgensen, W. L. Perfluoroalkanes: conformational analysis and liquid-state properties from *ab initio* and Monte Carlo calculations. *J. Phys. Chem. A* **105**, 4118 (2001).

[152] Bonifácio, R. P.; Filipe, E. J. M.; McCabe, C.; Costa Gomes, M. F.; Pádua, A. A. H. Predicting the solubility of xenon in n-hexane and n-perfuorohexane: a simulation and theoretical study. *Molec. Phys.* **100**, 2547 (2002).

[153] McCabe, C.; Galindo, A.; Gil-Villegas, A.; Jackson, G. Predicting the high-pressure phase equilibria of binary mixtures of perfluoro-n-alkanes + n-alkanes using the SAFT-VR approach. *J. Phys. Chem. B* **102**, 8060 (1998).

[154] Hesse, P.; Battino, R.; Scharlin, P.; Wilhelm, E. Solubility of gases in liquids. 20. Solubility of He, Ne, Ar, Kr, N_2, O_2, CH_4, CF_4, and SF_6 in n-alkanes n-C_lH_{2l+2} ($6 \leq l \leq 16$) at 298.15 K. *J. Chem. Eng. Data* **41**, 195 (1996).

[155] Wilcock, R.; Battino, R.; Danforth, W.; Wilhelm, E. The solubility of gases in Liquids. ll. The solubility of He, Ne, Ar, Kr, O_2, N_2, CO, CO_2, CH_4, CF_4, and SF_6 in n-octane, 1-octanol, n-decane, and 1-decanol at 1 atm and 283 to 313 K. *J. Chem. Thermodynamics* **10**, 817 (1978).

[156] Makranczy J.; Megyery-Balog, K.; Rusz, L.; patyi, L. Solubility of gases in normal-alkanes. *Hungarian J. Ind. Chem.* **4**, 269 (1976).

[157] Brown, J. A.; Mears, W. H. Physical properties of n-perfluorobutane. *J. Phys. Chem.* **62**, 960 (1958).

[158] Barber, E, J.; Cady, G. H. Vapor Pressures of perfluoropentanes. *J. Phys. Chem.* **60**, 504 (1956).

[159] Burger, L. L.; Cady, G. H. Physical properties of perfluoropentanes. *J. Am. Chem. Soc.* **73**, 4243 (1951).

[160] Caço A. I.; Dias, A. M. A.; Piñeiro, M.; Coutinho, J. A. P.; Marrucho, I. M. Unpub-lished results.

[161] Steele, W. V.; Chirico, R. D.; Knipmeyer, S. E.; Nguyen, A. Vapor pressure, heat capacity, and density along the saturation line. Measurements for cyclohexanol, 2-cyclohexen-1-one, 1,2-dichloropropane, 1,4-di-*tert*-butylbenzene, ($\pm$)-2-ethylhexanoic acid, 2-(methylamino)ethanol, perfluoro-*n*-heptane, and sulfolane. *J. Chem. Eng. Data* **42**, 1021 (1997).

[162] Kreglewski, A. volume X, 11-12. Bulletin de l'Academie Polonaise des Sciences, 1962.

[163] Hariharan, A.; Harris, J. G. Structure and thermodynamics of the liquid-vapor interface of fluorocarbons and semifluorinated alkane diblocks: a molecular dynamics study. *J. Chem. Phys.* **101**, 4156 (1994).

[164] Kiselev, S. B.; Ely, J. F. Simplified crossover SAFT equation of state for pure fluids and fluid mixtures. *Fluid Phase Equilib.* **174**, 93 (2000).

[165] Duce, C.; Tinè, M.; Lepori, L.; Matteoli, E. VLE and LLE of perfluoroalkane + alkane mixtures. *Fluid Phase Equilib.* **199**, 197 (2002).

[166] Scott, R. L.; Van Konynenburg, P. H. Van der Waals and related models for hydrocarbon mixtures. *Discuss. Faraday Soc.* **49**, 87 (1970).

[167] Filipe, E. J. M.; Dias, L. M. B.; Calado, J. C. G.; McCabe, C.; Jackson, G. Is xenon an "ennobled" alkane? *Phys. Chem. Chem. Phys.* **4**, 1618 (2002).

[168] Kennan, R.; Pollack, G. Solubility of xenon in perfluoroalkanes: Temperature dependence and thermodynamics. *J. Chem. Phys.* **89**, 517 (1988).

[169] Dias, A. M. A.; Freire, M. G.; Coutinho, J. A. P.; Marrucho, I. M. Unpublished results.

[170] Mack, H. G.; Oberhammer, H. An *ab initio* approach to the interaction of CF_4 and CH_4 with O_2, CO_2, N_2 and CO. The nature of the interaction force in perfluorochemical artificial blood. *J. Chem. Phys.* **87**, 2158 (1987).

[171] Peters, C. J.; Gauter, K. Occurrence of holes in ternary fluid multiphase systems of near-critical carbon dioxide and certain solutes. *Chem. Reviews* **99**, 419 (1999).

[172] Passarello, J. P.; Benzaghou, S.; Tobaly, P. Modeling mutual solubility of *n*-alkanes and CO_2 using SAFT equation of state. *Ind. Eng. Chem. Res.* **39**, 2578 (2000).

[173] Galindo, A.; Blas, F. J. Theoretical examination of the global fluid phase behavior and critical phenomena in carbon dioxide + *n*-alkane binary mixtures. *J. Phys. Chem. B* **106**, 4503 (2002).

[174] Shaver, R. D.; Robinson, Jr., R. L.; Gasem, K. A. M. Automated apparatus for equilibrium phase compositions, densities, and interfacial tensions: data for carbon dioxide + decane. *Fluid Phase Equilib.* **179**, 43 (2001).

[175] Chester, T. L.; Haynes, B. S. Estimation of pressure-temperature critical loci of CO_2 binary mixtures with methyl-tert-butyl ether, ethyl acetate, methyl-ethyl ketone, dioxane and decane. *J. Supercritical Fluids* **11**, 15 (1997).

[176] Ziegler, J. W.; Chester, T. L. *Critical loci of binary mixtures containing CO_2*. Innovations in Supercritical Fluids. Science an thecnology; Hutchenson, K. W.; Foster, N. R. (editors); ACS Symposium series, 1995.

[177] Jennings, D. W.; Chang, F.; Bazaan, V.; Teja, A. S. Vapor-liquid equilibria for carbon dioxide + 1-pentanol. *J. Chem. Eng. Data* **37**, 337 (1992).

[178] Staby, A.; Mollerup, J. Measurement of mutual solubilities of 1-pentanol and supercritical carbon dioxide. *J. Supercritical Fluids* **6**, 15 (1993).

[179] Jorgensen, W. L.; Madura, J. D.; Swenson, C. J. Optimized intermolecular potential functions for liquid hydrocarbons. *J. Am. Chem. Soc.* **106**, 6638 (1984).

[180] Panagiotopoulos, A. Z. Monte Carlo methods for phase equilibria of fluids. *J. Phys. Condens. Matter* **12**, R25 (2000).

[181] Ladd, A. J. C.; Woodcock, L. V. Interfacial and co-existence properties of the Lennard-Jones system at the triple point. *Molec. Phys.* **36**, 611 (1978).

[182] Holcomb, C. D.; Clancy, P.; Thompson, S. M.; Zollweg, J. A. A critical study of simulations of the Lennard-Jones liquid-vapor interface. *Fluid Phase Equilib.* **75**, 185 (1992).

[183] Holcomb, C. D.; Clancy, P.; Zollweg, J. A. A critical study of the simulation of the liquid-vapour interface of a Lennard-Jones fluid. *Molec. Phys.* **78**, 437 (1993).

[184] Gelb, L. D.; Müller, E. A. Location of phase equilibria by temperature-quench molecular dynamics simulations. *Fluid Phase Equilib.* **203**, 1 (2002).

[185] Alejandre, J.; Tildesley, D. J.; Chapela, G. A. Fluid phase equilibria using molecular dynamics: the surface tension of chlorine and hexane. *Molec. Phys.* **85**, 651 (1995).

[186] Trokhymchuk, A.; Alejandre, J. Computer simulations of the liquid/vapor interface in Lennard-Jones fluids: some questions and answers. *J. Chem. Phys.* **111**, 8510 (1999).

[187] Shi, W.; Johnson, J. K. Histogram reweighting and finite-size scaling study of the Lennard-Jones fluids. *Fluid Phase Equilib.* **187-188**, 171 (2001).

[188] Rivera, J. L.; Alejandre, J.; Nath, S. K.; de Pablo, J. J. Thermodynamic and transport properties of nitrogen and butane mixtures. *Molec. Phys.* **98**, 43 (2000).

[189] Goujon, F.; Malfreyt, P.; Boutin, A.; Fuchs, A. H. Direct Monte Carlo simulations of the equilibrium properties of *n*-pentane liquid-vapor interface. *J. Chem. Phys.* **116**, 8106 (2002).

[190] Goujon, F.; Malfreyt, P.; Boutin, A.; Fuchs, A. H. Vapour-liquid phase equilibria of *n*-alkanes by direct Monte Carlo simulations. *Mol. Sim.* **27**, 99 (2002).

[191] Rivera, J. L.; Predota, M.; Chialvo, A. A.; Cummings, P. T. Vapor-liquid equilibrium simulations of the SCPDP model of water. *Chem. Phys. Lett.* **357**, 189 (2002).

[192] Tuckerman, M. E.; Berne, B. J.; Martyna, G. J. Molecular dynamics algorithm for multiple time scales: systems with long range forces. *J. Chem. Phys.* **94**, 6811 (1991).

[193] Andersen, H. C. A velocity version of the shake algorithm for molecular dynamics calculations. *J. Comput. Phys.* **52**, 24 (1983).

[194] Mundy, C. J.; Siepmann, J. I.; Klein, M. L. Calculation of the shear viscosity of decane using a reversible multiple time-step algorithm. *J. Chem. Phys.* **102**, 3376 (1995).

[195] Islam, M. R. Emerging technologies in enhanced oil recovery. *Energy Sources* **21**, 97 (1999).

[196] Macleod, D. B. Relation between surface tension and density. *Trans. Faraday Soc.* **19**, 38 (1923).

[197] Weinaug, C. F.; Katz, D. L. Surface tensions of methane-propane mixtures. *Ind. Eng. Chem.* **35**, 239 (1943).

[198] Miqueu, C. *Modélisation á température et pression élevés de la tension superficielle de composants des fluides pétroliers et de leurs mélanges synthétiques ou réels.* Ph. D. thesis, Université de Pau et des Pays de l'Adour, France, 2001.

[199] Guggenheim, E. A. The principle of corresponding states. *J. Chem. Phys.* **13**, 253 (1945).

[200] Zuo, Y.-X.; Stenby, E. H. Corresponding-states parachor models for the calculation of interfacial tensions. *Can. J. Chem. Eng.* **75**, 1130 (1997).

[201] Queimada, A. J.; Marrucho, I. M.; Coutinho, J. A. P. Surface tension of pure heavy *n*-alkanes: a corresponding states approach. *Fluid Phase Equilib.* **183-184**, 229 (2001).

[202] Cornelisse, P. M. W.; Peters, C. J.; de Swaan Arons, J. Application of the Peng-Robinson equation of state to calculate interfacial tensions and profiles at vapour-liquid interfaces. *Fluid Phase Equilib.* **82**, 119 (1993).

[203] Cornelisse, P. M. W.; Peters, C. J.; de Swaan Arons, J. Non-classical interfacial tension and fluid phase behaviour. *Fluid Phase Equilib.* **117**, 312 (1996).

[204] Evans, R. *Fundamentals of inhomogeneous fluids.* Marcel Dekker; Henderson, D. (editors), New York, 1992.

[205] Segura, C. J.; Chapman, W. G.; Shukla, K. P. Associating fluids with four bonding sites against a hard wall: density functional theory. *Molec. Phys.* **90**, 759 (1997).

[206] Blas, F. J.; Martín del Río, E.; de Miguel, E.; Jackson, G. An examination of the vapour-liquid interface of associating fluids using a SAFT-DFT approach. *Molec. Phys.* **99**, 1851 (2001).

[207] Gloor, G. J.; Blas, F. J.; Martín del Río, E.; de Miguel, E.; Jackson, G. A SAFT-DFT approach for the vapour-liquid interface of associating fluids. *Fluid Phase Equilibria* **194-197**, 521 (2002).

[208] Gude, M.; Teja, A. S. Vapor-liquid critical properties of elements and compounds. 4. Aliphatic alkanols. *J. Chem. Eng. Data* **40**, 1025 (1995).

[209] Miqueu, C.; Broseta, D.; Satherley, J.; Mendiboure, B.; Lachaise, J.; Graciaa, A. An extended scaled equation for the temperature dependence of the surface tension of pure compounds inferred from an analysis of experimental data. *Fluid Phase Equilib.* **172**, 169 (2000).

[210] Lide, D. R. *CRC Handbook of chemistry and physics.* CRC Press, 83 edition, 2002.

[211] Rolo, L. I.; Caço, A. I.; Queimada, A. J.; Marrucho, I. M.; Coutinho, J. A. P. Surface tension of heptane, decane, hexadecane, eicosane, and some of their binary mixtures. *J. Chem. Eng. Data* **47**, 1442 (2002).

[212] Águila-Hernández, J. *Tensión superficial de n-alcanos y de cíclicos-alcanos*. Ph. D. thesis, Universidad Autnoma de Puebla, Mexico, 1987.

[213] Hsu, J. J.-C.; Nagarajan, N.; Robinson, Jr., R. L. Equilibrium phase compositions, phase densities, and interfacial tensions for CO_2 + hydrocarbon systems. 1. CO_2 + n-butane. *J. Chem. Eng. Data* **30**, 485 (1985).

[214] Hicks, C. P.; Young, C. L. The gas-liquid critical properties of binary mixtures. *Chem. Rev.* **75**, 119 (1975).

Appendix A

The mathematical description of the soft-SAFT approach

A mathematical description of the soft-SAFT EOS is shown in this appendix. It is supposed to be a complement to the theoretical explanations in Chapter 2. Expressions for the Helmholtz free energy $\tilde{A}$, pressure $\tilde{P}$, chemical potential $\tilde{\mu}$ and fraction of nonbonded molecules X for multicomponent systems, as a function of temperature $\tilde{T}$, density $\tilde{\rho}$, composition x and molecular parameters, are provided. All the equations are given in a dimensionless form, and magnitudes that have been converted to nondimensional are indicated with a tilde ($\sim$) as a superscript. Please refer to the next section for the definitions of dimensionless variables.

A.1 Dimensionless variables

When writing thermodynamic magnitudes in a dimensionless form, it is imperative to choose a reference component. In the relationships below, i_{R} is the reference component, and σ_{R} and ϵ_{R} their corresponding LJ parameters. Evidently, when dealing with a pure fluid, $\sigma = \sigma_i = \sigma_{\mathrm{R}}$. In multicomponent systems, each component has its own σ_i parameter, and σ corresponds to the "averaged" value computed from mixing and combination rules (see eqs 2.2-2.6). Hence, this value depends on composition. The same holds for the energy LJ parameter.

Dimensionless thermodynamic variables and parameters are defined as follows:

$$\tilde{T} \;=\; \frac{T}{\epsilon_{\mathrm{R}}/k_{\mathrm{B}}} \qquad \text{(A.1)} \qquad\qquad \tilde{\sigma} \;=\; \frac{\sigma}{\sigma_{\mathrm{R}}} \qquad \text{(A.7)}$$

$$\tilde{\rho} \;=\; \rho N_{\mathrm{A}}\sigma_{\mathrm{R}}^{3} \qquad \text{(A.2)} \qquad\qquad \tilde{\epsilon} \;=\; \frac{\epsilon}{\epsilon_{\mathrm{R}}} \qquad \text{(A.8)}$$

$$\tilde{A} \;=\; \frac{A}{N_{\mathrm{A}}\epsilon_{\mathrm{R}}} \qquad \text{(A.3)} \qquad\qquad \tilde{\sigma}_{i,i\neq i_{\mathrm{R}}} \;=\; \frac{\sigma_{i}}{\sigma_{\mathrm{R}}} \qquad \text{(A.9)}$$

$$\tilde{P} \;=\; \frac{P\sigma_{\mathrm{R}}^{3}}{\epsilon_{\mathrm{R}}} \qquad \text{(A.4)} \qquad\qquad \tilde{\epsilon}_{i,i\neq i_{\mathrm{R}}} \;=\; \frac{\epsilon_{i}}{\epsilon_{\mathrm{R}}} \qquad \text{(A.10)}$$

$$\tilde{\mu} \;=\; \frac{\mu}{N_{\mathrm{A}}\epsilon_{\mathrm{R}}} \qquad \text{(A.5)} \qquad\qquad \tilde{k}^{\alpha_{i}\beta_{j}} \;=\; \frac{k^{\alpha_{i}\beta_{j}}}{\sigma_{\mathrm{R}}^{3}} \qquad \text{(A.11)}$$

$$\tilde{G} \;=\; \frac{G}{N_{\mathrm{A}}\epsilon_{\mathrm{R}}} \qquad \text{(A.6)} \qquad\qquad \tilde{\varepsilon}^{\alpha_{i}\beta_{j}} \;=\; \frac{\varepsilon^{\alpha_{i}\beta_{j}}}{\epsilon_{\mathrm{R}}} \qquad \text{(A.12)}$$

In the segment term of the soft-SAFT EOS and wherever the LJ radial distribution function is needed, densities and temperatures refer to the LJ reference fluid and, hence, they have to be converted in dimensionless form by using the "averaged" composition-dependent $\tilde{\sigma}$ and $\tilde{\epsilon}$ parameters (eqs 2.2-2.3). The variables that refer to the reference fluid will be denoted with the superscript rf. Consequently,

$$\tilde{T}^{\mathrm{rf}} = \frac{\tilde{T}}{\tilde{\epsilon}}, \tag{A.13}$$

and the density of LJ cores

$$\tilde{\rho}_{\mathrm{c}}^{\mathrm{rf}} = m\tilde{\rho}^{\mathrm{rf}} = m\tilde{\rho}\tilde{\sigma}^{3}. \tag{A.14}$$

A.2   Ideal term

The Helmholtz free energy of a pure ideal fluid is defined as,

$$\tilde{A}^{\mathrm{ideal}} = \tilde{T}\left(\ln\tilde{\rho} + \ln\lambda_{T}^{3} - 1\right). \tag{A.15}$$

Since the reference state is irrelevant in thermodynamic phase-equilibrium, and no (partial) derivative of the Helmholtz free energy with respect to the temperature will be needed, the thermal part of the ideal Helmholtz free energy can be ignored. Therefore,

$$\tilde{A}^{\mathrm{ideal}} = \tilde{T}\left(\ln\tilde{\rho} - 1\right). \tag{A.16}$$

For mixtures, the contribution of each component is weighted by its composition. The ideal pressure and chemical potential can be straightforwardly calculated using basic thermodynamic definitions:

$$\tilde{A}^{\text{ideal}} = \sum_i x_i \tilde{T} (\ln \tilde{\rho} - 1) + \tilde{T} \sum_i x_i \ln x_i = \tilde{T} \sum_i x_i (\ln \tilde{\rho} x_i - 1) \quad \text{(A.17)}$$

$$\tilde{P}^{\text{ideal}} = \tilde{\rho}^2 \left(\frac{\partial \tilde{A}^{\text{ideal}}}{\partial \tilde{\rho}} \right)_{\tilde{T}, x_k} = \tilde{\rho} \tilde{T} \quad \text{(A.18)}$$

$$\tilde{\mu}_i^{\text{ideal}} = \left(\frac{\partial \tilde{A}^{\text{ideal}}}{\partial x_i} \right)_{\tilde{T}, \tilde{\rho}, x_{k \neq i}} = \tilde{T} (\ln \tilde{\rho} x_i) \quad \text{(A.19)}$$

Eq A.18 corresponds to the ideal gas law and $\tilde{T} (\ln \tilde{\rho})$ is equivalent to the ideal Gibbs free energy $\tilde{G}^{\text{ideal}}$ of a pure fluid, since $\tilde{\mu}^{\text{ideal}} = \tilde{G}^{\text{ideal}}$ for a pure fluid.

A.3   Segment term

It is given here the LJ EOS of Johnson *et al.* [45], which is a modified Benedict-Webb-Rubin EOS, with temperature-dependent parameters (a_p, b_p and G_p) fitted to molecular simulation data of the LJ fluid. The corresponding equations follow.

For the calculation of the segment term in multicomponent systems, mixing and combination rules for the size and energy LJ parameters are required. The soft-SAFT EOS uses van der Waals one-fluid mixing rules (eqs 2.2-2.4) and the Lorentz-Berthelot combining rules (eqs 2.5-2.6).

$$\tilde{A}^{\text{ref}} = \tilde{\epsilon} \left(\sum_{p=1}^{8} \frac{a_p}{p} (\tilde{\rho}_c^{\text{rf}})^p + \sum_{p=1}^{6} b_p G_p \right) \quad \text{(A.20)}$$

$$\tilde{P}^{\text{ref}} = \tilde{\rho}^2 \left(\frac{\partial \tilde{A}^{\text{ref}}}{\partial \tilde{\rho}} \right)_{\tilde{T}, x_k} = \frac{1}{m \tilde{\sigma}^3} (\tilde{\rho}_c^{\text{rf}})^2 \left(\frac{\partial \tilde{A}^{\text{ref}}}{\partial \tilde{\rho}_c^{\text{rf}}} \right)_{\tilde{T}, x_k}$$

$$= \frac{\tilde{\epsilon}}{m \tilde{\sigma}^3} \left(\sum_{p=1}^{8} a_p (\tilde{\rho}_c^{\text{rf}})^{p+1} + F \sum_{p=1}^{6} b_p (\tilde{\rho}_c^{\text{rf}})^{2p+1} \right) \quad \text{(A.21)}$$

$$\tilde{\mu}^{\text{ref}} = \tilde{G}^{\text{ref}} = \tilde{A}^{\text{ref}} + \frac{\tilde{P}^{\text{ref}}}{\tilde{\rho}} = \tilde{A}^{\text{ref}} + m \tilde{\sigma}^3 \frac{\tilde{P}^{\text{ref}}}{\tilde{\rho}_c^{\text{rf}}} \quad \text{(A.22)}$$

Note that relationships A.13 and A.14 were used in the last two eqs.

A.4   Chain term

Only the chain term corresponding to a reference fluid of monomers is given. Equations are similar for dimers, and the general expression for the Helmholtz free energy was given in eq 2.8.

The chain term depends explicitly on composition and it also depends on the LJ radial distribution function of the reference fluid. Hence, the monomeric density $\tilde{\rho}_{\mathrm{c}}$ is needed for the computation of $g_{LJ}(\tilde{\sigma})$.

The Helmholtz free energy due to the formation of chains of component i, and its derivatives, read

$$\tilde{A}_i^{\mathrm{chain}} = \tilde{T}(1 - m_i)\ln\left[g_{LJ}(\tilde{\sigma})\right] \tag{A.23}$$

$$\left(\frac{\partial \tilde{A}_i^{\mathrm{chain}}}{\partial \tilde{\rho}}\right)_{\tilde{T},x_k} = \tilde{T}(1 - m_i)\frac{1}{g_{LJ}(\tilde{\sigma})}\left(\frac{\partial g_{LJ}(\tilde{\sigma})}{\partial \tilde{\rho}}\right)_{\tilde{T},x_k} \tag{A.24}$$

$$\left(\frac{\partial \tilde{A}_j^{\mathrm{chain}}}{\partial x_i}\right)_{\tilde{T},\tilde{\rho},x_{k\neq i}} = \tilde{T}(1 - m_j)\frac{1}{g_{LJ}(\tilde{\sigma})}\left(\frac{\partial g_{LJ}(\tilde{\sigma})}{\partial x_i}\right)_{\tilde{T},\tilde{\rho},x_{k\neq i}} \tag{A.25}$$

The empirical function fitted by Johnson *et al.* [53] for the pair correlation function of the LJ fluid evaluated at the bonding distance, and its derivatives, follow. Parameters a_{pq} where fitted to molecular simulation data.

$$g_{LJ}(\tilde{\sigma}) = 1 + \sum_{p=1}^{5}\sum_{q=1}^{5}a_{pq}\left(\tilde{\rho}_{\mathrm{c}}^{\mathrm{rf}}\right)^p\left(\tilde{T}^{\mathrm{rf}}\right)^{1-q} \tag{A.26}$$

$$\left(\frac{\partial g_{LJ}(\tilde{\sigma})}{\partial \tilde{\rho}}\right)_{\tilde{T},x_k} = m\tilde{\sigma}^3\left(\frac{\partial g_{LJ}(\tilde{\sigma})}{\partial \tilde{\rho}_{\mathrm{c}}^{\mathrm{rf}}}\right)_{\tilde{T},x_k}$$

$$= m\tilde{\sigma}^3\sum_{p=1}^{5}p\sum_{q=1}^{5}a_{pq}\left(\tilde{\rho}_{\mathrm{c}}^{\mathrm{rf}}\right)^{p-1}\left(\tilde{T}^{\mathrm{rf}}\right)^{1-q} \tag{A.27}$$

$$\left(\frac{\partial g_{LJ}(\tilde{\sigma})}{\partial x_i}\right)_{\tilde{T},\tilde{\rho},x_{k\neq i}} = \sum_{p=1}^{5}\sum_{q=1}^{5}a_{pq}\left(\tilde{\rho}_{\mathrm{c}}^{\mathrm{rf}}\right)^p\left(\tilde{T}^{\mathrm{rf}}\right)^{1-q}\left[p\frac{m_i}{m}\right.$$

$$\left. +\frac{p}{\tilde{\sigma}^3}\left(\frac{\partial \tilde{\sigma}^3}{\partial x_i}\right)_{x_{k\neq i}} - \frac{(1-q)}{\tilde{\epsilon}}\left(\frac{\partial \tilde{\epsilon}}{\partial x_i}\right)_{x_{k\neq i}}\right] \tag{A.28}$$

Next two expressions, equivalent to eqs 2.2-2.4, correspond to the van der Waals' mixing rules. Derivatives of the "averaged" size and energy parameters are also needed.

$$\tilde{\sigma}^3 \quad = \quad \frac{\sum\limits_{i}\sum\limits_{j} x_i x_j m_i m_j \tilde{\sigma}_{ij}^3}{\left(\sum\limits_{i} x_i m_i\right)^2} \tag{A.29}$$

$$\tilde{\epsilon}\tilde{\sigma}^3 \quad = \quad \frac{\sum\limits_{i}\sum\limits_{j} x_i x_j m_i m_j \tilde{\epsilon}_{ij}\tilde{\sigma}_{ij}^3}{\left(\sum\limits_{i} x_i m_i\right)^2} \tag{A.30}$$

$$\left(\frac{\partial \tilde{\sigma}^3}{\partial x_i}\right)_{x_{k\neq i}} \quad = \quad \frac{2m_i}{m}\left(\sum_j x_{c_j}\tilde{\sigma}_{ij}^3 - \tilde{\sigma}^3\right)$$

$$= \quad \frac{m_i}{m}\left[\left(\frac{\partial \tilde{\sigma}^3}{\partial x_{c_i}}\right)_{x_{k\neq i}} - 2\tilde{\sigma}^3\right] \tag{A.31}$$

$$\left(\frac{\partial \left(\tilde{\epsilon}\tilde{\sigma}^3\right)}{\partial x_i}\right)_{x_{k\neq i}} \quad = \quad \frac{2m_i}{m}\left(\sum_j x_{c_j}\tilde{\epsilon}_{ij}\tilde{\sigma}_{ij}^3 - \tilde{\epsilon}\tilde{\sigma}^3\right)$$

$$= \quad \frac{m_i}{m}\left[\left(\frac{\partial \left(\tilde{\epsilon}\tilde{\sigma}^3\right)}{\partial x_{c_i}}\right)_{x_{k\neq i}} - 2\tilde{\epsilon}\tilde{\sigma}^3\right] \tag{A.32}$$

Combining eq A.28 with eqs A.31-A.32,

$$\left(\frac{\partial g_{LJ}\left(\tilde{\sigma}\right)}{\partial x_i}\right)_{\tilde{T},\tilde{\rho},x_{k\neq i}} \quad = \quad \sum_{p=1}^{5}\sum_{q=1}^{5} a_{pq}\left(\tilde{\rho}_{\mathrm{c}}^{\mathrm{rf}}\right)^p\left(\tilde{T}^{\mathrm{rf}}\right)^{1-q}\frac{m_i}{m}\left\{p\left[-1 + \frac{1}{\tilde{\sigma}^3}\left(\frac{\partial \tilde{\sigma}^3}{\partial x_{c_i}}\right)_{x_{k\neq i}}\right]\right.$$

$$- (1-q)\left[\frac{1}{\tilde{\epsilon}\tilde{\sigma}^3}\left(\frac{\partial\left(\tilde{\epsilon}\tilde{\sigma}^3\right)}{\partial x_{c_i}}\right)_{x_{k\neq i}}\right.$$

$$\left.\left. -\frac{1}{\tilde{\sigma}^3}\left(\frac{\partial \tilde{\sigma}^3}{\partial x_{c_i}}\right)_{x_{k\neq i}}\right]\right\} \tag{A.33}$$

The pressure and chemical potentials depend on the derivatives previously written.

$$\tilde{A}^{\text{chain}} = \sum_i x_i \tilde{A}_i^{\text{chain}} \tag{A.34}$$

$$\tilde{\mu}_i^{\text{chain}} = \left(\frac{\partial \tilde{A}^{\text{chain}}}{\partial x_i} \right)_{\tilde{T},\tilde{\rho},x_{k \neq i}}$$

$$= \tilde{A}_i^{\text{chain}} + \sum_j x_j \left(\frac{\partial \tilde{A}_j^{\text{chain}}}{\partial x_i} \right)_{\tilde{T},\tilde{\rho},x_{k \neq i}} \tag{A.35}$$

$$\tilde{A}^{\text{chain}} = \tilde{T} \sum_i x_i \left(1 - m_i \right) \ln \left[g_{LJ} \left(\tilde{\sigma} \right) \right] \tag{A.36}$$

$$\tilde{P}^{\text{chain}} = \tilde{\rho}^2 \left(\frac{\partial \tilde{A}^{\text{chain}}}{\partial \tilde{\rho}} \right)_{\tilde{T},x_k} = \tilde{\rho}^2 \sum_i x_i \left(\frac{\partial \tilde{A}_i^{\text{chain}}}{\partial \tilde{\rho}} \right)_{\tilde{T},x_k} \tag{A.37}$$

$$\tilde{P}^{\text{chain}} = \tilde{T} \tilde{\rho}^2 \left(1 - m \right) \frac{1}{g_{LJ} \left(\tilde{\sigma} \right)} \left(\frac{\partial g_{LJ} \left(\tilde{\sigma} \right)}{\partial \tilde{\rho}} \right)_{\tilde{T},x_k} \tag{A.38}$$

$$\tilde{\mu}_i^{\text{chain}} = \tilde{T} \left[\left(1 - m_i \right) \ln \left[g_{LJ} \left(\tilde{\sigma} \right) \right] \right.$$

$$\left. + \left(1 - m \right) \frac{1}{g_{LJ} \left(\tilde{\sigma} \right)} \left(\frac{\partial g_{LJ} \left(\tilde{\sigma} \right)}{\partial x_i} \right)_{\tilde{T},\tilde{\rho},x_{k \neq i}} \right] \tag{A.39}$$

A.5   Association term

The association contribution of component i in a mixture is given in terms of the temperature, the number of association sites M_i, and X_i^α, the fraction of molecules i not bonded at site α. The Helmholtz free energy reads

$$\tilde{A}_i^{\text{assoc}} = \tilde{T} \left[\sum_\alpha \left(\ln X_i^\alpha - \frac{X_i^\alpha}{2} \right) + \frac{M_i}{2} \right] \tag{A.40}$$

$$\tilde{A}^{\text{assoc}} = \sum_i x_i \tilde{A}_i^{\text{assoc}} \tag{A.41}$$

The chemical potential

$$
\begin{aligned}
\tilde{\mu}_i^{\text{assoc}} &= \left(\frac{\partial \tilde{A}^{\text{assoc}}}{\partial x_i} \right)_{\tilde{T},\tilde{\rho},x_{k\neq i}} \\
&= \tilde{A}_i^{\text{assoc}} + \sum_j x_j \left(\frac{\partial \tilde{A}_j^{\text{assoc}}}{\partial x_i} \right)_{\tilde{T},\tilde{\rho},x_{k\neq i}} \quad\quad\quad\text{(A.42)}
\end{aligned}
$$

requires the evaluation of the next partial derivative.

$$
\left(\frac{\partial \tilde{A}_j^{\text{assoc}}}{\partial x_i} \right)_{\tilde{T},\tilde{\rho},x_{k\neq i}} = \tilde{T} \sum_\alpha \left(\frac{1}{X_j^\alpha} - \frac{1}{2} \right) \left(\frac{\partial X_j^\alpha}{\partial x_i} \right)_{\tilde{T},\tilde{\rho},x_{k\neq i}} \quad\quad\text{(A.43)}
$$

Therefore, combining A.40 and A.43 in A.42,

$$
\begin{aligned}
\tilde{\mu}_i^{\text{assoc}} = \tilde{T} &\left[\sum_\alpha \left(\ln X_i^\alpha - \frac{X_i^\alpha}{2} \right) + \frac{M_i}{2} \right. \\
&\left. + \sum_j x_j \sum_\alpha \left(\frac{1}{X_j^\alpha} - \frac{1}{2} \right) \left(\frac{\partial X_j^\alpha}{\partial x_i} \right)_{\tilde{T},\tilde{\rho},x_{k\neq i}} \right]. \quad\quad\text{(A.44)}
\end{aligned}
$$

The next derivative will be required for the calculation of the pressure corresponding to the association term.

$$
\left(\frac{\partial \tilde{A}_i^{\text{assoc}}}{\partial \tilde{\rho}} \right)_{\tilde{T},x_k} = \tilde{T} \left[\sum_\alpha \left(\frac{1}{X_i^\alpha} - \frac{1}{2} \right) \left(\frac{\partial X_i^\alpha}{\partial \tilde{\rho}} \right)_{\tilde{T},x_k} \right] \quad\quad\text{(A.45)}
$$

To sum up, the Helmholtz free energy of association is given by

$$
\tilde{A}^{\text{assoc}} = \tilde{T} \sum_i x_i \left[\sum_\alpha \left(\ln X_i^\alpha - \frac{X_i^\alpha}{2} \right) + \frac{M_i}{2} \right] \quad\quad\text{(A.46)}
$$

where $\alpha =$A,B,C,..., the last letters denoting specific association sites.

Using eq A.45, the pressure is given by

$$
\begin{aligned}
\tilde{P}^{\text{assoc}} &= \tilde{\rho}^2 \left(\frac{\partial \tilde{A}^{\text{assoc}}}{\partial \tilde{\rho}} \right)_{\tilde{T},x_k} = \tilde{\rho}^2 \sum_i x_i \left(\frac{\partial \tilde{A}_i^{\text{assoc}}}{\partial \tilde{\rho}} \right)_{\tilde{T},x_k} \\
&= \tilde{T} \tilde{\rho}^2 \sum_i x_i \sum_\alpha \left(\frac{1}{X_i^\alpha} - \frac{1}{2} \right) \left(\frac{\partial X_i^\alpha}{\partial \tilde{\rho}} \right)_{\tilde{T},x_k} \quad\quad\text{(A.47)}
\end{aligned}
$$

In eqs A.40 to A.47, the only unknowns are X_i^α and its density and composition derivatives. X_i^α was given in eq 2.12, and the association strength $\Delta^{\alpha_i \beta_j}$ in eq 2.15. They are written again next, but in a dimensionless form.

$$X_i^\alpha \quad = \quad \frac{1}{1 + \tilde{\rho} \sum\limits_j x_j \sum\limits_\beta X_j^\beta \tilde{\Delta}^{\alpha_i \beta_j}} \tag{A.48}$$

$$\tilde{\Delta}^{\alpha_i \beta_j} \quad = \quad 4\pi \left[\exp\left(\frac{\tilde{\varepsilon}^{\alpha_i \beta_j}}{\tilde{T}} \right) - 1 \right] \tilde{k}^{\alpha_i \beta_j} \tilde{I} \tag{A.49}$$

An empirical function for the dimensionless integral $\tilde{I}$ (eq 2.17), as a function of the reduced temperature and density, was provided by Müller and Gubbins [47],

$$\tilde{I} \quad = \quad \frac{1}{38400} \sum_{p=0}^{4} \sum_{q=0}^{4} a_{pq} \left(\tilde{\rho}_c^{\mathrm{rf}} \right)^p \left(\tilde{T}^{\mathrm{rf}} \right)^q \tag{A.50}$$

with constants a_{pq} given in their paper.

The derivatives of X require, at the same time, derivatives of the same variable:

$$\left(\frac{\partial X_j^\alpha}{\partial x_i} \right)_{\tilde{T}, \tilde{\rho}, x_{k \neq i}} = -\tilde{\rho} \left(X_j^\alpha \right)^2 \left\{ \sum_\beta X_i^\beta \tilde{\Delta}^{\alpha_j \beta_i} + \sum_k x_k \sum_\beta \left[X_k^\beta \left(\frac{\partial \tilde{\Delta}^{\alpha_j \beta_k}}{\partial x_i} \right)_{\tilde{T}, \tilde{\rho}, x_{k \neq i}} \right. \right.$$

$$\left. \left. + \tilde{\Delta}^{\alpha_j \beta_k} \left(\frac{\partial X_k^\beta}{\partial x_i} \right)_{\tilde{T}, \tilde{\rho}, x_{k \neq i}} \right] \right\} \tag{A.51}$$

$$\left(\frac{\partial X_i^\alpha}{\partial \tilde{\rho}} \right)_{\tilde{T}, x_k} = -\left(X_i^\alpha \right)^2 \sum_j x_j \left\{ \sum_\beta X_j^\beta \tilde{\Delta}^{\alpha_i \beta_j} + \tilde{\rho} \sum_\beta \left[X_j^\beta \left(\frac{\partial \tilde{\Delta}^{\alpha_i \beta_j}}{\partial \tilde{\rho}} \right)_{\tilde{T}, x_k} \right. \right.$$

$$\left. \left. + \tilde{\Delta}^{\alpha_i \beta_j} \left(\frac{\partial X_j^\beta}{\partial \tilde{\rho}} \right)_{\tilde{T}, x_k} \right] \right\} \tag{A.52}$$

At this point, we need to make a few assumptions to be able to calculate the association contribution analytically. We present four cases; the first three correspond to self-associating models and the last one is a cross-associating model.

Case 1. Cross-association (i.e., association between two different components) is not allowed, and all the association sites are equivalent, which means that $X_i^\alpha = X_i$, $\varepsilon^{\alpha_i \beta_i} = \varepsilon_i$ and $k^{\alpha_i \beta_i} = k_i$. With these assumptions, eq A.48 becomes

$$X_j \quad = \quad \frac{1}{1 + \tilde{\rho} x_j M_j' X_j \tilde{\Delta}^j} \tag{A.53}$$

Isolating $\tilde{\Delta}^j$,

$$\tilde{\Delta}^j = \frac{1 - X_j}{\tilde{\rho} x_j M_j' \left(X_j\right)^2} \tag{A.54}$$

where M_j' is the number of bonds allowed between two molecules of type j. Taking logarithms in each side of A.55,

$$\ln \tilde{\Delta}^j = \ln \left(1 - X_j\right) - \ln \tilde{\rho} - \ln x_j - \ln M_j' - 2 \ln X_j \tag{A.55}$$

At this point it is convenient to recover the next relationships,

$$\tilde{\Delta}^j = 4\pi \left[\exp\left(\frac{\tilde{\varepsilon}_j}{\tilde{T}}\right) - 1\right] \tilde{k}_j \tilde{I} \tag{A.56}$$

$$\tilde{\rho}_{c_i} = m_i \tilde{\rho}_i \tilde{\sigma}^3 \tag{A.57}$$

$$\tilde{\rho}_c = m \tilde{\rho} \tilde{\sigma}^3 \tag{A.58}$$

$$x_{ci} = \frac{m_i}{m} x_i \tag{A.59}$$

$$m = \sum_k m_k x_k \tag{A.60}$$

and to rewrite expressions A.29-A.30 in another way,

$$\tilde{\sigma}^3 = \sum_i \sum_j x_{c_i} x_{c_j} \tilde{\sigma}_{ij}^3 \tag{A.61}$$

$$\tilde{\epsilon} \tilde{\sigma}^3 = \sum_i \sum_j x_{c_i} x_{c_j} \tilde{\epsilon}_{ij} \tilde{\sigma}_{ij}^3 \tag{A.62}$$

Using eq A.55, we can write

$$\left(\frac{\partial \ln \tilde{\Delta}^j}{\partial x_i}\right)_{\tilde{T},\tilde{\rho},x_{k \neq i}} = \frac{1}{\tilde{I}}\left(\frac{\partial \tilde{I}}{\partial x_i}\right)_{\tilde{T},\tilde{\rho},x_{k \neq i}} = \left(\frac{-1}{1 - X_j} - \frac{2}{X_j}\right)\left(\frac{\partial X_j}{\partial x_i}\right)_{\tilde{T},\tilde{\rho},x_{k \neq i}}$$

$$-\frac{1}{x_j}\left(\frac{\partial x_j}{\partial x_i}\right)_{\tilde{T},\tilde{\rho},x_{k \neq i}} \tag{A.63}$$

$$\left(\frac{\partial \ln \tilde{\Delta}^i}{\partial \tilde{\rho}}\right)_{\tilde{T},x_k} = \frac{1}{\tilde{I}}\left(\frac{\partial \tilde{I}}{\partial \tilde{\rho}}\right)_{\tilde{T},x_k} = \frac{m \tilde{\sigma}^3}{\tilde{I}}\left(\frac{\partial \tilde{I}}{\partial \tilde{\rho}_c^{\mathrm{rf}}}\right)_{\tilde{T},x_k}$$

$$= \left(\frac{-1}{1 - X_i} - \frac{2}{X_i}\right)\left(\frac{\partial X_i}{\partial \tilde{\rho}}\right)_{\tilde{T},x_k} - \frac{1}{\tilde{\rho}} \tag{A.64}$$

Taking into account the following equality

$$\frac{1}{X_j} - \frac{1}{2} = -\frac{1}{2}\left(1 - X_j\right)\left(\frac{-1}{1 - X_j} - \frac{2}{X_j}\right) \tag{A.65}$$

and playing with the equations,

$$x_j M_j \left(\frac{1}{X_j} - \frac{1}{2}\right)\left(\frac{\partial X_j}{\partial x_i}\right)_{\tilde{T},\tilde{\rho},x_{k\neq i}} =$$

$$= -x_j M_j \frac{1}{2}\left(1 - X_j\right)\left(\frac{-1}{1 - X_j} - \frac{2}{X_j}\right)\left(\frac{\partial X_j}{\partial x_i}\right)_{\tilde{T},\tilde{\rho},x_{k\neq i}}$$

$$= \frac{-M_j}{2}\left(1 - X_j\right)\left[\left(\frac{\partial x_j}{\partial x_i}\right)_{\tilde{T},\tilde{\rho},x_{k\neq i}} + x_j\left(\frac{\partial \ln \tilde{\Delta}^j}{\partial x_i}\right)_{\tilde{T},\tilde{\rho},x_{k\neq i}}\right] \tag{A.66}$$

$$\tilde{\rho}\left(\frac{1}{X_i} - \frac{1}{2}\right)\left(\frac{\partial X_i}{\partial \tilde{\rho}}\right)_{\tilde{T},x_k} = -\frac{\tilde{\rho}}{2}\left(1 - X_i\right)\left(\frac{-1}{1 - X_i} - \frac{2}{X_i}\right)\left(\frac{\partial X_i}{\partial \tilde{\rho}}\right)_{\tilde{T},x_k}$$

$$= -\frac{1}{2}\left(1 - X_i\right)\left[1 + \tilde{\rho}\left(\frac{\partial \ln \tilde{\Delta}^i}{\partial \tilde{\rho}}\right)_{\tilde{T},x_k}\right] \tag{A.67}$$

$$\left(\frac{\partial x_j}{\partial x_i}\right)_{\tilde{T},\tilde{V},x_{k\neq i}} = \begin{cases} 0 & j \neq i \\ 1 & j = i \end{cases} \tag{A.68}$$

we can get the chemical potentials and the pressure of association, where the derivatives of $\tilde{I}$ are needed.

$$\tilde{\mu}_i^{\text{assoc}} = \tilde{T}\left\{M_i\left(\ln X_i + \frac{1 - X_i}{2}\right) - \sum_j \frac{M_j}{2}\left(1 - X_j\right)\left[\left(\frac{\partial x_j}{\partial x_i}\right)_{\tilde{T},\tilde{\rho},x_{k\neq i}}\right.\right.$$

$$\left.\left. + x_j\frac{1}{\tilde{I}}\left(\frac{\partial \tilde{I}}{\partial x_i}\right)_{\tilde{T},\tilde{\rho},x_{k\neq i}}\right]\right\} \tag{A.69}$$

$$\tilde{P}^{\text{assoc}} = -\frac{1}{2}\tilde{T}\tilde{\rho}\left[1 + \frac{\tilde{\rho}_c}{\tilde{I}}\left(\frac{\partial \tilde{I}}{\partial \tilde{\rho}_c}\right)_{\tilde{T},x_k}\right]\sum_i x_i M_i\left(1 - X_i\right) \tag{A.70}$$

$$\left(\frac{\partial \tilde{I}}{\partial \tilde{\rho}_c^{\text{rf}}}\right)_{\tilde{T},x_k} = \frac{1}{38400}\sum_{p=0}^{4} p \sum_{q=0}^{4} a_{pq}\left(\tilde{\rho}_c^{\text{rf}}\right)^{p-1}\left(\tilde{T}^{\text{rf}}\right)^q \tag{A.71}$$

Using these useful relationships,

$$
\left(\frac{\partial \tilde{\epsilon}}{\partial x_{c_i}} \right)_{x_{k \neq i}} = \frac{1}{\tilde{\sigma}^3} \left[\left(\frac{\partial \left(\tilde{\epsilon} \tilde{\sigma}^3 \right)}{\partial x_{c_i}} \right)_{x_{k \neq i}} - \tilde{\epsilon} \left(\frac{\partial \tilde{\sigma}^3}{\partial x_{c_i}} \right)_{x_{k \neq i}} \right] \tag{A.72}
$$

$$
\left(\frac{\partial \tilde{\sigma}^3}{\partial x_{c_i}} \right)_{x_{k \neq i}} = 2 \sum_j x_{c_j} \tilde{\sigma}_{ij}^3 \tag{A.73}
$$

$$
\left(\frac{\partial \left(\tilde{\epsilon} \tilde{\sigma}^3 \right)}{\partial x_{c_i}} \right)_{x_{k \neq i}} = 2 \sum_j x_{c_j} \tilde{\epsilon}_{ij} \tilde{\sigma}_{ij}^3 \tag{A.74}
$$

the derivative of I with respect to the composition can be obtained:

$$
\begin{aligned}
\left(\frac{\partial \tilde{I}}{\partial x_i} \right)_{\tilde{T}, \tilde{\rho}, x_{k \neq i}} &= \frac{1}{38400} \sum_{p=0}^4 \sum_{q=0}^4 a_{pq} \left(\tilde{\rho}_c^{\mathrm{rf}} \right)^p \left(\tilde{T}^{\mathrm{rf}} \right)^q \left[p \frac{m_i}{m} + \frac{p}{\tilde{\sigma}^3} \left(\frac{\partial \tilde{\sigma}^3}{\partial x_i} \right)_{x_{k \neq i}} \right. \\
&\quad \left. - \frac{q}{\tilde{\epsilon}} \left(\frac{\partial \tilde{\epsilon}}{\partial x_i} \right)_{x_{k \neq i}} \right] \\
&= \frac{1}{38400} \sum_{p=0}^4 \sum_{q=0}^4 a_{pq} \left(\tilde{\rho}_c^{\mathrm{rf}} \right)^p \left(\tilde{T}^{\mathrm{rf}} \right)^q \frac{m_i}{m} \left\{ p \left[-1 + \frac{1}{\tilde{\sigma}^3} \left(\frac{\partial \tilde{\sigma}^3}{\partial x_{c_i}} \right)_{x_{k \neq i}} \right] \right. \\
&\quad \left. - q \left[\frac{1}{\tilde{\epsilon} \tilde{\sigma}^3} \left(\frac{\partial \left(\tilde{\epsilon} \tilde{\sigma}^3 \right)}{\partial x_{c_i}} \right)_{x_{k \neq i}} - \frac{1}{\tilde{\sigma}^3} \left(\frac{\partial \tilde{\sigma}^3}{\partial x_{c_i}} \right)_{x_{k \neq i}} \right] \right\} \tag{A.75}
\end{aligned}
$$

The mathematical procedure for the next cases is similar to the previous case, hence no additional comment will be made.

Case 2. Cross-association is not allowed, component l has 3 association sites, $M_l = 3$, and the following assumptions hold. $X_l^A = X_l^B$, $X_l^C = 2X_l^A - 1$, $\varepsilon_l^{A_l C_l} = \varepsilon_l^{B_l C_l} = \varepsilon_l$, and $k_l^{A_l C_l} = k_l^{B_l C_l} = k_l$.

$$
X_l^A = \frac{1}{1 + \tilde{\rho} x_l \left(2X_l^A - 1 \right) \tilde{\Delta}^l} \tag{A.76}
$$

$$
\tilde{\Delta}^l = \frac{1 - X_l^A}{\tilde{\rho} x_l X_l^A \left(2X_l^A - 1 \right)} \tag{A.77}
$$

$$
\ln \tilde{\Delta}^l = \ln \left(1 - X_l^A \right) - \ln \tilde{\rho} - \ln x_l - \ln X_l^A - \ln \left(2X_l^A - 1 \right) \tag{A.78}
$$

$$\left(\frac{\partial \ln \tilde{\Delta}^l}{\partial x_i}\right)_{\tilde{T},\tilde{\rho},x_{k\neq i}} = \frac{1}{\tilde{I}}\left(\frac{\partial \tilde{I}}{\partial x_i}\right)_{\tilde{T},\tilde{\rho},x_{k\neq i}} = \left[\frac{-1}{1-X_l^A} - \frac{1}{X_l^A}\right.$$

$$\left. - \frac{2}{2X_l^A-1}\right]\left(\frac{\partial X_l^A}{\partial x_i}\right)_{\tilde{T},\tilde{\rho},x_{k\neq i}} - \frac{1}{x_j}\left(\frac{\partial x_l}{\partial x_i}\right)_{\tilde{T},\tilde{\rho},x_{k\neq i}} \quad (A.79)$$

$$\left(\frac{\partial \ln \tilde{\Delta}^l}{\partial \tilde{\rho}}\right)_{\tilde{T},x_k} = \frac{1}{\tilde{I}}\left(\frac{\partial \tilde{I}}{\partial \tilde{\rho}}\right)_{\tilde{T},x_k} = \frac{m\tilde{\sigma}^3}{\tilde{I}}\left(\frac{\partial \tilde{I}}{\partial \tilde{\rho}_c^{\mathrm{rf}}}\right)_{\tilde{T},x_k}$$

$$= \left(\frac{-1}{1-X_l^A} - \frac{1}{X_l^A} - \frac{2}{2X_l^A-1}\right)\left(\frac{\partial X_i}{\partial \tilde{\rho}}\right)_{\tilde{T},x_k} - \frac{1}{\tilde{\rho}} \quad (A.80)$$

$$\sum_\alpha \left(\frac{1}{X_l^\alpha} - \frac{1}{2}\right)\left(\frac{\partial X_l^\alpha}{\partial \tilde{\rho}}\right)_{\tilde{T},x_k} = 2\left(\frac{1}{X_l^A} + \frac{1}{2X_l^A-1} - 1\right)\left(\frac{\partial X_l^A}{\partial \tilde{\rho}}\right)_{\tilde{T},x_k} \quad (A.81)$$

$$\frac{1}{X_l} + \frac{1}{2X_l-1} - 1 = -(1-X_l)\left(\frac{-1}{1-X_l} - \frac{1}{X_l} - \frac{2}{2X_l-1}\right) \quad (A.82)$$

$$2x_l\left(\frac{1}{X_l^A} + \frac{1}{2X_l^A-1} - 1\right)\left(\frac{\partial X_l^A}{\partial x_i}\right)_{\tilde{T},\tilde{\rho},x_{k\neq i}} =$$

$$= -2x_l\left(1-X_l^A\right)\left(\frac{-1}{1-X_l^A} - \frac{1}{X_l^A} - \frac{2}{2X_l^A-1}\right)\left(\frac{\partial X_l^A}{\partial x_i}\right)_{\tilde{T},\tilde{\rho},x_{k\neq i}}$$

$$= -2\left(1-X_l^A\right)\left[\left(\frac{\partial x_l}{\partial x_i}\right)_{\tilde{T},\tilde{\rho},x_{k\neq i}} + x_l\left(\frac{\partial \ln \tilde{\Delta}^l}{\partial x_i}\right)_{\tilde{T},\tilde{\rho},x_{k\neq i}}\right] \quad (A.83)$$

$$2\tilde{\rho}\left(\frac{1}{X_l^A} + \frac{1}{2X_l^A-1} - 1\right)\left(\frac{\partial X_l^A}{\partial \tilde{\rho}}\right)_{\tilde{T},x_k} =$$

$$= -2\tilde{\rho}\left(1-X_l^A\right)\left(\frac{-1}{1-X_l^A} - \frac{1}{X_l^A} - \frac{2}{2X_l^A-1}\right)\left(\frac{\partial X_l^A}{\partial \tilde{\rho}}\right)_{\tilde{T},x_k}$$

$$= -2\left(1-X_l^A\right)\left[1 + \tilde{\rho}\left(\frac{\partial \ln \tilde{\Delta}^l}{\partial \tilde{\rho}}\right)_{\tilde{T},x_k}\right] \quad (A.84)$$

$$\left(\frac{\partial x_j}{\partial x_i}\right)_{\tilde{T},\tilde{V},x_{k\neq i}} = \begin{cases} 0 & j \neq i \\ 1 & j = i \end{cases} \quad (A.85)$$

$$\tilde{\mu}_i^{\text{assoc}} = \tilde{T}\left\{ M_i\left(\ln X_i + \frac{1-X_i}{2}\right) - \sum_j \frac{M_j}{2}\left(1-X_j^A\right)\left[\left(\frac{\partial x_j}{\partial x_i}\right)_{\tilde{T},\tilde{\rho},x_{k\neq i}}\right.\right.$$

$$\left.\left. + x_j \frac{1}{\tilde{I}}\left(\frac{\partial \tilde{I}}{\partial x_i}\right)_{\tilde{T},\tilde{\rho},x_{k\neq i}}\right]\right\}, \qquad \text{if } j=l, \ M_j = M_l+1 \qquad \text{(A.86)}$$

$$\tilde{P}^{\text{assoc}} = -\frac{1}{2}\tilde{T}\tilde{\rho}\left[1 + \frac{\tilde{\rho}_c}{\tilde{I}}\left(\frac{\partial \tilde{I}}{\partial \tilde{\rho}_c}\right)_{\tilde{T},x_k}\right]\sum_i x_i M_i\left(1-X_i\right),$$

$$\text{if } i=l, \ M_i = M_l+1 \qquad \text{(A.87)}$$

Case 3. Cross-association is not allowed, component l has 4 association sites, $M_l = 4$, and the following assumptions hold. $X_l^A = X_l^B = X_l^C$, $X_l^D = 3X_l^A - 2$, $\varepsilon_l^{A_iD_i} = \varepsilon_l^{B_iD_i} = \varepsilon_l^{C_iD_i} = \varepsilon_l$, and $k_l^{A_iD_i} = k_l^{B_iD_i} = k_l^{C_iD_i} = k_l$.

$$X_j^A = \frac{1}{1 + \tilde{\rho}x_l\left(3X_l^A - 2\right)\tilde{\Delta}^l} \qquad \text{(A.88)}$$

$$\tilde{\Delta}^j = \frac{1 - X_l^A}{\tilde{\rho}x_l X_l^A\left(3X_l^A - 2\right)} \qquad \text{(A.89)}$$

$$\ln\tilde{\Delta}^l = \ln\left(1 - X_l^A\right) - \ln\tilde{\rho} - \ln x_l - \ln X_l^A - \ln\left(3X_l^A - 2\right) \qquad \text{(A.90)}$$

$$\left(\frac{\partial \ln\tilde{\Delta}^l}{\partial x_i}\right)_{\tilde{T},\tilde{\rho},x_{k\neq i}} = \frac{1}{\tilde{I}}\left(\frac{\partial \tilde{I}}{\partial x_i}\right)_{\tilde{T},\tilde{\rho},x_{k\neq i}}$$

$$= \left(\frac{-1}{1-X_l^A} - \frac{1}{X_l^A} - \frac{3}{3X_l^A - 2}\right)\left(\frac{\partial X_l^A}{\partial x_i}\right)_{\tilde{T},\tilde{\rho},x_{k\neq i}}$$

$$- \frac{1}{x_l}\left(\frac{\partial x_l}{\partial x_i}\right)_{\tilde{T},\tilde{\rho},x_{k\neq i}} \qquad \text{(A.91)}$$

$$\left(\frac{\partial \ln\tilde{\Delta}^i}{\partial \tilde{\rho}}\right)_{\tilde{T},x_k} = \frac{1}{\tilde{I}}\left(\frac{\partial \tilde{I}}{\partial \tilde{\rho}}\right)_{\tilde{T},x_k} = \frac{m\tilde{\sigma}^3}{\tilde{I}}\left(\frac{\partial \tilde{I}}{\partial \tilde{\rho}_c^{\text{rf}}}\right)_{\tilde{T},x_k}$$

$$= \left(\frac{-1}{1-X_l^A} - \frac{1}{X_l^A} - \frac{3}{3X_l^A - 2}\right)\left(\frac{\partial X_l}{\partial \tilde{\rho}}\right)_{\tilde{T},x_k} - \frac{1}{\tilde{\rho}} \qquad \text{(A.92)}$$

$$\sum_{\alpha} \left(\frac{1}{X_l^{\alpha}} - \frac{1}{2} \right) \left(\frac{\partial X_l^{\alpha}}{\partial \tilde{\rho}} \right)_{\tilde{T}, x_k} = 3 \left(\frac{1}{X_l^A} + \frac{1}{3X_l^A - 2} - 1 \right) \left(\frac{\partial X_l^A}{\partial \tilde{\rho}} \right)_{\tilde{T}, x_k} \quad \text{(A.93)}$$

$$\frac{1}{X_l} + \frac{1}{3X_l - 2} - 1 = -(1 - X_l) \left(\frac{-1}{1 - X_l} - \frac{1}{X_l} - \frac{3}{3X_l - 2} \right) \quad \text{(A.94)}$$

$$3x_l \left(\frac{1}{X_l^A} + \frac{1}{3X_l^A - 2} - 1 \right) \left(\frac{\partial X_l^A}{\partial x_i} \right)_{\tilde{T}, \tilde{\rho}, x_{k \neq i}} =$$

$$= -3x_l \left(1 - X_l^A \right) \left(\frac{-1}{1 - X_l^A} - \frac{1}{X_l^A} - \frac{3}{3X_l^A - 2} \right) \left(\frac{\partial X_l^A}{\partial x_i} \right)_{\tilde{T}, \tilde{\rho}, x_{k \neq i}}$$

$$= -3 \left(1 - X_l^A \right) \left[\left(\frac{\partial x_l}{\partial x_i} \right)_{\tilde{T}, \tilde{\rho}, x_{k \neq i}} + x_l \left(\frac{\partial \ln \tilde{\Delta}^l}{\partial x_i} \right)_{\tilde{T}, \tilde{\rho}, x_{k \neq i}} \right] \quad \text{(A.95)}$$

$$3\tilde{\rho} \left(\frac{1}{X_l^A} + \frac{1}{3X_l^A - 2} - 1 \right) \left(\frac{\partial X_l^A}{\partial \tilde{\rho}} \right)_{\tilde{T}, x_k} =$$

$$= -3\tilde{\rho} \left(1 - X_l^A \right) \left(\frac{-1}{1 - X_l^A} - \frac{1}{X_l^A} - \frac{3}{3X_l^A - 2} \right) \left(\frac{\partial X_l^A}{\partial \tilde{\rho}} \right)_{\tilde{T}, x_k}$$

$$= -3 \left(1 - X_l^A \right) \left[1 + \tilde{\rho} \left(\frac{\partial \ln \tilde{\Delta}^l}{\partial \tilde{\rho}} \right)_{\tilde{T}, x_k} \right] \quad \text{(A.96)}$$

$$\left(\frac{\partial x_j}{\partial x_i} \right)_{\tilde{T}, \tilde{V}, x_{k \neq i}} = \left\{ \begin{array}{ll} 0 & j \neq i \\ 1 & j = i \end{array} \right. \quad \text{(A.97)}$$

$$\tilde{\mu}_i^{\text{assoc}} = \tilde{T} \left\{ M_i \left(\ln X_i + \frac{1 - X_i}{2} \right) - \sum_j \frac{M_j}{2} \left(1 - X_j^A \right) \left[\left(\frac{\partial x_j}{\partial x_i} \right)_{\tilde{T}, \tilde{\rho}, x_{k \neq i}} \right. \right.$$

$$\left. \left. + x_j \frac{1}{\tilde{I}} \left(\frac{\partial \tilde{I}}{\partial x_i} \right)_{\tilde{T}, \tilde{\rho}, x_{k \neq i}} \right] \right\} \qquad \text{if } j = l, \ M_j = M_l + 2 \quad \text{(A.98)}$$

$$\tilde{P}^{\text{assoc}} = -\frac{1}{2} \tilde{T} \tilde{\rho} \left[1 + \frac{\tilde{\rho}_c}{\tilde{I}} \left(\frac{\partial \tilde{I}}{\partial \tilde{\rho}_c} \right)_{\tilde{T}, x_k} \right] \sum_i x_i M_i \left(1 - X_i \right),$$

$$\text{if } i = l, \ M_i = M_l + 2 \quad \text{(A.99)}$$

Case 4. Cross-association between components 1 and 2, $M_1 = 1$, $M_2 = 1$, and no self-association.

$$X_1 = \frac{1}{1 + \tilde{\rho} x_2 X_2 \tilde{\Delta}^{AB}} \tag{A.100}$$

$$X_2 = \frac{1}{1 + \tilde{\rho} x_1 X_1 \tilde{\Delta}^{AB}} \tag{A.101}$$

$$x_1 (1 - X_1) = x_2 (1 - X_2) \tag{A.102}$$

$$X_1 = \frac{-1 + \tilde{\rho}\tilde{\Delta}^{AB} (x_1 - x_2) + \sqrt{1 + 2\tilde{\rho}\tilde{\Delta}^{AB} (x_1 + x_2) + \left(\tilde{\rho}\tilde{\Delta}^{AB}\right)^2 (x_1 - x_2)^2}}{2\tilde{\rho}\tilde{\Delta}^{AB} x_1} \tag{A.103}$$

$$\left(\frac{\partial X_1}{\partial x_i}\right)_{\tilde{T},\tilde{\rho},x_{k \neq i}} = -\tilde{\rho} (X_1)^2 \left[X_2 \tilde{\Delta}^{A\beta_i} + x_2 X_2 \left(\frac{\partial \tilde{\Delta}^{AB}}{\partial x_i}\right)_{\tilde{T},\tilde{\rho},x_{k \neq i}} \right.$$
$$\left. + x_2 \tilde{\Delta}^{AB} \left(\frac{\partial X_2}{\partial x_i}\right)_{\tilde{T},\tilde{\rho},x_{k \neq i}} \right] \tag{A.104}$$

$$\left(\frac{\partial X_1}{\partial \tilde{\rho}}\right)_{\tilde{T},x_k} = -(X_1)^2 x_2 \left[X_2 \tilde{\Delta}^{AB} + \tilde{\rho} X_2 \left(\frac{\partial \tilde{\Delta}^{AB}}{\partial \tilde{\rho}}\right)_{\tilde{T},x_k} \right.$$
$$\left. + \tilde{\rho}\tilde{\Delta}^{AB} \left(\frac{\partial X_2}{\partial \tilde{\rho}}\right)_{\tilde{T},x_k} \right] \tag{A.105}$$

$$\left(\frac{\partial X_2}{\partial x_i}\right)_{\tilde{T},\tilde{\rho},x_{k \neq i}} = \frac{x_1}{x_2} \left(\frac{\partial X_1}{\partial x_i}\right)_{\tilde{T},\tilde{\rho},x_{k \neq i}} - \frac{1 - X_1}{x_2} \left(\frac{\partial x_1}{\partial x_i}\right)_{x_{k \neq i}}$$
$$+ \frac{1 - X_2}{x_2} \left(\frac{\partial x_2}{\partial x_i}\right)_{x_{k \neq i}} \tag{A.106}$$

$$\left(\frac{\partial X_2}{\partial \tilde{\rho}}\right)_{\tilde{T},x_k} = \frac{x_1}{x_2} \left(\frac{\partial X_1}{\partial \tilde{\rho}}\right)_{\tilde{T},x_k} \tag{A.107}$$

$$
\left(\frac{\partial X_1}{\partial x_i}\right)_{\tilde{T},\tilde{\rho},x_{k\neq i}} = -\tilde{\rho}\left(X_1\right)^2\left\{\frac{X_2\tilde{\Delta}^{AB}\left[\frac{\tilde{\Delta}^{A\beta_i}}{\tilde{\Delta}^{AB}} + \frac{x_2}{\tilde{I}}\left(\frac{\partial \tilde{I}}{\partial x_i}\right)_{\tilde{T},\tilde{\rho},x_{k\neq i}}\right]}{1 + \tilde{\rho}x_1\left(X_1\right)^2\tilde{\Delta}^{AB}}\right.
$$

$$
\left. + \frac{\tilde{\Delta}^{AB}\left[\left(1-X_2\right)\left(\frac{\partial x_2}{\partial x_i}\right)_{x_{k\neq i}} - \left(1-X_1\right)\left(\frac{\partial x_1}{\partial x_i}\right)_{x_{k\neq i}}\right]}{1 + \tilde{\rho}x_1\left(X_1\right)^2\tilde{\Delta}^{AB}}\right\} \qquad \text{(A.108)}
$$

$$
\left(\frac{\partial X_1}{\partial \tilde{\rho}}\right)_{\tilde{T},x_k} = \frac{-x_2\left(X_1\right)^2 X_2\left[\tilde{\Delta}^{AB} + \tilde{\rho}\left(\frac{\partial \tilde{\Delta}^{AB}}{\partial \tilde{\rho}}\right)_{\tilde{T},x_k}\right]}{1 + \tilde{\rho}x_1\left(X_1\right)^2\tilde{\Delta}^{AB}}
$$

$$
= \frac{-x_2\left(X_1\right)^2 X_2\tilde{\Delta}^{AB}\left(1 + \frac{\tilde{\rho}_c}{\tilde{I}}\left(\frac{\partial \tilde{I}}{\partial \tilde{\rho}_c}\right)_{\tilde{T},x_k}\right)}{1 + \tilde{\rho}x_1\left(X_1\right)^2\tilde{\Delta}^{AB}} \qquad \text{(A.109)}
$$

$$
\tilde{\mu}_i^{\text{assoc}} = \tilde{T}\left\{\ln X_i + \frac{1}{2}\left(1-X_i\right) + \left(\frac{1}{X_2} - \frac{1}{2}\right)\left[\left(1-X_2\right)\left(\frac{\partial x_2}{\partial x_i}\right)_{x_{k\neq i}}\right.\right.
$$

$$
\left. - \left(1-X_1\right)\left(\frac{\partial x_1}{\partial x_i}\right)_{x_{k\neq i}}\right]
$$

$$
- x_1\left(\frac{1}{X_1} + \frac{1}{X_2} - 1\right)\tilde{\rho}\left(X_1\right)^2\left\{\frac{X_2\tilde{\Delta}^{AB}\left[\frac{\tilde{\Delta}^{A\beta_i}}{\tilde{\Delta}^{AB}} + \frac{x_2}{\tilde{I}}\left(\frac{\partial \tilde{I}}{\partial x_i}\right)_{\tilde{T},\tilde{\rho},x_{k\neq i}}\right]}{1 + \tilde{\rho}x_1\left(X_1\right)^2\tilde{\Delta}^{AB}}\right.
$$

$$
\left.\left. + \frac{\tilde{\Delta}^{AB}\left[\left(1-X_2\right)\left(\frac{\partial x_2}{\partial x_i}\right)_{x_{k\neq i}} - \left(1-X_1\right)\left(\frac{\partial x_1}{\partial x_i}\right)_{x_{k\neq i}}\right]}{1 + \tilde{\rho}x_1\left(X_1\right)^2\tilde{\Delta}^{AB}}\right\}\right\} \qquad \text{(A.110)}
$$

$$
\tilde{P}^{\text{assoc}} = \tilde{T}\tilde{\rho}^2 x_1\left(\frac{1}{X_1} + \frac{1}{X_2} - 1\right)\left\{\frac{-x_2\left(X_1\right)^2 X_2\tilde{\Delta}^{AB}\left[1 + \frac{\tilde{\rho}_c}{\tilde{I}}\left(\frac{\partial \tilde{I}}{\partial \tilde{\rho}_c}\right)_{\tilde{T},x_k}\right]}{1 + \tilde{\rho}x_1\left(X_1\right)^2\tilde{\Delta}^{AB}}\right\} \qquad \text{(A.111)}
$$

Publications

The following publications have arisen from this thesis work:

1. Pàmies, J. C.; Vega, L. F. Vapor-liquid equilibria and critical behavior of heavy n-alkanes using transferable parameters from the soft-SAFT equation of state. *Ind. Eng. Chem. Res.* **40**, 2532 (2001).

2. Pàmies, J. C.; Vega, L. F. Critical properties of homopolymer fluids studied by a Lennard-Jones statistical associating fluid theory. *Molec. Phys.* **100**, 2519 (2002).

3. Pàmies, J. C.; McCabe, C.; Cummings, P. T.; Vega, L. F. Coexistence densities of methane and propane by canonical molecular dynamics and Gibbs ensemble Monte Carlo simulations. *Mol. Sim.* **29**, 463 (2003).

4. Florusse L. J; Pàmies, J. C.; Vega, L. F. Peters, C. J.; Meijer, H. Solubility of hydrogen in heavy n-alkanes: experiments and SAFT modeling. *AIChE J.*, in press (2003).

5. Dias A. M. A.; Pàmies, J. C.; Coutinho, J. A. P.; Marrucho , I. M.; Vega, L. F. SAFT modeling of the solubility of gases in perfluoroalkanes. *J. Phys. Chem. B*, accepted (2003).

6. Herdes, C.; Pàmies, J. C.; Marcos, R.; Vega, L. F. SAFT and Monte Carlo simulations: influence of the location of association sites on the thermodynamics of freely-jointed Lennard-Jones chains. In preparation (2003).

7. Pàmies, J. C.; Vega, L. F. Fluid phase behavior of carbon dioxide mixtures with alkanes and alkanols from the soft-SAFT equation of state. In preparation (2003).

8. Pàmies, J. C.; Vega, L. F. Interfacial tensions from a SAFT + density gradient theory approach. In preparation (2003).

9. Pàmies, J. C.; Vega, L. F. Vapor pressures of long chains from the soft-SAFT dimer theory. In preparation (2003).

Curriculum Vitae

Josep C. Pàmies was born in Tarragona, Spain, on the 20th of July of 1976. He started the five-year studies of chemical engineering in 1994 at the Universitat Rovira i Virgili. After some exams and a five-month stay in industry, working on the inference of properties by neural networks, he could start doing some research at the fluid mechanics group, where he learned about macroscopic modelling and the numerical solving of Navier-Stokes equations to study the influence of the flux structure on the photolytic cycle of the tropospheric nitrogen. He obtained his bachelor's degree in chemical engineering on July, 1999. After a few months doing research at the Bioengineering & Bioelectrochemistry group of the same university, working on colloidal gold electrodeposition, he noticed that experimental work and he were incompatible. At the same time, he joined the molecular modelling group, where he started to work on the project of soft-SAFT, under the supervision of Dr. Lourdes Vega. There he began to see things also from a molecular point of view. In October 1999, he enroled in the graduate studies in Chemical and Process Engineering at the Universitat Rovira i Virgili, holding a scholarship from the same university. Three months thereafter, he was awarded a predoctoral scholarship from the government of Catalonia. After successfully passing a number of courses, he obtained the Diploma d'Estudis Avançats (Diploma of advanced studies) in October 2001, which stated that he was suitable to do research. During the four-year research period, it was time to go abroad, and he stayed the three last months of 2000 in Knoxville, TN, learning about the direct simulation of interfaces by molecular dynamics, under the supervision of professor Peter Cummings and Dr. Clare McCabe. Later on, in 2002, he stayed other three months in Delft, The Netherlands, working on the modelling of the solubility of gases in long chains with the soft-SAFT theory, under the supervision of professor Cor J. Peters.

Josep C. Pàmies has published five research articles in international journals, and he is preparing some more. He has more than five publications in international conference proceedings, and has contributed by means of oral or poster presentations to more than 15 conferences. He was a member of the organizing committee of two

national conferences and one international symposium, the latter being organized on the occasion of having together the select members of the evaluation committee that, on the 11th of December of 2003, based on the lights of the present study, will decide if he deserves the doctor's degree.

Resum

En aquest treball s'han desenvolupat tècniques de modelització molecular, concretament la teoria estadística dels fluids associants (en anglès, SAFT) i la simulació molecular (Monte Carlo i dinàmica molecular), i s'han aplicat a l'àrea de la termodinàmica molecular moderna. Les tècniques esmentades s'han utilitzat en l'estudi del comportament de propietats de sistemes fluids en equilibri termodinàmic, principalment equilibris líquid-vapor, però també coexistència líquid-líquid i comportament crític. També són objecte d'aquest treball de tesi les propietats d'interfases planes des d'un enfoc de la SAFT juntament amb la teoria del gradient de la densitat. Els sistemes reals tractats inclouen n-alcans purs, 1-alcanols, n-perfluoroalcans, hidrogen, oxigen, xenó, diòxid de carboni i algunes de les seves mescles.

Les propietats termofísiques afecten molts dels aspectes del disseny i de l'operació de plantes químiques. Per una banda, les dades de propietats i els models predictius són la matèria primera del disseny de processos químics. Per altra banda, la simulació de processos ha esdevingut l'eina principal per al desenvolupament, disseny, escalat i optimització de processos químics. Les propietats termofísiques i, particularment, les d'equilibri de fases, són doncs entrades clau per al desenvolupament d'aquests models de procés.

Les propietats termofísiques es poden obtenir experimentalment i mitjançant models teòrics, ja sigui des del punt de vista fenomenològic o molecular. Tanmateix, avui en dia les mesures experimentals només es duen a terme per a sistemes o condicions termodinàmiques en les cuals els models existents fallen o no són prou exactes. Els models fenomenològics són un camí físicament raonable de representar dades experimentals, però degut a la seva capacitat limitada de predicció, normalment no funcionen fora del rang d'ajust dels seus paràmetres. Una perspectiva molecular, contràriament, permet derivar relacions fonamentals entre les forces intermoleculars subjacents i el comportament macroscòpic resultant dels fluids. Un avantatge important d'utilitzar un model molecular és que els paràmetres tenen sentit físic i són independents de les condicions termodinàmiques. A més, l'ús conjunt de teories moleculars i simulacions proporciona una forma de determinar separadament l'efecte de les

forces intermoleculars i l'efecte de les aproximacions de les teories en el comportament macroscòpic.

Tal com s'explicita en el títol d'aquesta tesi, aquest treball s'inclou en el camp de la modelització molecular. El treball tracta del desenvolupament d'eines precises i fiables de la modelització molecular per a la predicció del comportament termodinàmic de fluids complexes. La teoria estadística dels fluids associants, la teoria del gradient de la densitat, i simulacions moleculars, tan Monte Carlo com dinàmica molecular, s'han utilitzat per a l'estudi del comportament de les propietats *bulk* (del sí del fluid) i interfacials de fluids de tipus cadena en equilibri termodinàmic. Els sistemes reals tractats inclouen n-alcans purs, 1-alcanols, n-perfluoroalcans, hidrogen, oxigen, xenó, dióxid de carboni i algunes de les seves mescles.

Una versió de l'equació d'estat SAFT, l'anomenada equació soft-SAFT, basada en un potencial d'interacció *soft* (suau) entre molècules, el potencial Lennard-Jones, s'ha emprat en l'estudi de l'equilibri de fases i el comportament crític de fluids de tipus cadena. S'ha proposat un conjunt de paràmetres moleculars optimitzats per als primers membres de les sèries dels n-alcans, 1-alcanols i n-perfluoroalcans, que correlacionen linealment amb el nombre de carbonis de la cadena. La utilització d'aquests paràmetres de forma transferible permet la predicció correcta del diagrama de fases de cadenes llargues i mescles, sense necessitat d'optimitzar paràmetres de mescla en molts casos. Es demostra que l'equació dóna molt bons resultats en les prediccions d'equilibris de fases i comportament crític de n-alcans i mescles binàries assimètriques d'aquests. També es prova que l'equació soft-SAFT és capaç de predir quantitativament les propietats crítiques per longituds de cadena relativament grans, mostrant un canvi cap a comportament de camp mitjà quan s'assoleix el règim de longitud de cadena infinita. A més, suposant que el volum i l'energia dispersiva per molècula mantenen la proporcionalitat respecte el pes molecular per cadenes molt llargues, s'ha trobat que l'equació prediu un valor per al factor de compressibilitat crític igual a 1/5 per cadenes de longitud infinita.

La solubilitat d'hidrogen en cadenes llargues de n-alcans és una altra de les aplicacions exitoses de l'equació d'estat soft-SAFT. Es demostra que el model soft-SAFT proporciona resultats molt acurats i fiables per aquests sistemes molt assimètrics. L'extensió de l'equació a sistemes amb associació creuada permet la descripció correcta de la solubilitat d'oxigen en n-perfluoroalcans. Es remarca de nou la importància dels paràmetres amb sentit físic, mostrant tendències raonables i mitjançant la comparació dels paràmetres amb valors d'altres models quan és possible. L'estudi de mescles binàries de dióxid de carboni conclou que, per una descripció correcta d'aquests sistemes, l'efecte del quadrupol del dióxid de carboni s'ha d'incloure en el model SAFT.

L'equació soft-SAFT s'ha acoblat a la teoria del gradient de la densitat de Cahn i Hilliard per al càlcul de propietats d'interfases planes de n-alcans, 1-alcanols i algunes

de les seves mescles. Es mostra que les propietats interfacials de compostos purs i mescles en condicions subcrítiques es poden predir correctament amb aquesta aproximació teòrica. Adicionalment, un tractament de *crossover* milloraria la descripció de mescles en les quals hi ha un punt crític.

Encara que la major part del treball s'ha enfocat cap al desenvolupament d'una eina fiable i precisa basada en SAFT per a la predicció del comportament termodinàmic de fluids complexos, les simulacions moleculars també s'han emprat per al càlcul de propietats *bulk* i interfacials de fluids simples. En particular, s'ha extès un codi de dinàmica molecular per al càlcul de propietats interfacials. També es presenta la influència del radi de tall del potencial d'interacció molecular en les densitats coexistents.

Aquest treball de tesi vol sobretot posar èmfasi en què les claus d'un ús apropiat de les eines de modelització molecular són la selecció de models específics adequats, representatius de l'estructura i les interaccions rellevants del sistema real, i l'ús de paràmetres que haurien de mostrar tendències físiques (dins una sèrie química) i ser transferibles (dins una mateixa sèrie química i a altres compostos) sempre que sigui possible.

Resumen

En este trabajo se han desarrollado técnicas de modelado molecular, concretamente la teoría estadística de los fluidos asociantes (en inglés, SAFT) y la simulación molecular (Monte Carlo y dinámica molecular), y se han aplicado en el área de la termodinámica molecular moderna. Las técnicas mencionadas se han utilizado en el estudio del comportamiento de propiedades de sistemas fluidos en equilibrio termodinámico, principalmente equilibrios líquido-vapor, pero también coexistencia líquido-líquido y comportamiento crítico. También son objeto de este trabajo de tesis las propiedades de interfases planas desde un enfoque de la SAFT juntamente con la teoría del gradiente de la densidad. Los sistemas reales tratados incluyen n-alcanos puros, 1-alcanoles, n-perfluoroalcanos, hidrógeno, oxígeno, xenón, dióxido de carbono y algunas de sus mezclas.

Las propiedades termofísicas afectan muchos de los aspectos del diseño y de la operación de plantas químicas. Por un lado, los datos de propiedades y los modelos predictivos son la materia prima del diseño de procesos químicos. Por otro lado, la simulación de procesos se ha convertido en la herramienta principal para el desarrollo, diseño, escalado y optimización de procesos químicos. Las propiedades termofísicas y, en particular, las de equilibrio de fases son, consecuentemente, entradas clave para el desarrollo de estos modelos de proceso.

Las propiedades termofísicas se pueden obtener experimentalmente y mediante modelos teóricos, ya sea des del punto de vista fenomenológico o molecular. Sin embargo, hoy en día las medidas experimentales sólo se llevan a cabo para sistemas o condiciones termodinámicas en las cuales los modelos existentes fallan o no son suficientemente exactos. Los modelos fenomenológicos son un camino físicamente razonable para representar datos experimentales, pero debido a su limitada capacidad de predicción, normalmente no funcionan fuera del rango de ajuste de sus parámetros. Una perspectiva molecular, por el contrario, permite derivar relaciones fundamentales entre las fuerzas intermoleculares subyacentes y el comportamiento macroscópico resultante de los fluidos. Una ventaja importante de utilizar un modelo molecular es que los parámetros tienen sentido físico y son independientes de las condiciones ter-

modinámicas. Además, el uso conjunto de teorías moleculares y simulaciones proporciona una forma de determinar separadamente el efecto de las fuerzas intermoleculares y el efecto de las aproximaciones de las teorías en el comportamiento macroscópico.

Tal como se explicita en el título de esta tesis, este trabajo se incluye en el campo del modelado molecular. El trabajo versa sobre el desarrollo de herramientas precisas y fiables del modelado molecular para la predicción del comportamiento termodinámico de fluidos complejos. Las teoría estadística de los fluidos asociantes, la teoría del gradiente de la densidad, y simulaciones moleculares, tanto Monte Carlo como dinámica molecular, se han utilizado para estudiar el comportamiento de las propiedades *bulk* (del seno del fluido) e interfaciales de fluidos de tipo cadena en equilibrio termodinámico. Los sistemas reales tratados incluyen n-alcanos puros, 1-alcanoles, n-perfluoroalcanos, hidrógeno, oxígeno, xenón, dióxido de carbono y algunas de sus mezclas.

Una versión de la ecuación de estado SAFT, la llamada ecuación soft-SAFT, basada en un potencial de interacción *soft* (suave) entre moléculas, el potencial Lennard-Jones, se ha usado en el estudio del equilibrio de fases y el comportamiento crítico de fluidos de tipo cadena. Se ha propuesto un conjunto de parámetros moleculares optimizados para los primeros miembros de las series de los n-alcanos, 1-alcanoles y n-perfluoroalcanos, que correlacionan linealmente con el número de carbonos de la cadena. La utilización de estos parámetros de forma transferible permite la predicción correcta del diagrama de fases de cadenas largas y mezclas, sin necesidad de optimizar parámetros de mezcla en muchos casos. Se demuestra que la ecuación da muy buenos resultados en las predicciones de equilibrios de fases y comportamiento crítico de n-alcanos y mezclas asimétricas de éstos. También se prueba que la ecuación soft-SAFT es capaz de predecir cuantitativamente las propiedades críticas de longitudes de cadena relativamente grandes, mostrando un cambio hacia comportamiento de campo medio cuando se alcanza el régimen de longitud de cadena infinita. Adicionalmente, asumiendo que el volumen y la energía dispersiva por molécula mantienen la proporcionalidad respecto al peso molecular para cadenas muy largas, se ha encontrado que la ecuación predice un valor para el factor de compresibilidad crítico igual a 1/5 para cadenas de longitud infinita.

La solubilidad de hidrógeno en cadenas largas de n-alcanos es otra de las aplicaciones exitosas de la ecuación de estado soft-SAFT. Se demuestra que el modelo soft-SAFT proporciona resultados muy exactos y fiables para estos sistemas muy asimétricos. La extensión de la ecuación a sistemas con asociación cruzada permite la descripción correcta de la solubilidad de oxígeno en n-perfluoroalcanos. Se remarca de nuevo la importancia de los parámetros con sentido físico, mostrando tendencias razonables y mediante la comparación de los parámetros con valores de otros modelos cuando es posible. El estudio de mezclas binarias de dióxido de carbono concluye que,

para una descripción correcta de estos sistemas, el efecto del cuadrupolo del dióxido de carbono debe incluirse en el modelo SAFT.

La ecuación soft-SAFT se ha acoplado a la teoría del gradiente de la densidad de Cahn y Hilliard para el cálculo de propiedades de interfases planas de n-alcanos, 1-alcanoles y algunas de sus mezclas. Se muestra que las propiedades interfaciales de compuestos puros y mezclas en condiciones subcríticas pueden predecirse correctamente con esta aproximación teórica. Adicionalmente, un tratamiento de *crossover* mejoraría la descripción de mezclas en las cuales aparece un punto crítico.

Aunque la mayor parte del trabajo se ha enfocado hacia el desarrollo de una herramienta fiable y precisa basada en SAFT para la predicción del comportamiento termodinámico de fluidos complejos, las simulaciones moleculares también se han utilizado para el cálculo de propiedades *bulk* e interfaciales de fluidos simples. En particular, se ha extendido un código de dinámica molecular para el cálculo de propiedades interfaciales. También se presenta la influencia del radio de corte del potencial de interacción molecular en las densidades coexistentes.

Este trabajo de tesis quiere sobretodo poner énfasis en que las claves de un uso apropiado de las herramientas de modelado molecular son la selección de modelos específicos adecuados, representativos de la estructura y las interacciones relevantes del sistema real, y el uso de parámetros que tendrían que mostrar tendencias físicas (dentro de una serie química) y ser transferibles (dentro de una misma serie química y a otros compuestos) siempre que sea posible.